UNIVERSITY OF CALIFORNIA, SAN DIEGO

Fluorescence and energy transfer studies of membrane protein folding

A dissertation submitted in partial satisfaction of the requirements
for the degree Doctor of Philosophy

in

Chemistry

by

Guipeun Kang

Committee in charge:

Professor Judy E. Kim, Chair
Professor Simpson Joseph
Professor Douglas Magde
Professor Douglas Smith
Professor Michael Tauber

2015

The Dissertation of Guipeun Kang is approved, and it is acceptable in quality and form for publication on microfilm and electronically:

_____

_____

_____

_____

_____
Chair

University of California, San Diego

2015

DEDICATION

To my parents, Ducksoo Kang and Young Joo Paik.

To my grand parents, Sung Hwan Paik and Sun Ok Lee.

TABLE OF CONTENTS

LIST OF FIGURES

LIST OF TABLES

ACKNOWLEDGEMENTS

It has been six years since I began the doctoral program. When I look back at every moment, my life was full of reasons for gratitude. Most of all, I express my sincere thanks to my advisor, Professor Judy E. Kim. Her enthusiasm for and insight into science always inspires me. In addition to having scientific expertise, she is a good mentor who motivates me in research and teaching. She has always listened to my opinion with amazing patience and support whatever I need and has been open-minded about all issues. I am very happy to have her guidance as my wonderful role model.

I also deeply appreciate my committee, Professor Michael Tauber, Professor Douglas Magde, Professor Simpson Joseph, and Professor Douglas Smith, for all of their benevolent support.

I express my appreciation to all former Kim group members. I deeply appreciate Dr. Katheryn Sanchez, Dr. Diana Schlamadinger, Dr. Hannah Shafaat, Dr. Vanessa Oklejas, Cyril Gary, and Bethany Larson Berg for all of the technical and emotional support and for being wonderful labmates. I am also very grateful to the present Kim group members for their generous support and cooperation. Ignacio López-Peña, Deeann Asamoto, Jen Daluz, and Justine Liang – I will miss the three o'clock coffee break a lot. In particular, I thank Dr. Brian Leigh, who always helped me regardless of whether the problem was scientific or non-scientific. I also want to say thank you so much to the outstanding undergraduates who work with me – Weihan Cao, Saajan Bhakta, Eric Y. Kim, and Ivan Kozachenko.

I extend my thanks to Dr. Sangho Park for his assistance in performing nanodiscs experiments. I also want to express my sincere thanks to Martha Stacklin for her strong support in developing English skills and fierceness. I am grateful to my previous advisor for my master degree, Professor Sihyun Ham, who kept encouraging me to study and stimulated my intellectual curiosity in science. I am very appreciative of the generous support of the ARCS Foundation and the Reuben H. Fleet Foundation.

Thanks to my family and friends, who always cheer me up. I thank my parents and sister, who always believed in me and encouraged me to step forward. I am thankful to my loving grandparents in heaven who gave me unstinting affection. I offer my thanks to all of my friends for filling me with refreshing energy. I cordially apologize for not being able to list all names here. I greatly appreciate my husband Sungje Byun for being an incredibly strong supporter of my life and my baby Heemang for being and doing the best.

I believe it may be karma to have met these people during my doctoral degree, and I sincerely appreciate all who offered me great kindness and warm support.

Chapter 3, in full, is a reprint of the material as it appears in Biochimica et Biophysica Acta (BBA) 1818, 2012, Kang, Guipeun; López-Peña, Ignacio; Oklejas, Vanessa; Gary, Cyril S.; Cao, Weihan; and Kim, Judy E. Elsevier S&T. The dissertation author was primary investigator and author of this paper.

Chapter 4, in part, is currently being prepared for submission for publication of the material. Kang, Guipeun; Asamoto, Deeann; and Kim, Judy E. The dissertation author was the primary investigator and author of this material.

Chapter 5, in part, is a reprint of the material as it appears in Encyclopedia of Analytical Chemistry, 2013, Kang, Guipeun; López-Peña, Ignacio; Bhakta, Saajan; Kim, Judy E. Wiley. The dissertation author was primary investigator and author of this paper. Sections 5.5.1 and 5.5.2 from the original publication focused on hydration, and these sections have been removed from Chapter 5 of this dissertation because previous group members were the lead researchers for hydration studies.

VITA

2006	Bachelor of Science, Sookmyung Women's University
2008	Master of Science, Sookmyung Women's University
2006-2008	Teaching Assistant, Sookmyung Women's University
2009-2010	Teaching Assistant, University of California, San Diego
2010-2013	Research Assistant, University of California, San Diego
2013-2015	Teaching Assistant, University of California, San Diego
2015	Doctor of Philosophy, University of California, San Diego

PUBLICATIONS

"Probing membrane protein structure and dynamics by fluorescence"
Guipeun Kang, Ignacio López-Peña, Saajan Bhakta, and Judy E. Kim ***Encylopedia of Analytical Chemistry,*** **2013** 1-21

"Förster resonance energy transfer as a probe of membrane protein folding"
Guipeun Kang, Ignacio López-Peña, Vanessa Oklejas, Cyril S. Gary, Weihan Cao, Judy E. Kim ***Biochimica et Biophysica Acta,*** **2012**, 1818, 154-161

"Tryptophan-Lipid Interactions in Membrane Protein Folding Probed by Ultraviolet Resonance Raman and Fluorescence Spectroscopy"
Katheryn M. Sanchez, Guipeun Kang, Beijing Wu, and Judy E. Kim ***Biophysical Journal,*** **2011,** 100, 2121-2130

"Structural and Thermodynamic Investigations on the Aggregation and Folding of Acylphosphatase by Molecular Dynamics Simulations and Solvation Free Energy Analysis"
Song-Ho Chong, Chewook Lee, Guipeun Kang, Mirae Park and Sihyun Ham ***Journal of the American Chemical Society,*** **2012**, 133, 7075-7083

"Tren-spaced rhodamine and pyrene fluorophores: Excimer modulation with metal ion complexation"
Min Hee Lee, Guipeun Kang, Sihyun Ham and Jong Seung Kim ***Supramolecular Chemistry,*** **2009**, *21. 135-141.*

"Ratiometry of monomer/excimer emission of dipyrenyl calix[4]arene in aqueous media"
Hyun Jung Kim, Duong Tuan Quang, Jooyeon Hong, Guipeun Kang, Sihyun Ham, and Jong Seung Kim ***Tetrahedron***, **2007**, 63, 10788-10792.

ABSTRACT OF THE DISSERTATION

Fluorescence and energy transfer studies of membrane protein folding

by

Guipeun Kang

Doctor of Philosophy in Chemistry

University of California, San Diego, 2015

Professor Judy E. Kim, Chair

Approximately 30 % of human genes encode for membrane proteins. Membrane proteins play important roles in cells as ion pumps, ligand receptors, and ion channels, and are targets for approximately 60 % of all therapeutic drugs. Despite their relevance in biology and biochemistry, membrane proteins account for only 1 % of the total number of reported protein structures (RCSB Protein Data Bank), and only 16 % of all protein

folding literature is related to membrane protein folding (literature search from 1990 – 2015, Web of Science). This dissertation presents spectroscopic studies of the *in vitro* folding mechanisms of outer membrane protein A (OmpA). Several optical tools are utilized, including circular dichroism (CD), tryptophan fluorescence, Förster resonance energy transfer (FRET), and ultraviolet resonance Raman (UVRR) spectroscopy. An improved method to determine free energies of unfolding of OmpA based on spectral decomposition is presented. Dynamics of OmpA folding in synthetic lipid bilayers of small unilamellar vesicles (SUVs) are investigated through studies of secondary and tertiary structures. CD and FRET data indicate that secondary and tertiary structures are formed within the first hour of folding, and strand extension and equilibration continues on a longer timescale. UVRR data complement the CD and FRET results, and reveal evolution of molecular interactions during folding. In particular, a tryptophan residue in the extra-vesicle portion of the pore (position 129) displays unusually intense Raman activity in the hydrogen-out-of-plane (HOOP) region. The increase in HOOP intensity is hypothesized to reflect perturbation of the indole ring electron density because of a nearby charged residue or hydroxyl group on neighboring threonine residue. More likely, hydrogen bonding of π electrons on tryptophan with hydroxyl group contributes to the overall stability in addition to hydrophobic contacts by neighboring hydrophobic residues. A relatively new folding environment of nanodiscs is also explored. Preliminary FRET and UVRR data show that OmpA folds and inserts into nanodiscs. Collectively, these measurements elucidate changes in secondary and tertiary structures as well as molecular interactions of tryptophan residues during membrane protein folding.

Chapter 1. Introduction

1.1 Membrane Protein Folding: An important, but challenging, topic of study

Membrane proteins play essential roles in cell membranes as transporter, receptor, channel, enzyme, and structural supporters of membranes. Hence, it is not surprising that the membrane protein family makes up ~ 60 % of current drug-targetable proteins.[1,2] Since membrane protein function is determined by the correlation between structure, dynamics, and environment, it is necessary to explore these fundamental aspects to understand disease-related malfunction of membrane proteins.[3]

Despite the biological and pharmaceutical importance of membrane proteins, there exists a gap between our knowledge of membrane proteins compared to soluble proteins. Since the first high-resolution structure of a soluble protein, myoglobin, was solved in 1960, it took 25 years to determine the first high-resolution structure of a membrane protein from photosynthetic reaction center of *Rhodopseudomonas viridis*.[4] While approximately 30 % of the human genes encode for membrane proteins,[5,6] less than 1 % of the 3-D structures of membrane proteins has been revealed over 100,000 of the total accessible protein structures in RCSB Protein Data Bank.[7,8]

Experimental difficulty is an obstacle to make faster progress in studies of membrane protein folding. First, membrane proteins are difficult to handle experimentally: they are hydrophobic, which makes them susceptible to aggregation, and the relatively low protein expression yields hamper progress. An additional challenge is that heterogeneous lipids are essential for the folding reaction and stabilization of the membrane protein. Membrane mimics, such as detergent micelles or liposomes, make *in*

vitro folding experiments for membrane proteins complicated. There are various factors that affect the kinetics of the folding process and the thermodynamic stability of membrane proteins. For example, the ratio of membrane protein to lipids is one of the determinants of folding kinetics,[9] and the carbon chain length and saturation level of the hydrocarbon tail impact the stability of membrane proteins.[10] Despite these challenges, membrane proteins are still vital and intriguing systems to explore as potential therapeutic targets. Significant efforts have been devoted to achieve a big picture of membrane protein folding for decades, but still there remain many unknown pieces. In this chapter, I will focus on previous achievements on membrane protein folding and theoretical backgrounds for application to climb "on the shoulders of Giants".

1.2 Membrane protein structural motifs and its folding mechanism

A cell envelope of gram-negative bacteria such as *E.coli* consists of an inner membrane and an outer membrane where the composition of lipids and the constituted proteins are different. In contrast to the symmetric inner membrane composed of phospholipids, the outer membrane contains phospholipids in the inner leaflet and lipopolysaccharide (LPS) in the outer leaflet. In addition, embedded integral membrane proteins have different structural motifs depending on where they are found: α-helix bundles reside in the inner membrane, and β-barrel structures are found in the outer membrane, as shown in Figure 1.1. Outer membrane proteins are less hydrophobic than inner membrane proteins due to the smaller number of hydrophobic residues, and this distribution enables outer membrane proteins secreted from the cytoplasm to cross the cytoplasmic membrane and reach the outer membrane.[11,12]

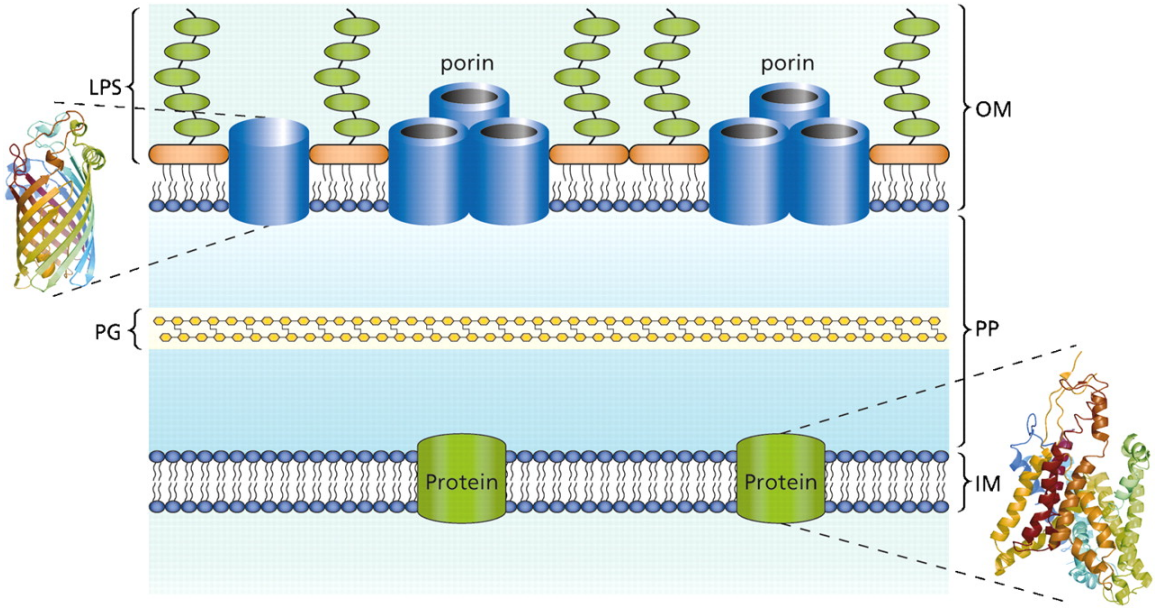

Figure 1.1 Structure of the Gram-negative bacterial cell envelope. Outer membrane (OM) contains phospholipids in the inner leaflet and LPS in the outer leaflet of the bilayer. β-barrel outer membrane proteins are located in OM. Inner membrane (IM) has symmetric leaflets containing phospholipids and α-helical membrane proteins. The peptidoglycan layer (PG) is located in the periplasmic region (PP). Figure is taken from reference.[12]

Different folding models have been proposed for α-helical bundles and β-barrel membrane proteins based on a two-stage model and a concerted mechanism, respectively. Popot and Engelman initially proposed the two-stage model for α-helical membrane proteins.[13] The first stage is formation of independent helices driven by hydrophobic interactions and backbone hydrogen bonds that form while inserting into the bilayer. The second stage is formation of helix-helix interactions to form tertiary and quaternary structures. A schematic of this two-stage model is depicted in Figure 1.2. The two-stage model successfully explained the experimental data for folding of α-helical segments of bacteriorhodopsin.[14] Recently, a three-stage model was suggested for helical systems, where the third state involved addition of internal polypeptide or a prosthetic group in a partitioning step following the second stage.[15]

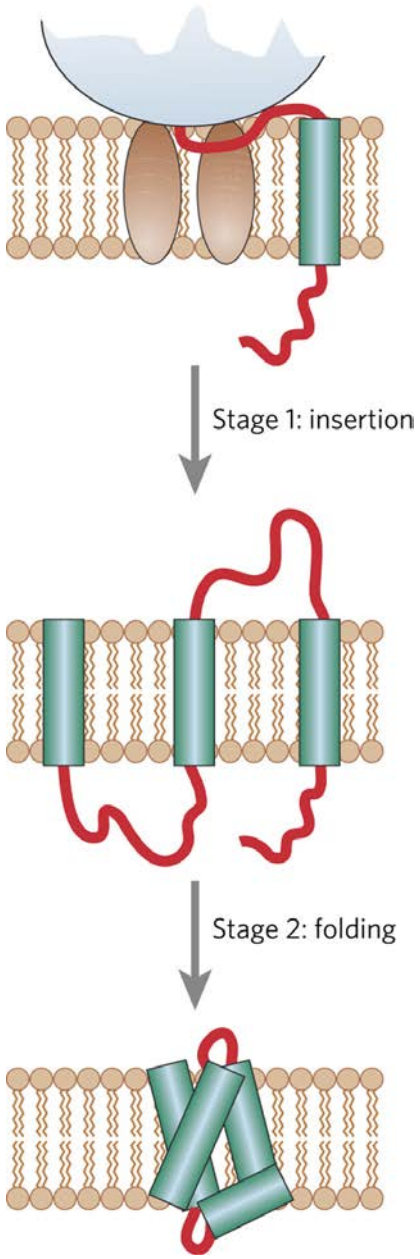

Figure 1.2 Schematic diagram for two-stage model of α-helical membrane protein folding. Figure is taken from reference.[16]

As opposed to the two-stage or three-stage models of α-helical bundles, β-barrels are known to fold and insert into lipid bilayer following a concerted folding mechanism.[17,18] While helices form internal backbone hydrogen bonds as a stable structure in the lipids and then develop tertiary structure between helices, β-barrels develop secondary and tertiary structures in a concerted manner through inter-strand hydrogen bonding networks.[9] This folding mechanism coupled with the insertion process was supported by extensive experiments of SDS-polyacrylamide gel electrophoresis (PAGE) and fluorescence spectroscopy, and these experiments revealed kinetically distinguished stages.[17,19] It has been proposed that OmpA assembles into preformed vesicles from soluble unfolded state (U) to the native refolded state (N) through three intermediate stages where OmpA first forms the misfolded configuration in water (I_W) by collapse. This misfolded intermediate may become an insoluble and irreversible aggregate (A), or it may interact with the membrane as a membrane-bound state (I_{M1}). This membrane-bound state then becomes a partially inserted state (I_{M2}) as shown in Figure 1.3. Throughout the dissertation, I will focus on utilizing spectroscopic techniques to probe the folding mechanism.

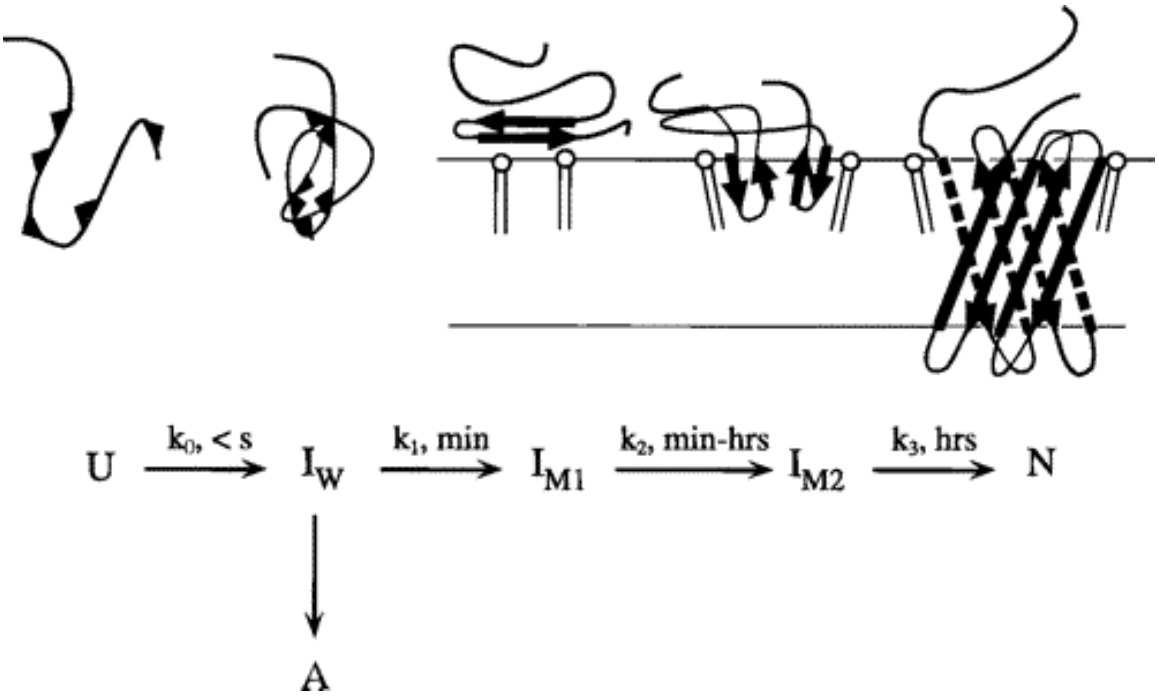

Figure 1.3 Schematic diagram for concerted mechanism of β-barrel integral membrane protein. Figure is taken from reference.[17]

1.3 Model membrane protein: Outer membrane protein A (OmpA)

The β-barrel membrane proteins consisting of 8 to 22 β-strands are found at the outer membrane of Gram-negative bacteria, chloroplasts, and mitochondria.[20,21] Here, the smallest outer membrane protein, Outer membrane protein A (OmpA) is chosen to investigate the folding mechanism. As one of the most abundant outer membrane proteins from *Escherichia coli*, OmpA serves as a bacteriophage receptor and a supporter of cell stability through physical linkage between peripheral domain and peptidoglycan.[11,22-24] OmpA not only provides these vital functions for the bacteria, but the protein also serves as a good model to study folding dynamics for several reasons. First, high resolution structures of OmpA have been revealed by X-ray crystallography[25,26] and nuclear magnetic resonance (NMR) spectroscopy.[27] These native-like structures are able to guide mutational studies and also help interpret experimental results. The eight antiparallel stranded protein forms a β-barrel monomer with 325 amino acids comprised of two domains: a transmembrane domain of ~ 171 residues incorporated in the bilayer, and a C-terminus peripheral domain of ~ 154 residues exposed to the periplasmic space. Second, OmpA spontaneously refolds and inserts into preformed lipid bilayers without the aid of detergent.[28] OmpA solubilized in 8 M urea solution refolds into detergent micelles or vesicles upon dilution of urea.[19,28-30] OmpA is also robust in terms of mutations in the N-terminal domain.[31] A final, but very important, benefit is that there are five tryptophan residues embedded in the interfacial region as shown in Figure 1.4. Tryptophan residues provide valuable information about the microenvironment near the indole side chain and structural changes during assembly, and can be interrogated by spectroscopic techniques such as fluorescence spectroscopy.

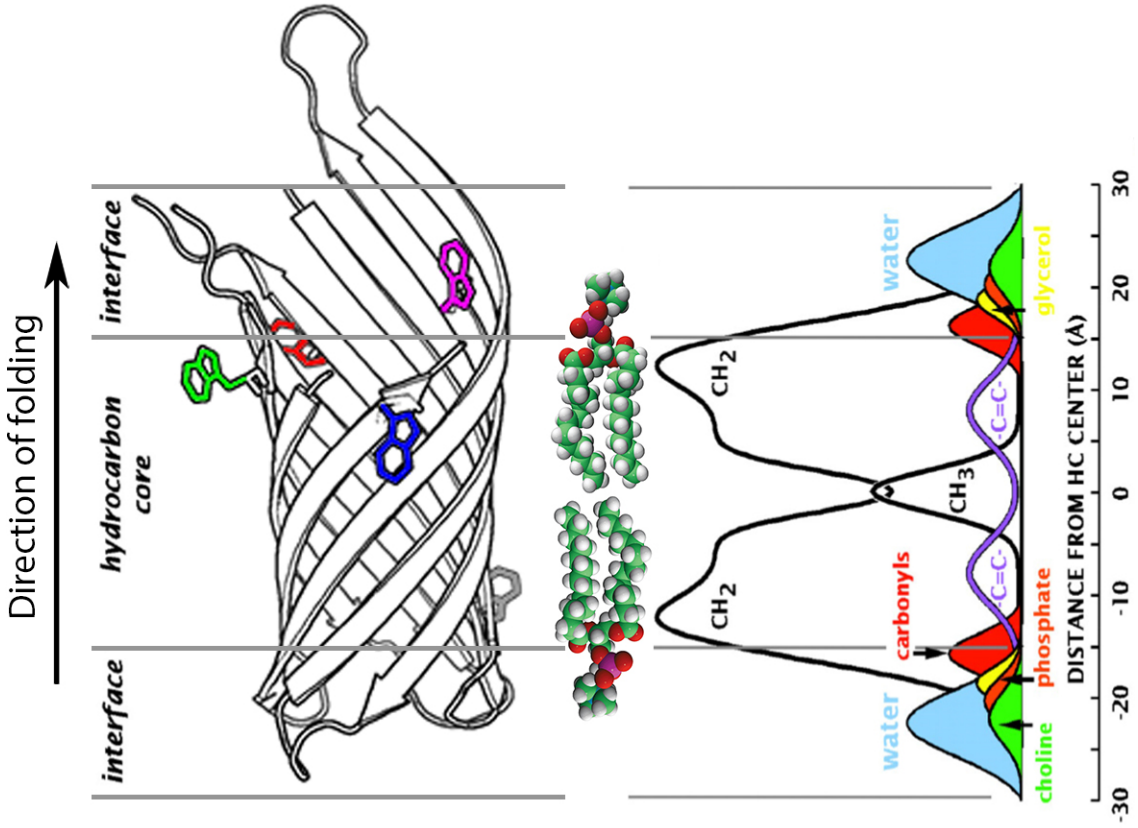

Figure 1.4 OmpA crystal structure (PDB: 1QJP) and experimental distribution of functional groups of a fluid lipid bilayer. Lipid models are from the Avanti Lipids website (www.avantilipids.com). OmpA refolds and inserts in an oriented manner in the presence of lipid bilayer, and five native tryptophan residues on OmpA are located at the lipid/water interface region. The figure on the right side shows the heterogeneous composition of phospholipids from reference.[32]

1.4 Photophysics of tryptophan in membrane proteins

The prevalence of tryptophan in membrane proteins is about twice what it is in soluble proteins[33,34], and this prevalence can be largely attributed to the co-existence of the hydrophobic indole side chain, and the heteroatom that is able to form hydrogen bonds.[35] The amphipathic characteristics enable tryptophan residues to play critical roles in anchoring the protein on the membrane[36,37], in stabilizing membrane proteins[38-40], and in minimizing hydrophobic mismatch.[41,42] Additionally, the indole side chain is a sensitive probe in biological systems to report conformational changes and molecular interactions.[43] For example, tryptophan emission of OmpA is sensitive to the polarity of the local environment near the indole group, and this property enables the emission spectrum to reflect conformational changes of the protein as shown in Figure 1.5.

There are two nearly-degenerate excited states in tryptophan that exhibit different sensitivities to polarity. These states are indicated ^1L_a or ^1L_b, and the transition moments are oriented perpendicular to each other (see Figure 1.5).[44,45] The ^1L_a and ^1L_b states absorb near 250-300 nm by $\pi \rightarrow \pi^*$ transitions. The ^1L_a transition moment is aligned through the nitrogen and hydrogen atoms on the pyrrole, which makes this state sensitive to polarity and hydrogen bonding. In most cases, therefore, emission of tryptophan in proteins results from this solvent-sensitive ^1L_a state. The sensitivity of tryptophan fluorescence to the environment makes this non-abundant residue a valuable probe to detect changes in structure and molecular interactions.

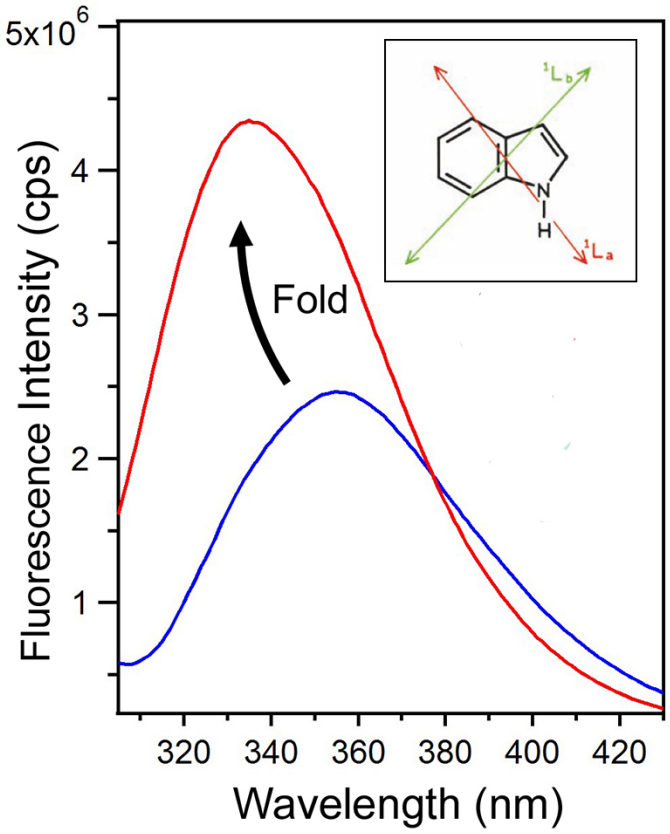

Figure 1.5 Emission spectra of OmpA in different environments: unfolded OmpA at 8 M urea solution (blue) and fully folded OmpA inserted in preformed, aqueous DMPC vesicles (red). The inset indicates the electronic transitions, ^1L_a and ^1L_b state, of tryptophan from reference.[44]

In β-barrel membrane proteins, tryptophan is localized at the water-bilayer interface, and typically points towards the lipid.[46] In, OmpA, there are five tryptophan residues, with four pointing towards the lipid at positions 7, 15, 57, and 143, and a single tryptophan facing the interior of the pore at position 102. In this dissertation, these tryptophan and other residues on OmpA were mutated to obtain site-selective information of local environment. Before discussing our work on OmpA, I would like to briefly mention a relevant experiment based on a fluorescence technique that was used to support the concerted folding mechanism of OmpA.

As discussed in chapter 1.2, the concerted folding mechanism for β-barrel membrane proteins is accepted as the primary path. Kleinschmidt *et al*. used time-resolved distance determinations by fluorescence quenching (TDFQ) to monitor the folding pathway of OmpA.[18,47] The TDFQ method facilitated real time measurements for translocation of tryptophan residues through the bilayer by utilizing brominated lipids as the fluorescence quencher. This experiment enabled characterization of the intermediate stages during OmpA folding and insertion into preformed lipid bilayer. To track site-specific relocation of tryptophan residues, the TDFQ experiment focused on single tryptophan OmpA residues at positions 15, 57, 102, and 143, located in the interior of the vesicle, and at position 7, located in the extra-vesicle region. As reminder, OmpA folds directionally, with positions 15, 57, 102, and 143 entering the lipid bilayer before position 7. The data suggested a concerted folding mechanism of OmpA. In 2002, Kleinschmidt *et al*. also proposed that the formation of secondary structure and tertiary structure were coupled during refolding into the lipid bilayer, and took place after tryptophan residues inserted into the lipid bilayer.[9]

Although significant understanding has been achieved, there still remains a fundamental question about how OmpA develops tertiary structure during folding. To investigate the structural dynamics in real time, Förster resonance energy transfer (FRET) technique is applied to OmpA during folding. As a first attempt to utilize FRET on OmpA, these experimental results could contribute to answer questions for membrane protein folding, and to supplement the applicable techniques for membrane proteins.

1.5 Förster resonance energy transfer (FRET) technique

In 1948, Förster proposed a theory that the probability of energy transfer depends upon the inverse sixth power of the distance between donor and acceptor.[48,49] This energy transfer occurs from an electronically excited state of a donor to a ground state acceptor through long-range dipole-dipole interactions. The energy transfer arises solely from a non-radiative process, and not from reabsorption of a photon or a collisional process (Figure 1.6).

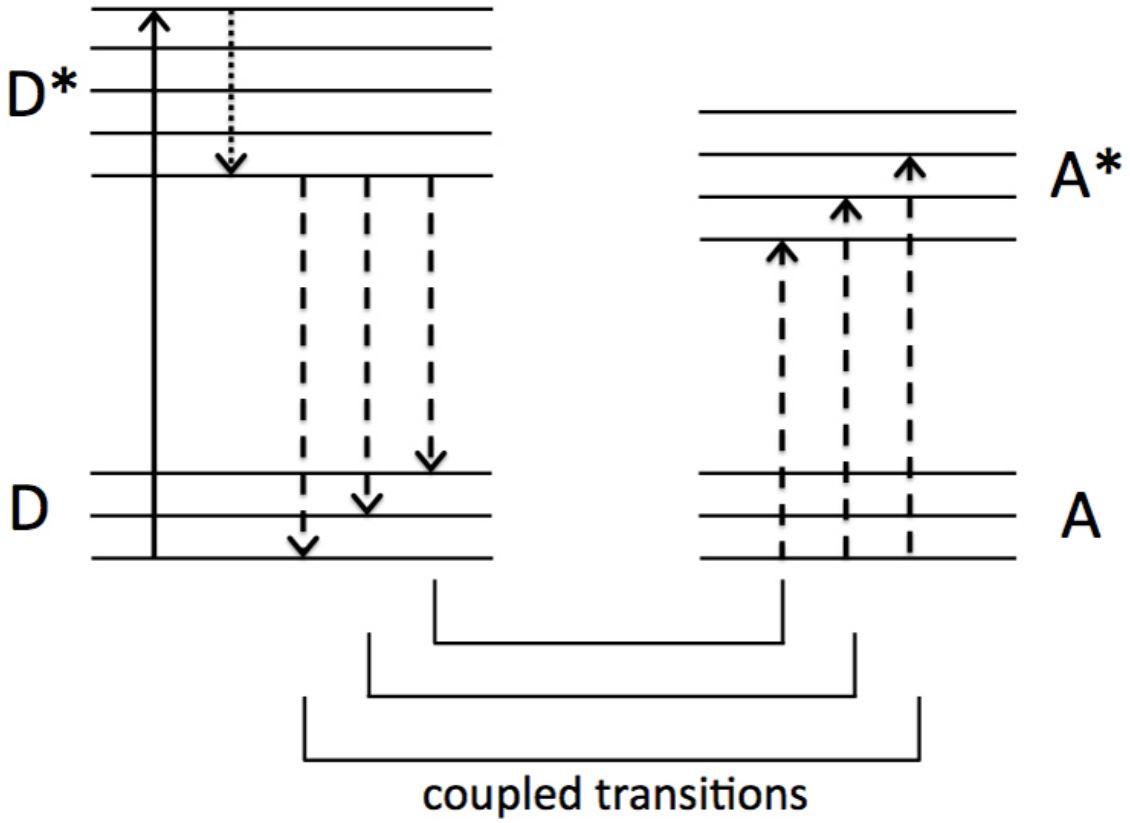

Figure 1.6 Schematic of energy transfer from the excited state of donor (D) to the ground state of acceptor (A). Radiative transition (solid), non-radiative transitions (dotted), energy transfer (dashed). Image adapted from reference.[49]

The transfer rate from donor to acceptor is given by Equation 1.1,

$$k_T = \frac{1}{\tau_D}\left(\frac{R_0}{r}\right)^6 \qquad 1.1$$

where τ_D is the donor excited state lifetime in the absence of acceptor, R_0 is Förster distance and r is the separation between donor and acceptor. This equation shows explicitly that the energy transfer rate is inversely proportional to sixth power of the distance. Förster distance, which is the distance at which the transfer efficiency is 50 %, is calculated as follows:

$$R_0^6 = 8.79 \times 10^{23}\left(\kappa^2 n^{-4} Q_D J(\lambda)\right) \quad (in\ \text{Å}^6) \qquad 1.2$$

where κ^2 is the orientation factor, *n* is the refractive index, Q_D is the quantum yield of donor in the absence of acceptor, and $J(\lambda)$ is the spectral overlap between emission of donor and absorption of acceptor chromophore. When one assumes isotropic motion within the excited-state lifetime, the orientation factor of 2/3 is conventionally used.[50] The refractive index and the quantum yield are typically fixed at appropriate values according to the system. The spectral properties of donor and acceptor are important to determine the Förster distance, and a wide selection of FRET-pairs covers most biological dynamics of interest.[44]

The rate of energy transfer can be interpreted in terms of a transfer efficiency (*E*), which is dependent on the separation (r) between donor and acceptor where the sensitive range of r lies between $0.5R_0$ and $1.5R_0$. The transfer efficiency can be calculated by donor fluorescence intensity in the presence and absence of acceptor, F_{DA} and F_D, respectively.[50] The labeling efficiency of the acceptor molecule, f_A, has to be taken into

account in the calculation of transfer efficiency to avoid misleading interpretation as shown in Equation 1.3.

$$E = \frac{R_0^6}{R_0^6 + r^6} = \left(1 - \frac{F_{DA} - F_D(1 - f_A)}{F_D f_A}\right) = \left(1 - \frac{F_{DA}}{F_D}\right)\frac{1}{f_A} \qquad 1.3$$

In 1967, Stryer and Haugland performed an experimental study by adopting poly-(L-proline)$_n$ oligomers (n = 5 - 12) in *trans* type II helix conformation as a "spectroscopic ruler".[51] They observed that transfer efficiency was dependent on distance by inserting proline spacers between donor and acceptor molecules that were covalently attached to each end of the peptides. Since this initial study by Stryer and Haugland, FRET has been widely used as a nanoscale "ruler" to shed light on the structural and dynamic information of biomolecular systems. FRET technique is sensitive to changes in conformation or environment by measurements of fluorescence intensity or lifetime. In addition, the applicable range of FRET is 10 – 100 Å, which corresponds to the range biomolecular structural changes. Lastly, FRET technique is a versatile method to combine with other spectroscopic instrumentation such as single molecule measurements.[52]

Here, we use the FRET technique for the membrane protein, OmpA. This protein is a good model system because it is well known that OmpA spontaneously folds and inserts into synthetic lipid bilayer. Furthermore, five intrinsic fluorophores, tryptophan, are naturally located at the water-bilayer interface region, which allows us to gain site-specific information about the surrounding environment from these native residues. One well studied FRET pair, tryptophan and 1,5-IAEDANS, has Förster distance of 24 Å, resulting in a useable FRET range between 12 Å ($0.5R_0$) and 36 Å ($1.5R_0$). Significant

advancements on optical instrumentation and on dye synthesis enable the FRET technique to become even more promising especially for biological systems that only limited approaches can access through *in vitro* and *in vivo* experiments.

1.6 Thesis overview

This dissertation focuses on two topics: 1) formation of secondary and tertiary structures during membrane protein folding by electronic spectroscopy and 2) molecular interactions during folding by vibrational spectroscopy. I describe our efforts to apply the FRET technique to OmpA. Chapter 2 describes detailed experimental procedures regarding the production of genetically engineered OmpA variants and membrane mimicking system for *in vitro* folding studies. Chapter 2 also includes the description of the spectroscopic tools utilized in experiments. Conformational dynamics of OmpA were investigated at different *in vitro* folding conditions by utilizing FRET, and are discussed in chapters 3 and 4. In chapter 5, practical applications in fluorescence are discussed for characterization of membrane proteins, such as thermodynamic stability by monitoring the spectroscopic parameters of tryptophan fluorescence. A new method was developed to improve the calculations of thermodynamic stability for membrane protein. Lastly, a future direction for experiments is suggested in chapter 6 to explore membrane protein dynamics by utilizing a different membrane system.

1.7 References

(1) Arinaminpathy, Y.; Khurana, E.; Engelman, D. M.; Gerstein, M. B. *Drug Discov Today* **2009**, *14*, 1130.

(2) Bakheet, T. M.; Doig, A. J. *Bioinformatics* **2009**, *25*, 451.

(3) Sachs, J. N.; Engelman, D. M. *Annu Rev Biochem* **2006**, *75*, 707.

(4) Deisenhofer, J.; Epp, O.; Miki, K.; Huber, R.; Michel, H. *Nature* **1985**, *318*, 618.

(5) Fagerberg, L.; Jonasson, K.; von Heijne, G.; Uhlen, M.; Berglund, L. *Proteomics* **2010**, *10*, 1141.

(6) Ahram, M.; Litou, Z. I.; Fang, R.; Al-Tawallbeh, G. *In silico biology* **2006**, *6*, 379.

(7) White, S. H. **Accessed 11 April 2015**.

(8) Berman, H. M.; Westbrook, J.; Feng, Z.; Gilliland, G.; Bhat, T. N.; Weissig, H.; Shindyalov, I. N.; Bourne, P. E. *Nucleic Acids Research* **2000**, *28*, 235.

(9) Kleinschmidt, J. H.; Tamm, L. K. *J. Mol. Biol.* **2002**, *324*, 319.

(10) Hong, H.; Tamm, L. K. *Proc. Natl. Acad. Sci. USA* **2004**, *101*, 4065.

(11) Koebnik, R.; Locher, K. P.; Van Gelder, P. *Molecular microbiology* **2000**, *37*, 239.

(12) Tommassen, J. *Microbiology-Sgm* **2010**, *156*, 2587.

(13) Popot, J. L.; Engelman, D. M. *Biochemistry* **1990**, *29*, 4031.

(14) Kahn, T. W.; Engelman, D. M. *Biochemistry* **1992**, *31*, 6144.

(15) Engelman, D. M.; Chen, Y.; Chin, C. N.; Curran, A. R.; Dixon, A. M.; Dupuy, A. D.; Lee, A. S.; Lehnert, U.; Matthews, E. E.; Reshetnyak, Y. K.; Senes, A.; Popot, J. L. *FEBS Lett* **2003**, *555*, 122.

(16) Bowie, J. U. *Nature* **2005**, *438*, 581.

(17) Kleinschmidt, J. H.; Tamm, L. K. *Biochemistry* **1996**, *35*, 12993.

(18) Kleinschmidt, J. H.; den Blaauwen, T.; Driessen, A. J. M.; Tamm, L. K. *Biochemistry* **1999**, *38*, 5006.

(19) Surrey, T.; Jahnig, F. *J Biol Chem* **1995**, *270*, 28199.

(20) Schulz, G. E. *Current Opinion in Structural Biology* **2000**, *10*, 443.

(21) Wimley, W. C. *Curr Opin Struct Biol* **2003**, *13*, 404.

(22) Morona, R.; Klose, M.; Henning, U. *J Bacteriol* **1984**, *159*, 570.

(23) Wang, Y. *Biochem. Bioph. Res. Comm.* **2002**, *292*, 396.

(24) Park, J. S.; Lee, W. C.; Yeo, K. J.; Ryu, K. S.; Kumarasiri, M.; Hesek, D.; Lee, M.; Mobashery, S.; Song, J. H.; Kim, S. I.; Lee, J. C.; Cheong, C.; Jeon, Y. H.; Kim, H. Y. *FASEB journal : official publication of the Federation of American Societies for Experimental Biology* **2012**, *26*, 219.

(25) Grigorieff, N.; Ceska, T. A.; Downing, K. H.; Baldwin, J. M.; Henderson, R. *J Mol Biol* **1996**, *259*, 393.

(26) Pautsch, A.; Schulz, G. E. *Nature Structural Biology* **1998**, *5*, 1013.

(27) Arora, A.; Abildgaard, F.; Bushweller, J. H.; Tamm, L. K. *Nat. Struct. Biol.* **2001**, *8*, 334.

(28) Surrey, T.; Jahnig, F. *Proc. Natl. Acad. Sci. USA* **1992**, *89*, 7457.

(29) Kleinschmidt, J. H.; Wiener, M. C.; Tamm, L. K. *Protein Sci* **1999**, *8*, 2065.

(30) Schweizer, M.; Hindennach, I.; Garten, W.; Henning, U. *European journal of biochemistry / FEBS* **1978**, *82*, 211.

(31) Koebnik, R. *J Mol Biol* **1999**, *285*, 1801.

(32) White, S. H.; Ladokhin, A. S.; Jayasinghe, S.; Hristova, K. *J Biol Chem* **2001**, *276*, 32395.

(33) Schiffer, M.; Chang, C. H.; Stevens, F. *Protein Eng.* **1992**, *5*, 213.

(34) von Heijne, G. *Embo J* **1986**, *5*, 3021.

(35) Killian, J. A.; von Heijne, G. *Trends Biochem. Sci.* **2000**, *25*, 429.

(36) de Planque, M. R. R.; Kruijtzer, J. A. W.; Liskamp, R. M. J.; Marsh, D.; Greathouse, D. V.; Koeppe, R. E.; de Kruijff, B.; Killian, J. A. *J Biol Chem* **1999**, *274*, 20839.

(37) de Planque, M. R. R.; Bonev, B. B.; Demmers, J. A. A.; Greathouse, D. V.; Koeppe, R. E.; Separovic, F.; Watts, A.; Killian, J. A. *Biochemistry* **2003**, *42*, 5341.

(38) Sanchez, K. M.; Gable, J. E.; Schlamadinger, D. E.; Kim, J. E. *Biochemistry* **2008**, *47*, 12844.

(39) Sanchez, K. M.; Kang, G. P.; Wu, B. J.; Kim, J. E. *Biophys. J.* **2011**, *100*, 2121.

(40) Hong, H.; Park, S.; Jiménez, R. H. F.; Rinehart, D.; Tamm, L. K. *J. Am. Chem. Soc.* **2007**, *129*, 8320.

(41) de Planque, M. R. R.; Killian, J. A. *Mol Membr Biol* **2003**, *20*, 271.

(42) Petrache, H. I.; Zuckerman, D. M.; Sachs, J. N.; Killian, J. A.; Koeppe, R. E.; Woolf, T. B. *Langmuir* **2002**, *18*, 1340.

(43) Vivian, J. T.; Callis, P. R. *Biophys. J.* **2001**, *80*, 2093.

(44) Lakowicz, J. R. *Springer: New York* **2006**.

(45) Callis, P. R. *Method Enzymol* **1997**, *278*, 113.

(46) Wimley, W. C. *Protein Sci* **2002**, *11*, 301.

(47) Kleinschmidt, J. H.; Tamm, L. K. *Biochemistry* **1999**, *38*, 4996.

(48) Förster, T. *Ann Phys-Berlin* **1948**, *2*, 55.

(49) Forster, T. *Discuss Faraday Soc* **1959**, 7.

(50) dosRemedios, C. G.; Moens, P. D. J. *J. Struct. Biol.* **1995**, *115*, 175.

(51) Stryer, L.; Haugland, R. P. *Proc Natl Acad Sci U S A* **1967**, *58*, 719.

(52) Sahoo, H. *J Photoch Photobio C* **2011**, *12*, 20.

Chapter 2. Methods

2.1 Expression, isolation and purification of OmpA variants

The procedure for the expression, isolation, and purification of OmpA was performed as described in previous reports;[1] this procedure was originally adapted and modified from Surrey *et al*.[2,3] The standard operating procedure for OmpA growth was established by Dr. Katheryn Sanchez.[4] Figure 2.1 briefly describes a series of sequential steps for the preparation of a pure OmpA sample. Herein, I focus on the protocol for producing the transmembrane domain OmpA variants that were used for the experiments.

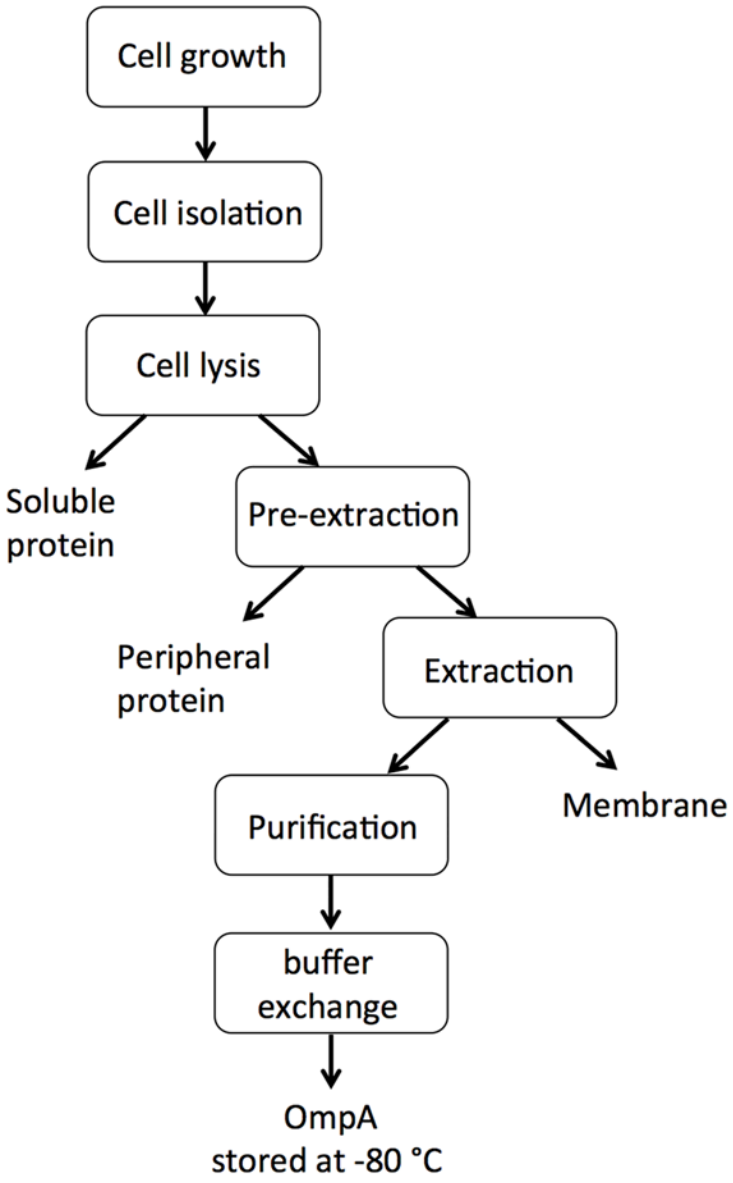

Figure 2.1 Schematic diagram for the expression, isolation, and purification of OmpA.

The *E.coli* JF733 strain lacking OmpA and OmpF (Genetic Stock Center, Yale University) was used to overexpress OmpA mutants. Cell growth was initiated from the frozen OmpA stock mixed with LB and glycerol. The growing cells in the log phase in a culture tube were spread on an agar/ampicillin plate and kept in a 37 °C incubator. Once colonies formed (approximately 12-15 hours), the plate was moved to a 4 °C fridge to prevent overgrowth, and used within 1 week. From the plate, a single colony was selected and used to inoculate 300 mL of sterile LB media containing 0.5 % glucose, 0.05 mg/mL ampicillin, and 0.17 M NaCl at 37 °C for overnight growth. An aluminum foil cap was sufficiently loose to allow air circulation during shaking at 180 rpm. The next morning, the absorbance at 600 nm was recorded, and the cells were transferred into two 250 mL sterilized centrifuge bottles and pelleted by centrifugation. The cell pellet was washed twice with fresh LB/ampicillin media and resuspended in ~ 20 mL of LB/ampicillin solution. The cell resuspension was evenly distributed into six 1 L flasks of LB media followed by injection of 1 mL of 1 M isopropyl β-D-thiogalactoside (IPTG) to each flask to overexpress the protein. The six flasks were placed in a shaker at 37 °C and were shaken at 180 rpm until the OD_{600} was approximately 1 or slightly greater than 1. When reaching this point, the cells were harvested by centrifugation at 6000 rpm for 10 minutes repeatedly until the entire 6 L cell solution was pelleted. The pellet was washed with 10 mM Tris-HCl buffer twice and weighed. The wet cell obtained from a 6 L batch was ~ 10-15 g depending on the mutant type and was stored in a –80 °C freezer until it was ready for cell lysis.

The cells were lysed in order to collect the membrane proteins. For cell lysis, the cells were defrosted in an ice bath with stirring for 2-3 hours. The muddy cells were

dissolved by the addition of 55 mL of cold 0.75 M sucrose/10 mM Tris-HCl buffer and 55 mL of cold 20 mM EDTA/0.5 mg/mL lysozyme solution. Next, 1 mL of 100 mM PMSF in isopropanol was injected carefully and continuously stirred for 1 hour. (For convenience, a 10 mL stock solution of 100 mM PMSF solution was stored in a 4 °C fridge in a secondary container, and 1 mL was pulled from this stock solution as needed.) The cells in the ice bath were completely lysed by sonication using a ½" horn tip for 5 minutes at a 50 % duty cycle with 70 % maximum amplitude. The tip should be dipped in the solution, but the immersion depth should be carefully adjusted so that the tip does not touch the centrifuge bottle. The sonicated solution was centrifuged at 5000 rpm for 15 minutes to remove residual unlysed cells. The supernatant was spun down at 17,000 rpm for 90 minutes, resulting in a brownish-red pellet and yellowish transparent supernatant that contains soluble protein. The pellet contains membrane proteins, including OmpA.

OmpA was further isolated from the other membrane proteins. In the pre-extraction step, the brownish-red pellet of membrane proteins was fully dissolved in 3.5 M urea/20 mM Tris-HCl/0.05 % 2-mercaptoethanol (2-ME) solution (pH 9), and the color of the solution became transparent light brown. Once dissolved, the solution was spun down at 17,000 rpm for 2 hours, and this process separated the solution into a supernatant containing peripheral membrane proteins, and a pellet containing OmpA and membrane fragments. Afterward, the pellet was suspended in 70 mL of a 1:1 mixture of an extraction buffer (8 M urea/20 mM Tris-HCl/0.1 % 2-ME, pH 8.5) and isopropanol. Centrifugation of the solution at 17,000 rpm for 1.5 hours resulted in crude OmpA in the supernatant.

Anion exchange chromatography with a HiTrap Q Sepharose Fast Flow (GE Healthcare) was used to purify the crude OmpA solution. The column was equilibrated with buffer A (8 M urea/15 mM Tris-HCl/0.05 % 2-ME, pH 8.5) prior to injection of the protein. After the crude OmpA solution was loaded, the NaCl concentration was linearly increased from 0 to 200 mM by the addition of buffer B (8 M urea/15 mM Tris-HCl/0.05 % 2-ME/200 mM NaCl, pH 8.5). The eluted OmpA was collected in 2 mL glass test tubes. The fractions containing OmpA were identified by measuring the absorption spectra. Additionally, SDS-polyacrylamide gel electrophoresis (PAGE) was optionally utilized to confirm the purity of OmpA. The fractions containing purified OmpA were combined for desalting, and the solution was changed to the concentration buffer (8 M urea/20 mM KPi, pH 7.3). The purified OmpA solution was concentrated using Amicon ultrafiltration (PM-10 or YM-10 for full-length OmpA and YM-3 for truncated OmpA), and the protein stock (200 – 300 μM) was stored at –80 °C for further experiments.

2.2 Site-directed mutagenesis and dye conjugation to OmpA

Site-directed mutagenesis was performed on the plasmid pET1102 to obtain the following OmpA mutants using a QuickChange II site-directed mutagenesis kit (Agilent technologies): (1) single tryptophan OmpA variants where tryptophan was placed at one of the native tryptophan positions (7, 15, 57, 102, or 143), or at a non-native position (Y129 and F170) for the full-length OmpA as well as its transmembrane (TM), truncated domain where the periplasmic portion was removed. (To distinguish TM, truncated OmpA mutants from full-length OmpA variants, the Greek symbol Δ is added to the end of the mutant name for truncated variants), (2) single tryptophan and single cysteine OmpA mutants where a tryptophan residue was located at one of the positions 15, 57,

129, or 143, and a cysteine residue was placed at one of the positions 7 or 57 on the TM, truncated domain OmpA, and (3) single cysteine OmpA variants where the cysteine residue was encoded at one of the positions 7 or 57 on the TM, truncated domain OmpA. The reason cysteine residues were placed on the TM domain of OmpA was because there are no native cysteine residues in the TM portion, whereas there are two essential cysteine residues in the soluble tail. Polymerase chain reaction (PCR) was used to generate modified DNA from the original DNA template and the DNA primer, and the PCR products were sequenced before transformation into the propagating cell strain (XL1-Blue competent cells). After sequencing, DNA that was extracted using QIAprep spin miniprep kit (Qiagen) was transformed into the JF733 cell strain to generate a cell stock of OmpA mutants. The DNA sequence of wild-type OmpA is shown in Figure 2.2, and shows the positions for the tryptophan and cysteine mutations, and the STOP codon to truncate the protein to eliminate the soluble domain. The nomenclature of the OmpA variants used in the experiments is tabulated in Tables 2.1 and 2.2.

1:GCT CCG AAA GAT AAC ACC TGG TAC ACT GGT GCC AAA CTG GGC TGG TCT CAG TAC

A_1 P K D N T W_7 Y T G A K L G W_{15} S Q Y

19: CAT GAC ACT GGT TTC ATC AAC AAC AAT GGC CCG ACC CAT GAA AAC CAA CTG GGC

H D T G F I N N N G P T H E N Q L G

37: GCT GGT GCT TTT GGT GGT TAC CAG GTT AAC CCG TAT GTT GGC TTT GAA ATG GGT

A G A F G G Y Q V N P Y V G F E Met G

55:TAC GAC TGG TTA GGT CGT ATG CCG TAC AAA GGC AGC GTT GAA AAC GGT GCA TAC

Y D W_{57} L G R Met P Y K G S V E N G A Y

73: AAA GCT CAG GGC GTT CAA CTG ACC GCT AAA CTG GGT TAC CCA ATC ACT GAC GAC

K A Q G V Q L T A K L G Y P I T D D

91: CTG GAC ATC TAC ACT CGT CTG GGT GGC ATG GTA TGG CGT GCC GAC ACT AAA TCC

L D I Y T R L G G Met V W_{102} R A D T K S

109:AAC GTA TAC GGT AAA AAC CAC GAC ACC GGC GTT TCT CCG GTC TTC GCT GGC GGT

N V Y G K N H D T G V S P V F A G G

127:GTT GAG TAC GCG ATC ACT CCT GAA ATC GCT ACC CGT CTA GAA TAC CAG TGG ACC

V E Y_{129} A I T P E I A T R L E Y Q W_{143} T

145:AAC AAC ATC GGT GAC GCA CAC ACC ATC GGC ACT CGT CCG GAC AAC GGC ATG CTG

N N I G D A H T I G T R P D N G Met L

163: AGC CTG GGT GTT TCC TAC CGT TTC GGT CAG GGC GAA GCA GCT CCA GTA GTT GCT

S L G V S Y R F_{170} G Q G E A A P_{177} V V A

181: CCG GCT CCA GCT CCG GCA CCG GAA GTA CAG ACC AAG CAC TTC ACT CTG AAG TCT

P A P A P A P E V Q T K H F T L K S

199:GAC GTT CTG TTC AAC TTC AAC AAA GCA ACC CTG AAA CCG GAA GGT CAG GCT GCT

D V L F N F N K A T L K P E G Q A A

217:CTG GAT CAG CTG TAC AGC CAG CTG AGC AAC CTG GAT CCG AAA GAC GGT TCC GTA

L D Q L Y S Q L S N L D P K D G S V

235:GTT GTT CTG GGT TAC ACC GAC CGC ATC GGT TCT GAC GCT TAC AAC CAG GGT CTG

V V L G Y T D R I G S D A Y N Q G L

253: TCC GAG CGC CGT GCT CAG TCT GTT GTT GAT TAC CTG ATC TCC AAA GGT ATC CCG

S E R R A Q S V V D Y L I S K G I P

271:GCA GAC AAG ATC TCC GCA CGT GGT ATG GGC GAA TCC AAC CCG GTT ACT GGC AAC

A D K I S A R G Met G E S N P V T G N

289:ACC TGT GAC AAC GTG AAA CAG CGT GCT GCA CTG ATC GAC TGC CTG GCT CCG GAT

T C D N V K Q R A A L I D C L A P D

307:CGT CGC GTA GAG ATC GAA GTT AAA GGT ATC AAA GAC GTT GTA ACT CAG CCG CAG

R R V E I E V K G I K D V V T Q P Q

325: GCT TAA

A_{325} Stop

Figure 2.2 DNA and the amino acid sequence of wild-type (WT) OmpA. WT OmpA has five native tryptophan residues (positions 7, 15, 57, 102, and 143) indicated in blue. Positions of additional mutations sites where tryptophan was incorporated are shown in green (positions 129 and 170). The positions of the cysteine for dye conjugation are underlined (7 and 57). The STOP codon is introduced at position 177 and shown in red; placement of this STOP codon results in TM OmpA (truncated) mutants where the soluble domain has been removed.

Table 2.1 Summary of the OmpA truncated variants for FRET experiments. The first column lists the name of the mutant. Donor (D) and acceptor (A) locations are indicated in the second and third columns, and the description of each mutant is included in the fourth column. Molar absorptivities are listed in the last column. 1,5-IAEDANS is the acceptor, and abbreviated as Dns. For all mutants that contain single-tryptophan residues or no trp residues, unwanted trp residues were mutated to phe. LY = dye labeling yield.

OmpA mutant	Donor (Trp)	Acceptor (Dns)	Description	Molar absorptivity, ε_{280} ($M^{-1}cm^{-1}$)
W15Δ	15	none	Donor-only	26,018
W57Δ	57	none	Donor-only	26,018
W129Δ	129	none	Donor-only	24,441
W143Δ	143	none	Donor-only	26,018
W15/F7CdnsΔ	15	7	D-A on same strand across bilayer	26,018+LY×1,192
W57/F7CdnsΔ	57	7	D-A across bilayer	26,018+LY×1,192
W143/F7CdnsΔ	143	7	D-A across bilayer	26,018+LY×1,192
W129/F57CdnsΔ	129	57	D-A across bilayer	24,441+LY×1,192
W129/F7CdnsΔ	129	7	D-A across pore	24,441+LY×1,192
W143/F57CdnsΔ	143	57	D-A across pore	26,018+LY×1,192
W0/F7CdnsΔ	none	7	Acceptor-only	20,501+LY×1,192
W0/F57CdnsΔ	none	57	Acceptor-only	20,501+LY×1,192
W0Δ	none	none	No donor, No acceptor	20,501

Table 2.2 Summary of OmpA variants. The first column lists the name of the OmpA mutant. Tryptophan locations are indicated in the second column, and the description of each mutant is included in the third column. Molar absorptivities are listed in the last column. FL = full length (325 residues), TM = transmembrane, truncated variant (176 residues). For all mutants that contain single-tryptophan residues or no trp residues, unwanted trp residues were mutated to phe.

OmpA variant	Trp locations	Description	ε_{280} ($M^{-1}cm^{-1}$)
WT	7,15,57,102,143	Native FL OmpA	54,394
W0	none	FL OmpA with no trp	26,809
W7	7	FL OmpA with single trp	32,326
W15	15	FL OmpA with single trp	32,326
W57	57	FL OmpA with single trp	32,326
W102	102	FL OmpA with single trp	32,326
W129	129	FL OmpA with single trp	30,749
W143	143	FL OmpA with single trp	32,326
W170	170	FL OmpA with single trp	32,326
WTΔ	7,15,57,102,143	TM OmpA with five native trp	48,086
W0Δ	none	TM OmpA with no trp	20,501
W7Δ	7	TM OmpA with single trp	26,018
W15Δ	15	TM OmpA with single trp	26,018
W57Δ	57	TM OmpA with single trp	26,018
W102Δ	102	TM OmpA with single trp	26,018
W129Δ	129	TM OmpA with single trp	24,441
W143Δ	143	TM OmpA with single trp	26,018
W170Δ	170	TM OmpA with single trp	26,018

For the cysteine-containing OmpA mutants, a dye molecule, 1,5-IAEDANS (5-((((2-iodoacetyl)amino)ethyl)amino)naphthalene-1-sulfonic acid, Molecular Probes), was conjugated at the cysteine residue. A schematic diagram for the conjugation reaction of 1,5-IAEDANS to the cysteine residue is provided in Figure 2.3. Specific dye labeling is enabled by selective reaction of 1,5-IAEDANS with the sulfhydryl group of the cysteine residue on TM OmpA mutants. Concentrated pure OmpA (50-100 μM in 8 M urea/20 mM KPi solution, pH 7.3) was initially mixed with a tenfold excess of a reducing agent, tris(2-carboxyethyl)phosphine (TCEP) (stock concentration of 10 mM), and stirred under nitrogen gas for 1 h. Lyophilized 1,5-IAEDANS powder (Molecular Probes) initially dissolved to 2–3 mM in dimethyl sulfoxide (DMSO) was then added to the protein solution to react with the cysteine residue at position 7 or 57 for approximately 5 h under nitrogen atmosphere in the dark. The reaction was quenched by the addition of tenfold excess 2-mercaptoethanol (2-ME) to consume excess thiol-reactive dye. Unreacted dye was separated from the protein by passing the sample down a desalting column (10-DG, Bio-Rad). The labeled OmpA sample was washed several times with fresh buffer (8 M urea/20 mM KPi, pH 7.3), concentrated by Amicon ultrafiltration, and finally stored at −80 °C for the further usage.

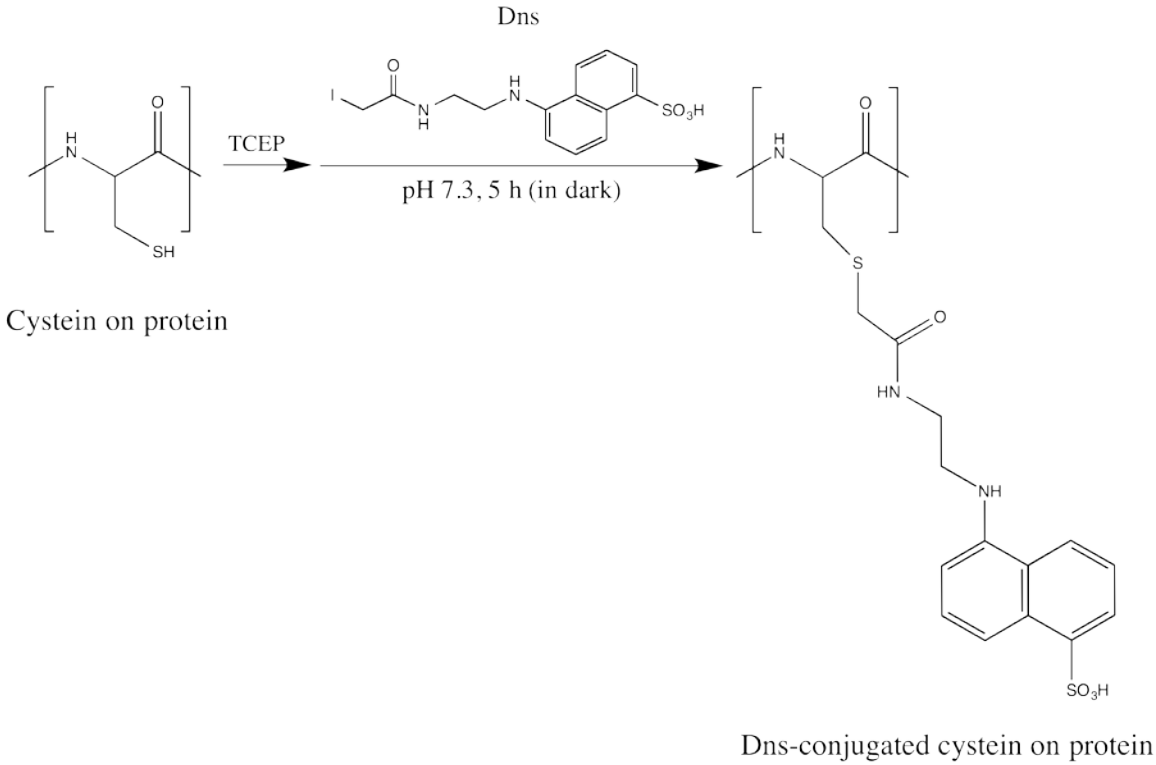

Figure 2.3 The reaction for conjugating the cysteine residue of OmpA with 1,5-IAEDANS (Dns). For the reaction, the cysteine residue was reduced using TCEP solution prior to the addition of the dye molecule.

2.3 Polyproline peptide as a representative of a "spectroscopic ruler"

Since Stryer and Haugland verified Förster theory by varying the distance between the naphthyl donor and the dansyl acceptor chromophore in polyproline peptides,[5] the application of FRET to polyproline peptides as a "spectroscopic ruler" has been investigated experimentally and theoretically.[6,7] Here, polyproline peptides that are known to be rigid were utilized to confirm that the energy transfer from the donor (Trp) at the N-terminus to the acceptor (Dns) at the C-terminus of the peptide depended on the number of proline spacers; these peptides were labelled with the same donor and acceptor as the labeled OmpA. The following polyproline peptides were purchased from American Peptide Company (> 95 % purity): Ac-Trp-$(Pro)_6$-Cys-NH_2 (donor-only peptide), Ac-Ala-$(Pro)_6$-Cys-Dns-NH_2 (acceptor-only peptide), Ac-Trp-$(Pro)_6$-Cys-Dns-NH_2 (donor+acceptor peptide with six proline spacer), and Ac-Trp-$(Pro)_9$-Cys-Dns-NH_2 (donor+acceptor peptide with nine proline spacer). Table 2.3 summarizes the peptides, and Figure 2.4 shows the fluorescence spectra of these polyproline peptides.

For the peptide with six and nine proline spacers, the experimental end-to-end distances determined by FRET were 23.1 Å and 29.2 Å, respectively. The value of R_0 was calculated to be 23 Å using equation 1.2 and the spectral overlap between the emission spectra of the donor-only polypeptides and the absorption spectra of the acceptor-only polypeptides, assuming a κ^2 of 2/3, n of 1.33, and Q_D of 0.13. The FRET efficiency was calculated by comparing the tryptophan fluorescence intensity in the presence of an acceptor with that in the absence of an acceptor, as shown in equation 1.3.

For the Cowan and McGavin coordinates, the end-to-end separations of the peptides with six and nine proline residue were estimated to be 18.7 Å and 27.9 Å,

respectively.[8] The calculated FRET distance of the polypeptide with six proline spacers was inconsistent with the crystallographic configuration, yet the value was compatible with a previously reported FRET distance distribution of 23.4 Å.[9] Although the FRET distance differed from the crystallographic distance of six-mer polyproline, the experimental conditions were apparently different from each other, making it difficult to compare the absolute values. Furthermore, the primary goal of this polyproline experiment was to test the sensitivity of the FRET technique, which successfully detected the dependence of the tryptophan fluorescence intensity on the acceptor and donor locations. Thus, these data show that the FRET technique with this specific pair of donor-acceptor molecules is a reasonable method for measuring internal distances of OmpA during a folding reaction.

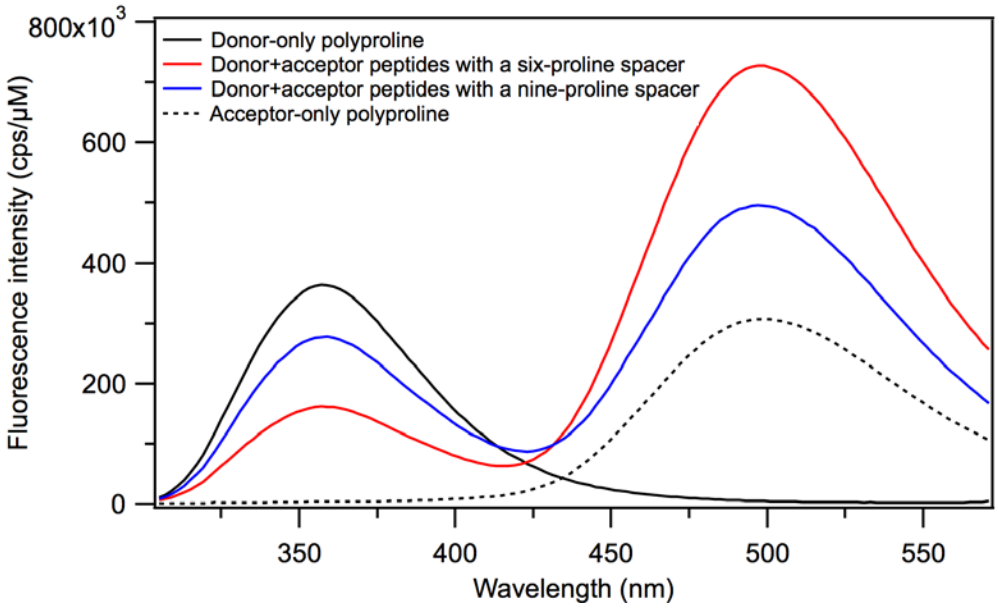

Figure 2.4 Fluorescence spectra of four polyproline peptides in phosphate buffer. Donor-only polyproline peptide is shown with a black solid curve. Donor+acceptor peptides with a six-proline and nine-proline spacer are shown as red and blue curves, respectively. The black-dotted spectrum is for the acceptor-only polyproline peptide.

Table 2.3 Summary of the polyproline peptides for FRET experiments. The first column lists the name of the peptide and the second column includes the description of the peptide. The third and the fourth columns describe molar absorptivities at 280 and 337 nm for donor-only, donor-acceptor, and acceptor-only peptides.

Peptide name	Description	ε_{280} ($M^{-1}cm^{-1}$)	ε_{337} ($M^{-1}cm^{-1}$)
Ac-Trp-$(Pro)_6$-Cys-NH_2	donor-only peptide	5,517	0
Ac-Trp-$(Pro)_6$-Cys-Dns-NH_2	donor+acceptor peptide with six proline spacer	6,709	5,960
Ac-Trp-$(Pro)_9$-Cys-Dns-NH_2	donor+acceptor peptide with nine proline spacer	6,709	5,960
Ac-Trp-$(Pro)_9$-Cys-Dns-NH_2	acceptor-only peptide	1,192	5,960

2.4 Preparation of small unilamellar vesicles

Small unilamellar vesicles (SUVs) were prepared based on a published procedure.[1] First, 25 mg/mL 1,2-dimyristoyl-*sn*-glycero-3-phosphocholine (DMPC, transition temperature of 24 °C) and 25 mg/mL 1,2-dipalmitoyl-*sn*-glycero-3-phosphocholine (DPPC, transition temperature of 41 °C) dissolved in chloroform were purchased from Avanti Polar Lipids. The solution was aliquoted into 1 mL portions in glass vials that were cleaned with a base bath and oven-dried. The 1 mL aliquot of the lipids solution was stored in a –20 °C freezer for further usage.

The 1 mL aliquot of DMPC or DPPC solution was dried under nitrogen gas for several hours. Once completely dried, the white lipid powder was resuspended in 1 mL of 20 mM KPi buffer (pH 7.3) using a water bath sonicator (Branson), and the solution was transferred to a plastic Falcon tube; the process was repeated five times to obtain a final lipids concentration of 5 mg/ml. Subsequently, the resuspended lipid solution was sonicated using an ultrasonicator microtip for 30 minutes at a 50 % duty cycle with 30 % maximum amplitude, resulting in a solution of ~ 50 nm diameter SUVs. During the sonication process, the Falcon tube containing DMPC (or DPPC) solution was immersed in a room temperature water bath (or a hot tap water bath). The sonicated solution was filtered through a 0.22 μm filter to remove particulates, such as titanium dust. The filtered lipid solution was stored in a 37 °C incubator overnight to equilibrate prior to the experiment on the following day.

2.5 Spectroscopic techniques that were used

2.5.1 Absorption spectroscopy

Steady-state absorption spectra were recorded on an Agilent 8453 UV-visible spectrophotometer to determine the protein concentration and labeling efficiency. The final protein concentration and labeling yields for each experiment were measured after dilution of the stock solutions into the appropriate buffer solutions to obtain optical densities in a useable range. The dilution step was necessary because of the instrumental detection limit and light scattering from vesicles. The protein concentration and labeling yields were estimated using the molar absorptivities listed in Tables 2.1, 2.2, and 2.3:

2.5.2 Steady-state fluorescence spectroscopy

Steady-state fluorescence spectra were obtained with a Jobin Yvon-SPEX Fluorolog FL3-11 spectrofluorometer. Protein samples at ~ 5 μM were excited at 290 nm (4 nm band-pass), and the OmpA emission was collected from 305 nm to 570 nm (4 nm band-pass) in 2 nm intervals with an integration time of 0.8 seconds. The protein sample was held in a 10 mm x 4 mm fused silica cuvette covered with a rubber septum, and stirred with a micro stir bar at 33 °C. The spectra for the corresponding buffer solutions were also obtained under the same experimental conditions to correct for background from factors such as lipids scattering and the water Raman signal.

2.5.3 Circular dichroism spectroscopy

Circular dichroism (CD) measurements were performed on an AVIV CD-215 (Aviv Associates, Lakewood, NJ). CD spectra were obtained from 190 nm to 260 nm at 1 nm intervals with an average acquisition time of 5 seconds and a bandwidth of 1 nm. The ~ 6 μM protein sample was held in a fused quartz cuvette with a 1 mm pathlength. The sample was manually mixed before being placed in the CD sample chamber purged with nitrogen gas, and the sample was held at 33 °C during the measurements. Corrected CD

spectra were obtained by subtracting the corresponding blank spectra (same buffer solution except for the presence of protein).

2.5.4 Ultraviolet resonance Raman spectroscopy

Ultraviolet resonance Raman (UVRR) spectra were obtained using a tunable Ti:sapphire laser (Photonics industries) setup that was described elsewhere.[10] To obtain the tryptophan vibrational spectra of OmpA, a ~ 20 μM OmpA sample was probed using an excitation wavelength of 228 nm. The fundamental wavelength of 912 nm passed through a lithium triborate (LBO) crystal for second harmonic generation, followed by a β-barium borate (BBO) crystal for fourth harmonic generation. The protein sample was flowed through a 100 μm (i.d.) fused-silica capillary at a rate of 0.16 mL/min. UVRR spectra of the OmpA mutants were collected for 5 or 10 minutes. Spectra of the buffer solution were also obtained. The buffer spectrum was subtracted from the OmpA spectrum, and residual background was removed by fitting an interpolated curve to the remaining background. All data analysis was performed using Igor Pro 6 (WaveMetrics) software.

2.6 References

(1) Sanchez, K. M.; Gable, J. E.; Schlamadinger, D. E.; Kim, J. E. *Biochemistry* **2008**, *47*, 12844.

(2) Surrey, T.; Jahnig, F. *Proc. Natl. Acad. Sci. USA* **1992**, *89*, 7457.

(3) Surrey, T.; Schmid, A.; Jahnig, F. *Biochemistry* **1996**, *35*, 2283.

(4) Sanchez, K. M., University of California, San Diego, 2010.

(5) Stryer, L.; Haugland, R. P. *Proc Natl Acad Sci U S A* **1967**, *58*, 719.

(6) Schuler, B.; Lipman, E. A.; Steinbach, P. J.; Kumke, M.; Eaton, W. A. *P Natl Acad Sci USA* **2005**, *102*, 2754.

(7) Dolghih, E.; Ortiz, W.; Kim, S.; Krueger, B. P.; Krause, J. L.; Roitberg, A. E. *J Phys Chem A* **2009**, *113*, 4639.

(8) Cowan, P. M.; Mcgavin, S. *Nature* **1955**, *176*, 501.

(9) Lakowicz, J. R.; Wiczk, W.; Gryczynski, I.; Johnson, M. L. *P Soc Photo-Opt Ins* **1990**, *1204*, 192.

(10) Sanchez, K. M.; Neary, T. J.; Kim, J. E. *J. Phys. Chem. B* **2008**, *112*, 9507.

Chapter 3. Förster resonance energy transfer as a probe of membrane protein folding

3.1 Introduction

In the energy landscape theory of protein folding,[1-3] favorable contacts bias a nascent protein towards a three-dimensional structure that represents the global free energy minimum. The non-covalent intramolecular forces that contribute to the stability of the native structure have been characterized for soluble proteins.[4] In the case of membrane proteins, additional intermolecular interactions between the protein and lipid bilayer must be considered, but are not well understood.

Knowledge of the chemical and physical properties of the bilayer is essential for understanding membrane protein structure and folding. A bilayer exhibits at least two distinct chemical regions, the interfacial space and the hydrophobic core.[5] The interfacial region, which spans ~15 Å, is chemically heterogeneous and contains functional groups that may participate in hydrogen bonds and ionic interactions.[6] This region is important for backbone solvation and can induce secondary structure in a peptide that is otherwise unfolded in aqueous solution.[7,8] In the hydrophobic core, the low dielectric constant of ~2 may enhance some molecular interactions.[9,10] For example, the energies of backbone hydrogen bonds in water and in the bilayer have been calculated to be ~1 kcal/mol and ~5 kcal/mol, respectively.[11] This differential suggests that the energetic cost of desolvating the backbone is overcome by enhanced stability upon formation of secondary structure in

a bilayer. This principle underlies the requirement that membrane proteins must form secondary structure in a membrane.[12]

Other general themes for membrane protein structure have emerged. The distribution of amino acids in transmembrane helices has evolved to foster favorable interactions with the water-lipid interface and the hydrophobic core.[13] There is an asymmetric distribution of residues on the N- and C-terminus of membrane proteins, with some polar residues, such as arginine and lysine, more abundant on the N-terminus on account of "snorkeling" effects.[5] The amphipathic residues tyrosine and tryptophan are localized at the bilayer interface and form an aromatic belt region that may serve as the protein anchor in the membrane.[14,15] As expected, aliphatic amino acids are more prevalent in the hydrophobic core of the lipid bilayer, resulting in membrane protein surfaces that are more hydrophobic than their interior.[16,17]

Our understanding of membrane protein folding is inferior to our knowledge of membrane protein structure. For α-helical systems, a sequence of events has been described:[8,12,18-20] (i) interfacial partitioning, (ii) interfacial folding, (iii) insertion into the bilayer, and (iv) assembly of tertiary and quaternary structure in the bilayer. For β-barrel membrane proteins, a concerted mechanism of insertion and folding has been discussed.[21] It should be noted that these and other models for membrane protein folding are derived from a small set of proteins because of experimental difficulties. The challenge lies not only in identification of membrane proteins that undergo reversible folding, but also in successful application of a breadth of techniques to the membrane protein folding problem.

One system that has been utilized to elucidate folding mechanisms is the 325-residue Outer Membrane Protein A (OmpA). OmpA is a major structural component of the *E. coli* outer membrane, and also acts as a non-specific pore and phage receptor.[22,23] The N-terminus forms the transmembrane domain (171 residues) and the C-terminus constitutes the periplasmic region (154 residues). The transmembrane domain folds into a β-barrel pore that is comprised of eight antiparallel β-sheets; the structure of the periplasmic domain has not been resolved. OmpA serves as an ideal model system to study membrane protein folding because of the availability of high resolution NMR and X-ray structures,[24,25] ease of purification,[26] and ability to reversibly and spontaneously fold into lipid vesicles.[27] Additionally, there is significant prior work by our group and others on the photophysics, thermodynamics, and kinetics associated with the native tryptophan residues that serve as chromophores in spectroscopic studies.[15,28-30]

Utilization of techniques that report on global structural changes during a folding reaction enhances our comprehension of folding mechanisms. Förster resonance energy transfer (FRET) is a mechanism for energy transfer based on dipole-dipole interaction between donor and acceptor molecules that are separated by distance *r*. The efficiency for energy transfer scales as $1/r^6$, and this strong distance-dependence enables FRET to be a sensitive spectroscopic ruler for measuring separations between 10 and 100 Å.[31] Widespread availability of spectroscopic tools and the relative ease of site-specific attachment of extrinsic or intrinsic chromophores have facilitated a large number of FRET-based studies of proteins and oligonucleotides. For example, FRET has been used to measure intra- and intermolecular distances in large protein complexes, detect fluctuations in DNA, and probe the folding landscape of heme proteins.[32-34] Recent

experiments have focused on single-molecule FRET measurements of biomolecular dynamics.[35-38] FRET has also been applied to a limited number of membrane-bound systems to determine structures of peptides in membranes,[39,40] probe conformational changes in ion channels,[41] and investigate helix-helix associations.[42] These and other examples of biological FRET exemplify the wealth of knowledge that may be gained from this technique, and motivate our present study to elucidate the complex mechanisms of membrane protein folding using this powerful tool.

3.2 Materials and methods

3.2.1 Expression and purification of OmpA mutants

The procedure for expression, isolation, and purification of OmpA mutants is described elsewhere.[28] The starting plasmid was one that encoded for a cysteine-free, all-phe mutant of OmpA in which the five native tryptophan residues at positions 7, 15, 57, 102, and 143 were substituted with phenylalanine residues. Additionally, the C-terminal periplasmic domain was cleaved by introduction of a stop codon at position 177. This truncated, trp-free mutant consists of only the transmembrane domain, and is referred to as W0Δ(177-325). For simplicity, we omit designation of the deleted residues and abbreviate the notation as W0Δ, where Δ indicates Δ(177-325). Three types of truncated OmpA systems were generated from this initial W0Δ mutant for the current study: OmpA with a single tryptophan residue as the donor, OmpA with a single cysteine residue on which the 1,5-IAEDANS (dns) acceptor moiety may be covalently linked, and OmpA with both tryptophan and cysteine residues (donor + acceptor). Four donor-acceptor pairs as well as appropriate control systems were generated: donor at position 15 with acceptor at position 7 (**F15W/F7CdnsΔ**); donor at position 57 with acceptor at

position 7 (**F57W/F7CdnsΔ**); donor at position 143 with acceptor at position 7 (**F143W/F7CdnsΔ**); donor at position 143 with acceptor at position 57 (**F143W/F57CdnsΔ**); donor-only at position 15 (**F15WΔ**); donor-only at position 57 (**F57WΔ**); donor-only at position 143 (**F143WΔ**); acceptor-only at position 7 (**F7CdnsΔ**); and acceptor-only at position 57 (**F57CdnsΔ**). These mutants are summarized in Table 3.1, and distances between β-carbons from the X-ray structure are illustrated in Figure 3.1.

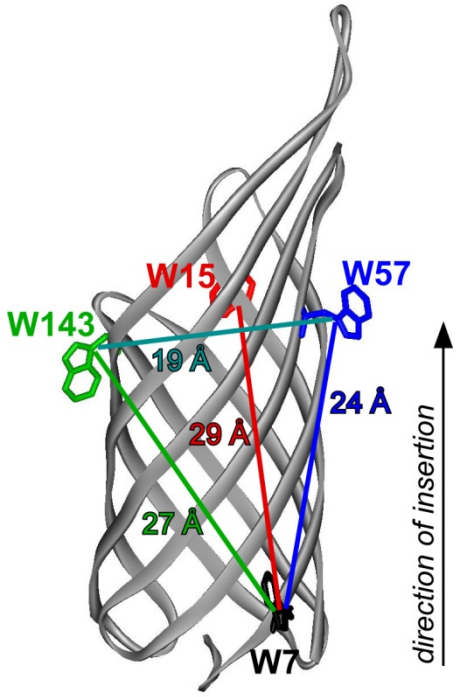

Figure 3.1 Structure of OmpA transmembrane domain (PDB ID: 1QJP) highlighting native residues in locations of tryptophan donor (positions 15, 57, and 143) or cysteine-linked dns acceptor (positions 7 and 57). Distances between β-carbons are indicated. Residues W7 and W15 are on the same strand. The unidirectional nature of insertion is shown.

Table 3.1 Summary of OmpA mutants. Residue positions of donor (D) and acceptor (A) as well as description of D and A locations are indicated.

Mutant	D	A	description
F15W/F7CdnsΔ	15	7	D-A on same strand, across bilayer
F57W/F7CdnsΔ	57	7	D-A across bilayer
F143W/F7CdnsΔ	143	7	D-A across bilayer
F143W/F57CdnsΔ	143	57	D-A across pore
F15WΔ	15	---	Donor-only
F57WΔ	57	---	Donor-only
F143WΔ	143	---	Donor-only
F7CdnsΔ	---	7	Acceptor-only
F57CdnsΔ	---	57	Acceptor-only

3.2.2 Labeling

Purified OmpA (~70 μM in 4-5 mL) was initially mixed with tenfold excess reducing agent, tris(2-carboxyethyl)phosphine (TCEP) (stock concentration of 10 mM), and stirred under nitrogen for 1 hour. Tenfold excess dns acceptor (1,5-IAEDANS is 5-((((2-iodoacetyl)amino)ethyl)amino)naphthalene-1-sulfonic acid, Molecular Probes) initially dissolved to 2-3 mM in dimethyl sulfoxide (DMSO) was added to the solution and allowed to react with the free cysteine residue at position 7 or 57 for approximately five hours under nitrogen atmosphere. The reaction was quenched by addition of tenfold excess 2-mercaptoethanol (2-ME). Unreacted dns was separated from the protein by passing the sample down a desalting column (10-DG, Bio-Rad). The labeled OmpA sample was washed several times with fresh 20 mM phosphate (KP_i) buffer (pH 7.3) that contained 8M urea, concentrated, and stored at -80 °C. Labeling yields were 66% (F143W/F57CdnsΔ), 100% (F57W/F7CdnsΔ), 100% (F15W/F7CdnsΔ), and 45% (F143W/F7CdnsΔ). These yields were determined from the UV-vis spectra and knowledge of the extinction coefficients: ε(337 nm, dns) = 5700 cm^{-1} M^{-1}; ε(280 nm, dns) = 4220 cm^{-1} M^{-1}; ε(280 nm, transmembrane OmpA with single tryptophan) = 26,020 cm^{-1} M^{-1}; and ε(280 nm, transmembrane OmpA with no tryptophan) = 20,500 cm^{-1} M^{-1}.

3.2.3 Preparation of vesicles

Small unilamellar vesicles (SUVs) were prepared following a published procedure [28]. Briefly, 20 mg of 1,2-dimyristoyl-sn-glycero-3-phosphocholine (DMPC, Avanti Polar Lipids) or 1,2-dipalmitoyl-*sn*-glycero-3-phosphocholine (DPPC, Avanti Polar Lipids) was dried under nitrogen gas. DMPC was utilized to probe the folding and

insertion of OmpA while DPPC provided an opportunity to probe the adsorbed, but not inserted, state of OmpA.[27,29] The lipid was resuspended in 20 mM KP_i buffer to a final concentration of 5 mg/mL. The aqueous solution of lipid was placed in a warm water bath and sonicated with a probe ultrasonicator microtip for one hour at 50% duty cycle. The SUV sample was then passed through a 0.22 μm filter, and equilibrated overnight at 37 °C prior to experiments.

3.2.4 Fluorescence and anisotropy measurements during folding reaction

Steady-state fluorescence measurements were performed with a Jobin Yvon-SPEX Fluorolo FL3-11 spectrofluorometer in a right-angle geometry using a 1 cm x 4 mm pathlength fused silica cuvette sealed with a rubber septum. The sample was excited along the 4 mm path, and emission was collected along the 1 cm path. The excitation wavelength for tryptophan was 290 nm, and that for the dns label was 330 nm. The excitation and emission bandpass were set to 4 nm for all unpolarized fluorescence spectra. The folding reaction was initiated by mixing a small volume of stock protein into an equilibrated SUV solution with constant stirring. Fluorescence spectra were acquired at specified time points following mixing: 2, 5, 10, 15, 20, 25, 30, 40, 50, 60, 120, 180, and 240 minutes. The final solution in these folding experiments contained ~6 μM OmpA, 0.5 M urea, 1 mg/mL DMPC in 20 mM KPi buffer at pH 7.3. The solution was kept at 33 °C during folding experiments in order to maintain DMPC in the fluid phase (T_m = 23 °C) or DPPC in the gel phase (T_m = 41°C). Spectra of SUV solutions that lacked protein were acquired at the beginning and end of each experiment.

Two additional experiments were performed to probe the contribution of aggregation and photobleaching to the observed signal. The extent of aggregation was

measured under the same conditions as the folding experiments, with the exception that SUVs were excluded from the sample. Aggregation was monitored via a blue-shift in the emission maximum; for example, F143WΔ exhibited a fluorescence maximum of 337 nm after incubating for three hours in 0.2 M urea solution. Photobleaching experiments were performed by injecting protein into a 20 mM KP_i/8 M urea solution, and monitoring the fluorescence spectra over a 240 minute window. These experiments confirmed that aggregation and photobleaching do not significantly contribute to the fluorescence spectra reported here.

Fluorescence anisotropy experiments were repeated twice under the same sample geometry conditions as the unpolarized fluorescence experiments. The polarized excitation wavelength was 290 nm, and polarized emission was obtained from 305 to 420 nm in 2 nm steps with excitation and emission bandpass set to 3 nm. Polarized spectra in the form of VV, VH, HV, and HH, where the first and second letter correspond to excitation and emission polarizations (V=vertical, H=horizontal), respectively, were acquired. Spectra of vesicle solutions that do not contain OmpA were also acquired and subtracted from corresponding OmpA spectra to remove contribution from scattering. The instrument response (G-factor) was determined using the model compound N-acetyl-L-tryptophanamide (NATA) and protein solutions; the G-factor was identical to within 5% when measured with these different samples.

3.3 Results

3.3.1 Folding yields for labeled protein

Donor-acceptor labeled OmpA was confirmed to fold and unfold via a gel-shift assay.[28,43] The labeled protein exhibited a folding yield of at least 70% after a 24-hour

incubation period in lipid solution (Figure 3.2). The yield of unfolding was ~90% after a 24-hour incubation period in 5 M urea solution. These yields are comparable to those observed for unlabeled transmembrane OmpA.[28]

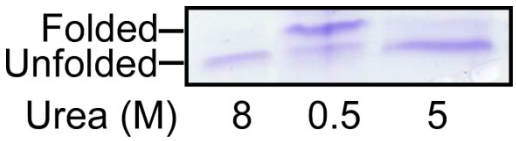

Figure 3.2 Gel-shift assay for F57W/F7CdnsΔ. Unfolded and folded OmpA have apparent molecular weights of 21 and 19 kDa, respectively. Lane 1 is stock unfolded OmpA, lane 2 is OmpA after 24 hour incubation in lipids, and lane 3 is OmpA after 24 hour incubation of folded protein in urea. Approximate urea concentrations are indicated.

3.3.2 FRET calculations and data

Spectral overlap of the donor-acceptor (tryptophan-dns) pair was measured for folded and unfolded OmpA. Figure 3.3 shows representative emission spectra of tryptophan in OmpA in the folded (λ_{max} = 330 nm) and unfolded (λ_{max} = 350 nm) states along with the absorption spectrum of model compound dns in aqueous solution. The absorption peak of dns that is covalently linked to folded or unfolded OmpA differs by less than 2 nm from the spectrum in aqueous solution (data not shown). The emission maximum of OmpA adsorbed on DPPC bilayers is between 339 and 347 nm, and depends on mutant (data not shown). Förster distances for the tryptophan-dns pair in OmpA can be calculated via the equation $R_0^6 = (8.79\times10^{23})(\kappa^2 n^{-4}\Phi_D J_{DA})$ where R_0 is the Förster distance (in Å), κ^2 is the orientation factor between the transition dipoles of the donor and acceptor (ranges from 0 to 4), n is the refractive index of the solvent, Φ_D is the quantum yield of the donor in the absence of acceptor, and J_{DA} is the overlap integral of the donor emission and acceptor absorption spectra.[31,44,45] For the unfolded state, we utilized the experimental absorption and emission spectra, and assumed values of ⅔ for κ^2, 0.13 for Φ_D, and 1.33 for n to calculate a Förster distance of 20.9 Å, which is consistent with prior published values of R_0 for the trp-dns pair.[44,45] The R_0 value for the folded state is 20.8 Å and was calculated using the appropriate overlap integral and the same values of κ^2, Φ_D, and n as the unfolded state. When a range of Φ_D values between 0.13 and 0.25 was utilized, the R_0 value varied 11.5 % for the folded state. In contrast to minor changes in R_0 because of shifts in spectral profile and quantum yield, alterations in κ^2 can have a significant impact on the Förster distance (discussed below).

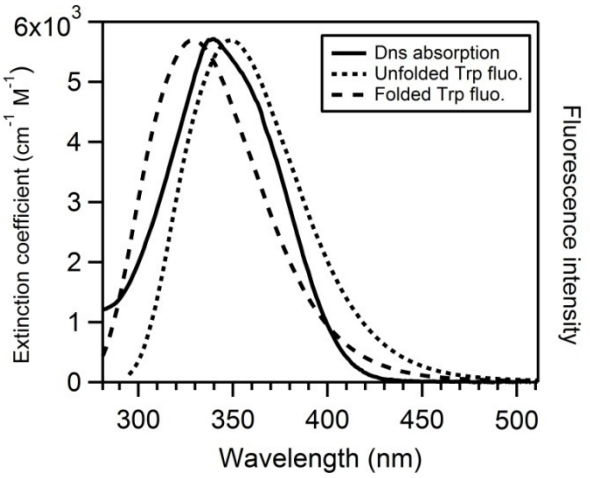

Figure 3.3 Absorption spectrum of dns acceptor (solid, left axis). Normalized fluorescence spectra of tryptophan donor in unfolded (dotted) and folded (dashed) OmpA are also shown (right axis).

FRET efficiencies were calculated for the four donor-acceptor labeled mutants with the following equation:[45]

$$E = 1 - \frac{F_{DA} - F_D(1 - f_A)}{F_D f_A} = \left(1 - \frac{F_{DA}}{F_D}\right)\frac{1}{f_A} \qquad 3.1$$

where E is the FRET efficiency, F_{DA} and F_D are the fluorescence intensity of the donor (tryptophan) in the presence and absence of dns acceptor, respectively, and f_A is the labeling yield for the specific mutant. F_{DA} and F_D were determined for each mutant as a function of time after mixing. Representative fluorescence data for donor-acceptor labeled OmpA, donor-only OmpA, and acceptor-only OmpA are shown in Figures 3.4 and 3.5; additional data are included in supporting information (Figure 3.6). FRET efficiencies are shown in Figure 3.7. For all mutants except F15W/F7CdnsΔ, evolution of the FRET efficiencies is consistent with donor and acceptor moving towards each other another as the protein folds and inserts into the bilayer. For these mutants, the FRET efficiencies evolve from as low as ~10% (unfolded in 8 M urea) to as high as 100% during the folding reaction. The fourth mutant in which donor and acceptor are on the same strand (F15W/F7CdnsΔ) displays the opposite trend in which donor and acceptor are moving apart, evidenced by the change in FRET efficiency from ~60% to ~0% during folding. FRET efficiencies for partially folded OmpA adsorbed on DPPC bilayers are also indicated in Figure 3.7. The estimated error for calculated FRET efficiencies is 20% for all mutants except F143W/F7CdnsΔ, and primarily reflects uncertainty in knowledge of labeling yields and protein concentrations. The error for the fourth mutant, F143W/F7CdnsΔ, is much larger (approximately 50%) because of the low labeling yield. It should be noted that the indicated FRET efficiencies have not taken into account the

minor population of protein that does not fold. The percentage of unfolded protein is expected to be similar for all mutants at less than 30%, and this unfolded population should exhibit no spectral shifts throughout the observation window. Therefore, this systematic error would impact the absolute FRET efficiencies, but not the shapes, of the FRET curves during a folding reaction.

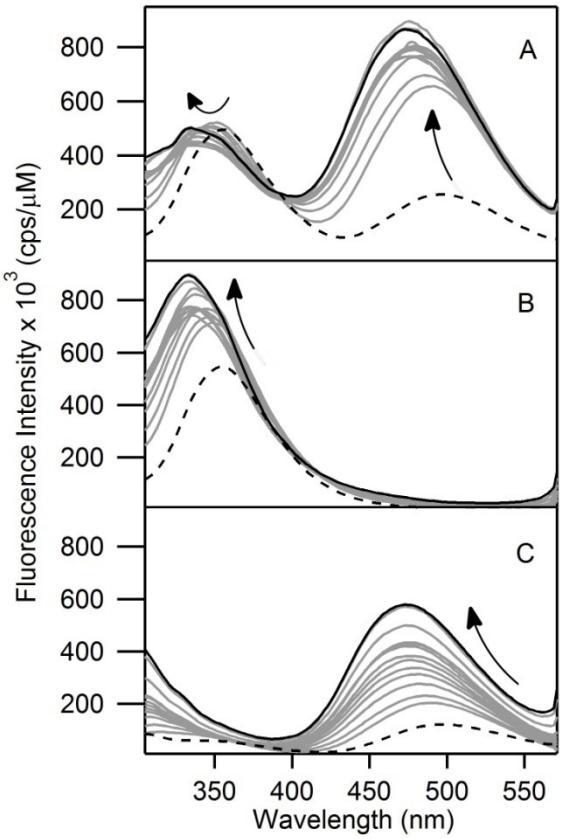

Figure 3.4 Fluorescence spectra during folding (gray and black, solid) and for the unfolded state in 8 M urea (dashed). Spectrum of the folded state after 240 minutes is indicated as the solid, bold, black curve. Spectra are of (A) donor-acceptor labeled mutant F57W/F7CdnsΔ; (B) donor-only (F57WΔ) mutant; and (C) acceptor-only (F7CdnsΔ) mutant.

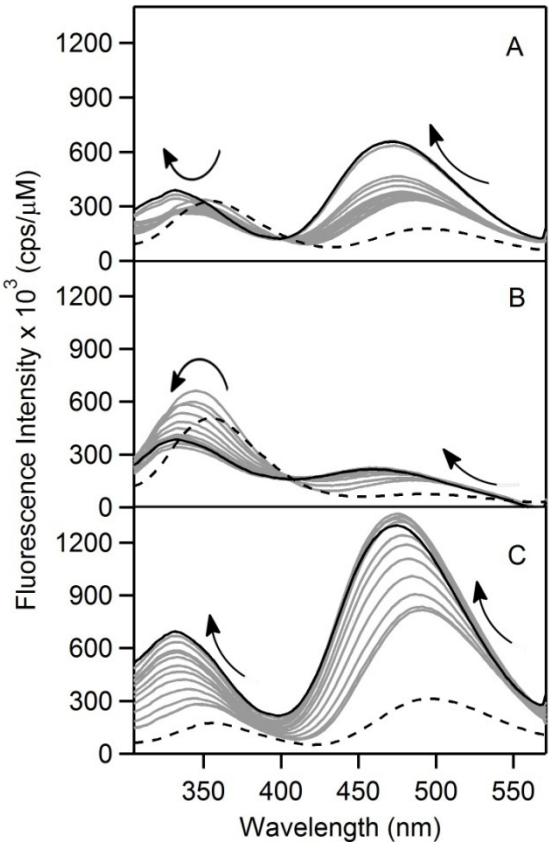

Figure 3.5 Fluorescence spectra during folding (gray and black, solid) and for the unfolded state in 8 M urea (dashed). Spectrum of the folded state after 240 minutes is indicated as the solid, bold, black curve. Spectra are of donor-acceptor labeled mutants (A) F143W/F57CdnsΔ; (B) F143W/F7CdnsΔ; and (C) F15W/F7CdnsΔ.

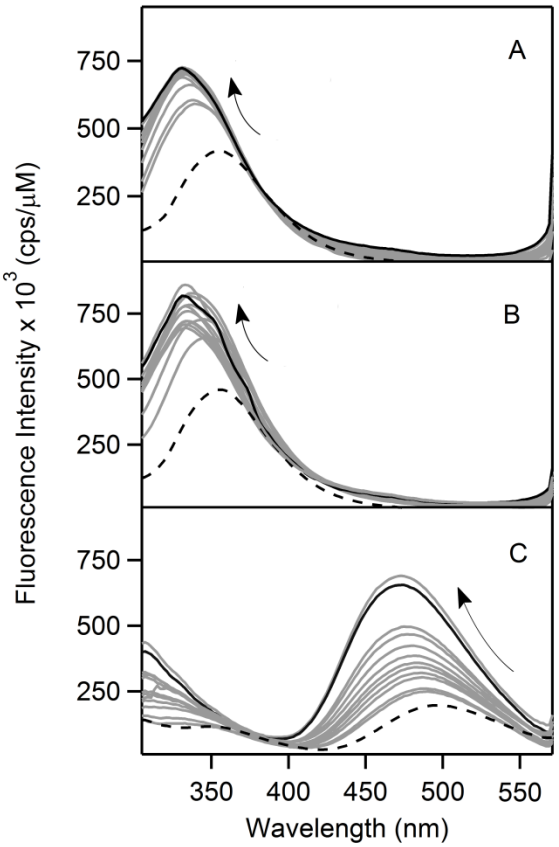

Figure 3.6 Fluorescence spectra during folding (gray and black, solid) and for the unfolded state in 8 M urea (dashed). Spectrum of the folded state after 240 minutes is indicated as the solid, bold, black curve. Spectra are for donor-only mutants (A) F15WΔ and (B) F143WΔ as well as for the acceptor-only mutant (C) F57CdnsΔ.

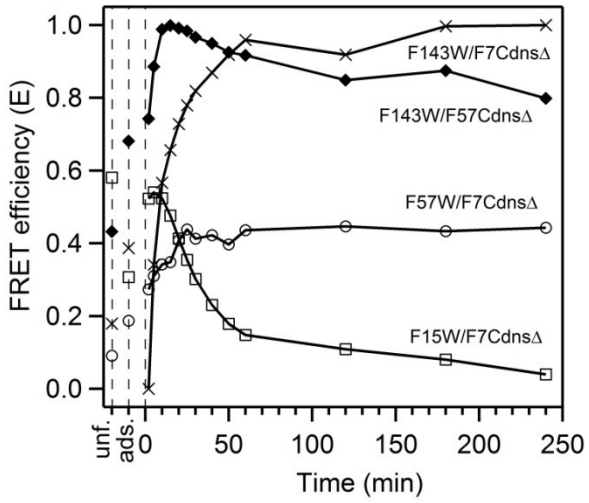

Figure 3.7 FRET efficiency of unfolded state ("unf.") in 8 M urea, adsorbed species ("ads.") on DPPC, and during folding reaction into DMPC. Solid lines that connect the data points are included to help guide the eye. The estimated error for calculated FRET efficiencies is 20% for all mutants except F143W/F7CdnsΔ; the error for F143W/F7CdnsΔ is approximately 50%. See text for details.

3.3.3 Tryptophan fluorescence shift and anisotropy

The evolution of the tryptophan blue-shift as a function of folding time is shown in supporting information (Figure 3.8). The kinetic traces for six of the seven OmpA mutants studied here are similar and indicate that ~75% of the fluorescence shift is completed within 60 minutes. The donor-acceptor labeled mutant F143W/F57CdnsΔ exhibits a fluorescence shift that is about twofold slower. This result indicates that traversal of the dns acceptor at position 57 through the bilayer may impede the folding kinetics (discussed below).

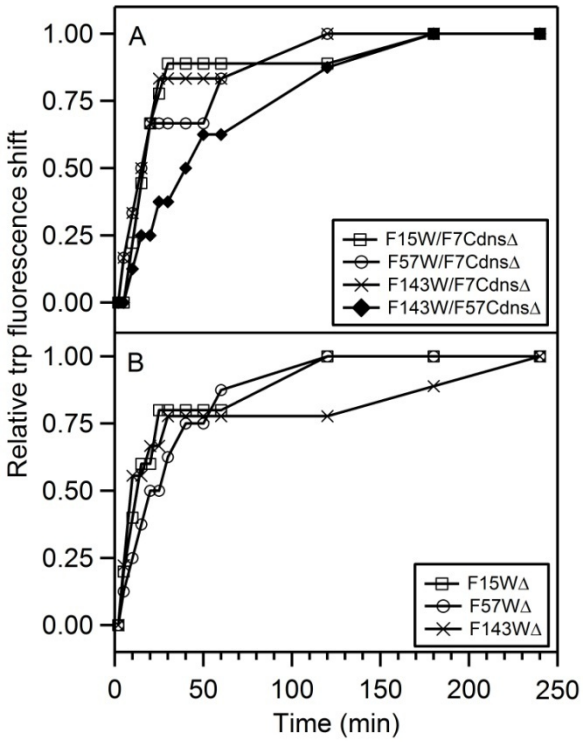

Figure 3.8 Relative tryptophan fluorescence blue-shift during folding of (A) donor-acceptor labeled OmpA, and (B) donor-only OmpA. The relative tryptophan fluorescence shift is calculated as $(\lambda_{obs}(t) - \lambda^{o}_{unf})/(\lambda^{o}_{fold} - \lambda^{o}_{unf})$ where $\lambda_{obs}(t)$ is the experimentally observed emission maximum at time *t*, λ^{o}_{unf} is the emission maximum for unfolded OmpA, and λ^{o}_{fold} is the emission maximum for folded OmpA.

Steady-state anisotropy measurements were performed to investigate the rotational flexibility of the tryptophan donor during the folding event (Figure 3.9). The enhanced anisotropy values of folded OmpA indicate loss of rotational flexibility in vesicles relative to unfolded OmpA in urea. In general, the anisotropy values are enhanced within minutes of initiating the folding reaction, and continue to increase on a timescale similar to those that characterize changes in FRET and tryptophan fluorescence. This finding supports a picture in which OmpA interacts closely with the membrane during folding, and this interaction gives rise to the measured anisotropy. The initial drop in anisotropy at t = 2 min for unfolded protein is likely an artifact that arises from injecting stock OmpA solution into the buffer solution; in this case, both solutions contain 8 M urea and are thus viscous. The implications of rotational restriction on FRET calculations are discussed below.

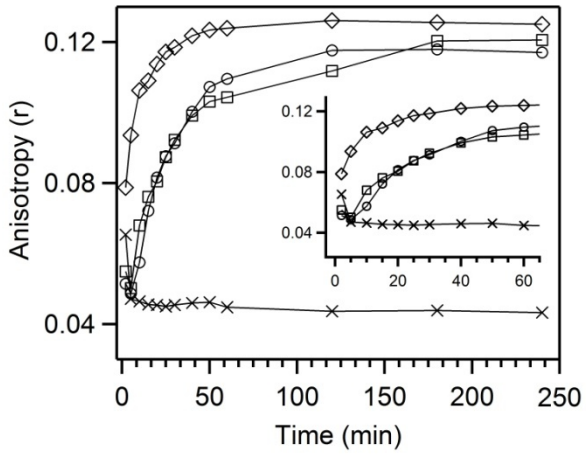

Figure 3.9 Average values of tryptophan anisotropy in the range 330-360 nm for OmpA donor-only mutants during folding reaction into DMPC bilayers: (◇)F143WΔ; (□)F15WΔ; and (○) F57WΔ. OmpA that is injected into a solution of 8 M urea is also shown for (×) F143WΔ. An expanded view of the initial 65 minutes is shown as the inset. The upper limit for error in anisotropy is estimated as ±0.02.

3.4 Discussion

3.4.1 Application of FRET to membrane protein folding

The application of FRET to membrane proteins is limited relative to analogous studies of soluble proteins because of challenges associated with labeling and folding membrane proteins. Here, we present FRET experiments on the 176-residue, transmembrane domain of OmpA. The selection of OmpA offers several advantages. First, β-barrel membrane proteins generally contain a greater fraction of polar residues than α-helical membrane proteins. A consequence of this property is that OmpA, unlike the α-helical protein bacteriorhodopsin, can be fully unfolded in denaturant, and refolded in the presence of lipid bilayer in a reversible and spontaneous manner.[46] Second, the availability of high-resolution structures guides the design of appropriate FRET mutants.[24,25] Finally, OmpA is a well-characterized system for membrane protein folding.[15,21,28-30,47-50] The observation that the transmembrane domain spontaneously inserts and folds into lipid bilayer in a unidirectional manner is especially advantageous for these FRET measurements.[27]

FRET mutants were selected for this initial study to probe the evolution of the following intraprotein distances: across the bilayer on different strands (F143W/F7CdnsΔ and F57W/F7CdnsΔ), across the bilayer on the same strand (F15W/F7CdnsΔ), and across the protein pore (F143W/F57CdnsΔ). The donor-acceptor pairs provide additional geometric constraints because three of the FRET pairs form the sides of a triangle, with donor and acceptor at the vertices. This combination of mutants enables study of the relative timescales for global structural changes, such as pore formation, bilayer traversal,

and strand extension. The current experiments not only complement prior work that probed intermolecular protein-lipid distances with the use of brominated lipids,[30,49] but may also enhance computational efforts in the expanding field of membrane protein folding.

Significant effort was devoted to characterizing the effect of labeling on the stability and kinetics of folding. The dns FRET acceptor has both hydrophobic (aromatic rings and hydrocarbon linker) and hydrophilic (sulfonate and amide groups) components and as a result, it is not straightforward to predict the effect of this extrinsic label on the folded state of OmpA. To our knowledge, there are no prior reports of *in vitro* FRET studies on membrane protein folding. Instead, a number of membrane proteins have been labeled with dyes on solvent-exposed residues to probe conformational changes and global interactions; nearly all of these examples utilized proteins in native membrane environments or solubilized in detergent.[42,51-53] As shown by SDS-PAGE analysis, OmpA that was labeled with dns inserts and folds into membranes with yields that are comparable to unlabeled OmpA. Additionally, the characteristic blue-shift of tryptophan fluorescence that accompanies folding[28,30] is preserved in the FRET mutants studied here. These measurements indicate that the presence of a covalently linked dns label at position 7 or 57 does not drastically alter the folded structure.

In contrast to these equilibrium measurements, the kinetics of insertion appears to be affected by the presence of a dns label at one of the positions. The single tryptophan residue at positions 15, 57 and 143 in the donor-only mutants of OmpA undergoes 75% of the fluorescence blue-shift within 60 minutes of folding. Attachment of a dns label at position 7 does not affect the kinetics. However, the presence of a dns label at position

57 impedes the kinetics such that the blue-shift occurs in ~100 rather than 60 minutes. One rational explanation for this perturbation is the unidirectional nature of insertion: residue 57 must traverse the bilayer whereas residue 7 is not required to cross the membrane. While it is plausible that the presence of the label at position 57 hinders the rate of insertion, we have not studied other OmpA mutants to confirm this hypothesis. Other experiments are currently underway.

3.4.2 Mechanisms of folding

An important goal of the present work is to elucidate mechanisms of folding. We acknowledge at the outset that the unfolded state in 8 M urea is not an adequate representation of the starting unfolded state for folding reactions. However, we pursued FRET measurements on OmpA in 8 M urea to investigate the protein in a presumably extended and unfolded conformation. The data in Figure 3.7 indicate that as expected, the FRET efficiencies for donor and acceptor pairs that are distant in sequence are low in 8 M urea, typically less than ~45%. The exception is F15W/F7CdnsΔ, for which the donor and acceptor are eight residues apart on the same strand. For this mutant, the FRET efficiency in 8 M urea is high at ~60%, indicating that a dynamic loop is likely formed between donor and acceptor in this denaturant. The presence of a loop is consistent with theoretical predictions that the probability of loop formation is maximum for a loop length of ten.[54]

Upon initiation of the folding event, the FRET results indicate that global changes occur on three different timescales. The most rapid change in FRET efficiency was observed for the mutant that reports on pore formation (F143W/F57CdnsΔ); this mutant exhibited a sharp increase in FRET efficiency that reached its maximum value of ~100%

in 15 minutes, followed by a slow decay in FRET signal over the remaining collection period. Evolution of FRET signal occurred on an intermediate timescale for the two mutants that probe bilayer traversal, F143W/F7CdnsΔ and F57W/F7CdnsΔ. The FRET signal for both mutants began to level off in ~60 minutes, with no significant change following this initial rise. The slowest change in FRET efficiency occurred for the mutant that probes strand extension across the bilayer, F15W/F7CdnsΔ. This mutant showed a large drop in FRET signal in the first 60 minutes, and continued to evolve until the last data point was measured at 240 minutes during the folding reaction.

The FRET data may be assembled to yield the following picture of OmpA insertion and folding into membranes (see Figure 3.10). Because the insertion process is known to be directional, the pore is at least partially formed during insertion. Specifically, the inserting portion of the protein is likely to assemble as a compact pore as it inserts into the bilayer. This initial formation is consistent with the early FRET response of the F143W/F57CdnsΔ mutant. It appears that the presence of the dns label at position 57 (described above) does not impact the formation of the pore despite its apparent effect on insertion kinetics. Bilayer traversal occurs on a slower timescale, on the order of 60 minutes. Here, the term "bilayer traversal" is not intended to suggest that the bilayer is a static medium in which the protein inserts. Rather, the dynamic nature of the bilayer plays a critical role in the folding process and therefore, it is more appropriate to consider "lipid-assisted protein folding" in which there are simultaneous changes in both protein and bilayer structure during folding.[29,55,56] However, since the current studies are limited to intraprotein FRET, we attribute the formation of a membrane-spanning domain to bilayer traversal. Following this ~60-minute period of bilayer

traversal, a long-time component that is attributed to strand extension and pore expansion persists over the 240-minute measurement window.

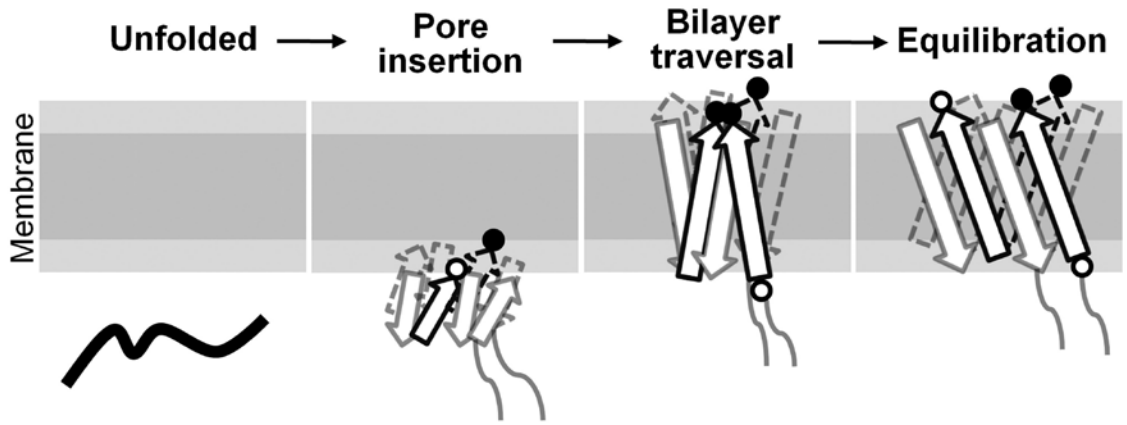

Figure 3.10 Schematic of OmpA folding into a membrane. Hydrophobic core and interfacial space of lipid bilayer are indicated as dark and light gray shaded regions, respectively. OmpA that is initially unfolded in 8 M urea forms at least a partial pore that begins to insert into the bilayer within the first 15 minutes of initiating the folding reaction. The protein continues to insert and traverse the bilayer for approximately 60 minutes following initiation. A long-time equilibration period lasts up to at least 240 minutes, during which period OmpA undergoes strand extension and pore expansion. Timescales and structural changes are based on evolution of FRET signal of specific donor (closed circle) and acceptor (open circle) pairs on the protein. See main text for additional details.

We also investigated the FRET signal for adsorbed intermediates that exhibit secondary structure, but does not insert into bilayers that are in the gel phase of DPPC.[47] For the three mutants in which donor and acceptor are distant in primary sequence, the adsorbed intermediates exhibited FRET efficiencies that are consistent with a compressed tertiary structure. This structure is more compact than the extended conformations in 8 M urea, but less compact than folded protein. The fourth mutant (F15W/F7CdnsΔ), in which the donor and acceptor are eight residues apart, shows the opposite trend where the adsorbed species is more extended than the unfolded state, but more compact than the folded species. These results suggest that while the β-sheet secondary structure of the adsorbed state resembles that of the folded state,[27,57] the tertiary structures of the adsorbed and folded states are dissimilar.

Results from the present FRET experiments build upon prior studies of OmpA that utilized tryptophan fluorescence, circular dichroism, and SDS-PAGE analyses.[21,30,57-59] In these earlier reports, three membrane-associated intermediates were identified, and the kinetics of folding was found to depend on several factors, including pH, temperature, and membrane properties. The emerging picture for the folding mechanism includes initial formation of an adsorbed (collapsed) intermediate, followed by folding and insertion into the membrane in a concerted manner.[21] Our results support this concerted picture, and provide additional insight into changes in tertiary structure. One important conclusion from the FRET measurements is that the pore appears to form early during the folding reaction, prior to completion of bilayer traversal and secondary structure formation. This pore formation may be associated with adsorption. It should be noted that we do not yet know the full extent of pore formation because the FRET pair is

located on the inserting portion of the protein. We are currently pursuing FRET measurements to monitor pore formation on the other end of the protein pore, near W7. Additional insight from the current studies is that the kinetics of bilayer traversal is coincident with the known blue-shift in fluorescence, and both occur on the order of ~60 minutes. This result suggests that the majority of the fluorescence blue-shift reported here and in prior reports can be attributed to formation of the membrane-spanning structure. Finally, the long-time component (~60-240 minutes) of folding that is observed as slow changes in the FRET signal and tryptophan fluorescence intensity (data not shown) may be attributed to equilibration of the protein in the bilayer. The current FRET results suggest that this equilibration may involve strand extension and pore expansion. This relaxation may also reflect slow changes in local solvation, such as expulsion of water from the protein/bilayer core. While this interpretation is consistent with prior reports, the current FRET data do not exclude the possibility of parallel folding pathways that exhibit different kinetics.

3.4.3 Interpretation of FRET distances

The conversion from FRET efficiency to intramolecular distance is, in principle, a straightforward task. However, for membrane proteins, we face several challenges. Here, we have shown that evolution of the absorption and emission profiles as well as the emission quantum yield during folding do not significantly alter the Förster distance for a given orientation factor; if orientational averaging of the donor and acceptor is assumed ($\kappa^2 = ⅔$), R_0 is calculated as 21 Å for the folded and unfolded states. However, it is possible that the use of ⅔ for κ^2 is not valid for folded OmpA, as has been discussed for dns-labeled bacteriorhodopsin.[60] Some deviation from the average value of ⅔ is

supported by steady-state and time-resolved fluorescence anisotropy measurements that indicate that the donor is rotationally hindered when OmpA is inserted and folded in a bilayer.[61]

The experimental difficulties of measuring the orientational factor have not precluded the wide use of FRET as a spectroscopic ruler. One reason for the quantitative success of FRET is that for systems that contain a heterogeneous population of conformations, the assumption of orientational averaging is valid.[62] For the majority of proteins in which donor and acceptor are covalently linked to solvent-exposed regions of the protein via flexible linkers, this assumption likely holds true. For OmpA and other membrane proteins, however, it is not known whether the folded protein exhibits preferential orientations of donor and acceptor within the membrane. The structural restrictions that complicate the interpretation of FRET data for membrane proteins can be overcome by selection of appropriate donor-acceptor pairs. In the case of tryptophan and dns, both molecules exhibit more than one transition dipole moment associated with overlapping electronic transitions.[63-65] The presence of these near-degenerate transitions significantly limits the range of possible κ^2 values such that errors in distances are likely less than 10%.[65] Therefore, the combination of structural heterogeneity and optimized photophysical properties enable FRET to be a useful probe despite the challenges associated with the orientation factor.

In the case where a protein structure is available, comparison of the apparent FRET distances, r' (using $\kappa^2 = ⅔$), with those from the crystal/NMR structure may provide insight into the extent of conformational heterogeneity.[31] The use of $\kappa^2 = ⅔$ for a membrane protein is not unprecedented, and was justified in a previous study of helix-

helix interactions of bacteriorhodopsin.[42] The evolution in distances between donor and acceptor for OmpA is summarized in the following form: r in 8 M urea → r' folded in membrane (with crystal structure distances from Figure 3.1 in parentheses). The distance changes are 31 Å → 22 Å (24 Å) for donor and acceptor across the bilayer (F57W/F7CdnsΔ), 27 Å → 13 Å (27 Å) for donor and acceptor across the bilayer (F143W/F7CdnsΔ), 22 Å → 16 Å (19 Å) Å for donor and acceptor across the pore (F143W/F57CdnsΔ), and 20 Å → 31 Å (29 Å) for donor and acceptor on the same strand across the bilayer (F15W/F7CdnsΔ). Satisfactory agreement between FRET and crystal structure distances for folded protein is achieved for three mutants, suggesting that κ^2 may not significantly deviate from the value of ⅔. This finding is consistent with other reports that indicate variation in κ^2 do not result in significant error.[44,66,67] The fourth mutant, F143W/F7CdnsΔ, exhibits a folded distance that is much smaller than expected given that the donor and acceptor must span the bilayer. This discrepancy likely arises because of the low labeling yield of 45% for this particular mutant, and this finding emphasizes the importance of high yields to obtain reliable results. Despite the overall agreement between crystallographic and FRET-based distances for the three mutants with high labeling yields, a more rigorous treatment of κ^2 would be necessary to confirm the absolute distances during folding.[31,60,68,69] Nonetheless, the qualitative trends reported here are likely to be valid.

3.5 Conclusion

The results presented here illustrate the application of FRET to the study of membrane protein folding. FRET experiments are advantageous because they provide

insight on intraprotein distances during a folding event, and results from this technique complement existing knowledge about secondary structure and local environment that is gained from other tools. Relative timescales for global changes, such as protein pore formation, bilayer traversal, and strand extension, help elucidate the mechanisms of protein insertion and folding into a synthetic bilayer. Despite the relative success of these initial FRET experiments, it is clear that several challenges persist. Low labeling yields and lack of knowledge of the orientation factor hinder facile quantitative assessment of distances. Nonetheless, qualitative insight is gained and motivates ongoing FRET experiments on membrane protein folding.

3.6 Acknowledgements

G.K. was supported by Heme and Blood Proteins Training Grant T32-DK007233. I.L.P. received funding from a National Science Foundation Alliance for Graduate Education and the Professoriate Fellowship (HRD-0450366), and C.G. acknowledges support from the UCSD Chancellor's Undergraduate Research Scholarship. This work was supported by the National Science Foundation (CHE-0645720).

Chapter 3, in full, is a reprint of the material as it appears in Biochimica et Biophysica Acta (BBA) 1818, 2012, Kang, Guipeun; López-Peña, Ignacio; Oklejas, Vanessa; Gary, Cyril S.; Cao, Weihan; and Kim, Judy E. Elsevier S&T. The dissertation author was primary investigator and author of this paper.

3.7 References

(1) Onuchic, J. N.; Luthey-Schulten, Z.; Wolynes, P. G. *Annu. Rev. Phys. Chem.* **1997**, *48*, 545.

(2) Dill, K. A.; Chan, H. S. *Nat. Struct. Biol.* **1997**, *4*, 10.

(3) Bryngelson, J. D.; Wolynes, P. G. *Proc. Natl. Acad. Sci. USA* **1987**, *84*, 7524.

(4) Dill, K. A. *Biochemistry* **1990**, *29*, 7133.

(5) Chamberlain, A. K.; Lee, Y.; Kim, S.; Bowie, J. U. *J. Mol. Biol.* **2004**, *339*, 471.

(6) Wiener, M. C.; White, S. H. *Biophys. J.* **1991**, *59*, 162.

(7) Kaiser, E.; Kezdy, F. *Proc. Natl. Acad. Sci. USA* **1983**, *80*, 1137.

(8) Wimley, W. C.; White, S. H. *Nat. Struct. Biol.* **1996**, *3*, 842.

(9) Dilger, J.; Fisher, L.; Haydon, D. *Chem. Phys. Lipids* **1982**, *30*, 159.

(10) Bowie, J. U. *Curr. Op. Struct. Biol.* **2011**, *21*, 42.

(11) Ben-Tal, N.; Sitkoff, D.; Topol, I. A.; Yang, A. S.; Burt, S. K.; Honig, B. *J. Phys. Chem. B* **1997**, *101*, 450.

(12) Jacobs, R. E.; White, S. H. *Biochemistry* **1989**, *28*, 3421.

(13) Ulmschneider, M. B.; Sansom, M. S. P. *Biochim. Biophys. Acta, Rev. Biomembr.* **2001**, *1512*, 1.

(14) Yau, W. M.; Wimley, W. C.; Gawrisch, K.; White, S. H. *Biochemistry* **1998**, *37*, 14713.

(15) Hong, H.; Park, S.; Jiménez, R. H. F.; Rinehart, D.; Tamm, L. K. *J. Am. Chem. Soc.* **2007**, *129*, 8320.

(16) Rees, D.; DeAntonio, L.; Eisenberg, D. *Science* **1989**, *245*, 510.

(17) Samatey, F. A.; Xu, C.; Popot, J. L. *Proc. Natl. Acad. Sci. USA* **1995**, *92*, 4577.

(18) Popot, J. L.; Engelman, D. M. *Biochemistry* **1990**, *29*, 4031.

(19) Popot, J. L.; Engelman, D. M. *Annu. Rev. Biochem.* **2000**, *69*, 881.

(20) White, S. H.; Wimley, W. C. *Annu. Rev. Biophys. Biomol. Struct.* **1999**, *28*, 319.

(21) Kleinschmidt, J. H. *Chem. Phys. Lipids* **2006**, *141*, 30.

(22) Wang, Y. *Biochem. Bioph. Res. Comm.* **2002**, *292*, 396.

(23) Sugawara, E.; Nikaido, H. *J. Biol. Chem.* **1992**, *267*, 2507.

(24) Arora, A.; Abildgaard, F.; Bushweller, J. H.; Tamm, L. K. *Nat. Struct. Biol.* **2001**, *8*, 334.

(25) Pautsch, A.; Schulz, G. E. *J. Mol. Biol.* **2000**, *298*, 273.

(26) Schweizer, M.; Hindennach, I.; Garten, W.; Henning, W. *Eur. J. Biochem.* **1978**, *82*, 211.

(27) Surrey, T.; Jahnig, F. *Proc. Natl. Acad. Sci. USA* **1992**, *89*, 7457.

(28) Sanchez, K. M.; Gable, J. E.; Schlamadinger, D. E.; Kim, J. E. *Biochemistry* **2008**, *47*, 12844.

(29) Sanchez, K. M.; Kang, G. P.; Wu, B. J.; Kim, J. E. *Biophysical Journal* **2011**, *100*, 2121.

(30) Kleinschmidt, J. H.; den Blaauwen, T.; Driessen, A. J. M.; Tamm, L. K. *Biochemistry* **1999**, *38*, 5006.

(31) Stryer, L. *Ann. Rev. Biochem.* **1978**, *47*, 819.

(32) Dockter, M. E.; Steinemann, A.; Schatz, G. *J. Biol. Chem.* **1978**, *253*, 311.

(33) Bonnet, G.; Krichevsky, O.; Libchaber, A. *Proc. Natl. Acad. Sci. USA* **1998**, *95*, 8602.

(34) Lyubovitsky, J. G.; Gray, H. B.; Winkler, J. R. *J. Am. Chem. Soc.* **2002**, *124*, 5481.

(35) Zhuang, X. W.; Kim, H.; Pereira, M. J. B.; Babcock, H. P.; Walter, N. G.; Chu, S. *Science* **2002**, *296*, 1473.

(36) Schuler, B.; Lipman, E. A.; Eaton, W. A. *Nature* **2002**, *419*, 743.

(37) Schuler, B.; Eaton, W. A. *Curr. Op. Struct. Biol.* **2008**, *18*, 16.

(38) Zhao, R.; Rueda, D. *Methods* **2009**, *49*, 112.

(39) Veatch, W.; Stryer, L. *J. Mol. Biol.* **1977**, *113*, 89.

(40) Lakowicz, J. R.; Gryczynski, I.; Laczko, G.; Wiczk, W.; Johnson, M. L. *Prot. Sci.* **1994**, *3*, 628.

(41) Cha, A.; Snyder, G. E.; Selvin, P. R.; Bezanilla, F. *Nature* **1999**, *402*, 809.

(42) Nannepaga, S. J.; Gawalapu, R.; Velaszuez, D.; Renthal, R. *Biochemistry* **2004**, *43*, 550.

(43) Tamm, L. K.; Arora, A.; Rinehart, D.; Szabo, G. *J. Biol. Chem.* **2000**, *275*, 1594.

(44) Wu, P. G.; Brand, L. *Analytical Biochemistry* **1994**, *218*, 1.

(45) Lakowicz, J. R. *Springer: New York* **2006**.

(46) Booth, P. J.; Templer, R. H.; Meijberg, W.; Allen, S. J.; Curran, A. R.; Lorch, M. *Crit. Rev. in Biochem. and Mol. Biol.* **2001**, *36*, 501.

(47) Dornmair, K.; Kiefer, H.; Jahnig, F. *J. Biol. Chem.* **1990**, *265*, 18907.

(48) Hong, H.; Tamm, L. K. *Proc. Natl. Acad. Sci. USA* **2004**, *101*, 4065.

(49) Kleinschmidt, J. H.; Tamm, L. K. *Biochemistry* **1999**, *38*, 4996.

(50) Ramakrishnan, M.; Qu, J.; Pocanschi, C. L.; Kleinschmidt, J. H.; Marsh, D. *Biochemistry* **2005**, *44*, 3515.

(51) Harris, G.; Renthal, R.; Tuley, J.; Robinson, N. *Biochem. and Biophys. Res. Comm.* **1979**, *91*, 926.

(52) Taniguchi, Y.; Ikehara, T.; Kamo, N.; Watanabe, Y.; Yamasaki, H.; Toyoshima, Y. *Photochem. Photobio.* **2007**, *83*, 311.

(53) Majumdar, D. S.; Smirnova, I.; Kasho, V.; Nir, E.; Kong, X.; Weiss, S.; Kaback, H. R. *Proc. Natl. Acad. Sci. USA* **2007**, *104*, 12640.

(54) Camacho, C. J.; Thirumalai, D. *Proc. Natl. Acad. Sci. USA* **1995**, *92*, 1277.

(55) Dowhan, W.; Bogdanov, M. *J. Biol. Chem.* **1999**, *274*, 36827.

(56) Dowhan, W.; Bogdanov, M. *Annu. Rev. Biochem.* **2009**, *78*, 515.

(57) Rodionova, N. A.; Tatulian, S. A.; Surrey, T.; Jaehnig, F.; Tamm, L. K. *Biochemistry* **1995**, *34*, 1921.

(58) Kleinschmidt, J. H.; Tamm, L. K. *Biochemistry* **1996**, *35*, 12993.

(59) Kleinschmidt, J. H.; Tamm, L. K. *J. Mol. Biol.* **2002**, *324*, 319.

(60) Renthal, R.; Cothran, M.; Dawson, N.; Harris, G. J. *Biochem. Biophys. Acta* **1987**, *897*, 384.

(61) Kim, J. E.; Arjara, G.; Richards, J. H.; Gray, H. B.; Winkler, J. R. *Journal of Physical Chemistry B* **2006**, *110*, 17656.

(62) Englert, A.; Leclerc, M. *Proc. Natl. Acad. Sci. USA* **1978**, *75*, 1050.

(63) Schlessi.J; Steinber.Iz; Pecht, I. *J. Mol. Biol.* **1974**, *87*, 725.

(64) Callis, P. R. *Fluorescence Spectroscopy* **1997**, *278*, 113.

(65) Haas, E.; Katchalskikatzir, E.; Steinberg, I. Z. *Biochemistry* **1978**, *17*, 5064.

(66) dosRemedios, C. G.; Moens, P. D. J. *J. Struct. Biol.* **1995**, *115*, 175.

(67) Lakowicz, J. R.; Gryczynski, I.; Wiczk, W.; Laczko, G.; Prendergast, F. C.; Johnson, M. L. *Biophys. Chem.* **1990**, *36*, 99.

(68) Hoefling, M.; Lima, N.; Haenni, D.; Seidel, C. A. M.; Schuler, B.; Grubmuller, H. *PLoS ONE* **2011**, *6*.

(69) Corry, B.; Jayatilaka, D.; Martinac, B.; Rigby, P. *Biophysical Journal* **2006**, *91*, 1032.

Chapter 4. Folding of a β-barrel membrane protein via Förster resonance energy transfer (FRET) and circular dichroism (CD)

4.1 Introduction

It is estimated that approximately 30 % of genes of all open reading frames encode as integral membrane proteins.[1,2] Integral membrane proteins fall into two classes depending on the structural motifs – α-helical and β-barrel membrane proteins. While α-helices are found in inner membranes of cell envelopes, β-barrel membrane proteins are found in the outer membrane of Gram-negative bacteria, chloroplast, and mitochondria of eukaryotic cells.[3] β-barrel integral membrane proteins are generally less hydrophobic than α-helical proteins because of the distribution of hydrophobic and hydrophilic residues.[4] Therefore, while hydrophobic α-helical membrane proteins such as bacteriorhodopsin are difficult to fully denature, β-barrel membrane proteins (e.g. OmpA) can be solubilized in high concentration of denaturant.[5,6] This ability to be easily denatured makes β-barrel membrane proteins convenient systems for studies of membrane protein folding. Thus, here we focus on a β-barrel membrane protein to investigate folding dynamics using spectroscopic methods.

β-barrel membrane proteins have been investigated in folding studies.[7,8] To reduce the energetic cost associated with exposed hydrogen bond donors and acceptors in a hydrophobic membrane, OmpA forms secondary structure while it inserts into the lipid bilayer, which in turn leads to formation of tertiary structure.[9] OmpA successfully refolds into both lipid bilayer and detergent micelles,[10,11] but it was suggested that there

are different folding processes and final structures depending on the medium in which the protein folds.[7,12,13] It is likely that different protein-environment interactions affect the conformation of the folded state, permeability of water through barrel pore, and flexibility of overall structure. Herein, we aim 1) to probe structural changes by tracking internal distances during folding into lipid bilayer, and 2) to compare the folded states of OmpA in a lipid bilayer and detergent micelle.

OmpA, which is a well-studied β-barrel membrane protein for *in vitro* folding experiments, was selected in the current experiments for reasons outlined in Chapter 1. Briefly, structures of OmpA are available through X-ray crystallographic and NMR studies.[14-16] The eight antiparallel strands of OmpA form a β-barrel monomer with 325 amino acids that constitute two domains: a transmembrane domain of ~ 171 residues that is incorporated into the hydrophobic membrane of phospholipids and a C-terminal peripheral domain of ~ 154 residues that is exposed to the periplasmic space. OmpA spontaneously refolds and inserts into preformed lipid bilayer without the aid of a detergent.[6,8] Lastly, five native tryptophan residues are embedded in the water-bilayer interfacial region as shown in Figure 4.1, and these intrinsic fluorophores are sensitive to the local environment. In combination with an appropriate energy acceptor, tryptophan residues in OmpA can reveal changes in distance during the folding process.

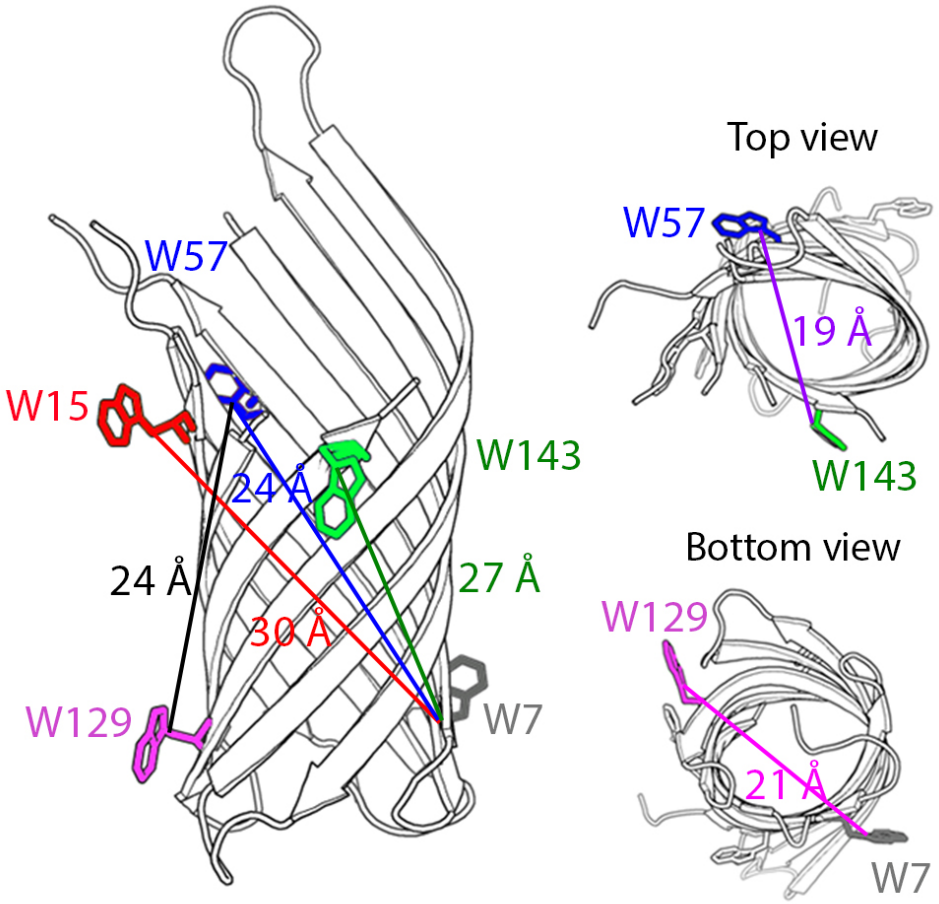

Figure 4.1 Structure of OmpA transmembrane domain (PDB code: 1QJP). Four native tryptophan residues at positions 7,15,57, and 143 are shown. One non-native tryptophan residue at position 129 has been modeled into the structure (Y129W). Distances correspond to C_γ-C_γ separation. Tryptophan donor is at position 15, 57, 129, or 143; IAEDANS acceptor is at position 7 or 57. See text for details.

Förster theory describes transfer of energy via dipole-dipole interactions between a donor and acceptor, and the transfer efficiency is inversely proportional to the sixth power of the distance.[17,18] FRET has been widely used for the measurement of inter- or intra-molecular dynamics on biomolecular systems.[19,20] The range of distances that can be accessed through FRET is generally accepted to be between $0.5R_0$ and $1.5R_0$, where R_0 is Förster distance.[21] When one assumes randomization of the orientations of donor and acceptor within the lifetime of the excited state, an orientation factor of 2/3 is conventionally used. The usage of 2/3 for κ^2 is a simplification, but one that is difficult to avoid given the challenges associated with determining κ^2. The use of 2/3 results in an error of ± 20% for distance, but still provides valuable data on the folding mechanisms.[22] Herein, FRET technique is utilized to probe the folding dynamics of OmpA in the presence of lipid bilayer as well as the refolded conformation in detergent micelles.

4.2 Methods and materials

4.2.1 Expression, purification, and labeling of OmpA

The protocol for the expression, isolation, and purification of OmpA is described in previous reports;[23] this procedure was originally adapted and modified from Surrey *et al*.[6] Three types of transmembrane (TM, 1-176 residues) OmpA mutants were generated by introducing a STOP codon at position 177 to remove the C-terminus (177-325 residues): (1) single tryptophan OmpA variants where one tryptophan residue was maintained at one of the native tryptophan positions (15, 57, or 143), or at a non-native position (Y129), (2) single tryptophan and single cysteine OmpA mutants where a tryptophan residue was located at one of the positions 15, 57, 129, or 143, and a cysteine residue was placed at one of the positions 7 or 57, and (3) single cysteine OmpA variants where the

cysteine residue was encoded at one of the positions 7 or 57. These families of mutants lead to donor-only, donor-acceptor, or acceptor-only proteins, respectively. To indicate that the mutants are truncated versions of OmpA that contain only the TM domain, the symbol Δ is added to the end of the mutant name.

For the cysteine-containing OmpA mutants, a dye molecule, 1,5-IAEDANS (5-((((2-iodoacetyl)amino)ethyl)amino)naphthalene-1-sulfonic acid, Molecular Probes; abbreviated as Dns), was conjugated at the cysteine residue. The protocol for dye conjugation reaction is described elsewhere and in Chapter 2.[24] Dye conjugated TM OmpA variants are classified as donor+acceptor OmpA, or acceptor-only OmpA depending on the presence or absence of a tryptophan donor, respectively.

A total of six unique donor+acceptor TM OmpA mutants were produced, along with their donor-only and acceptor-only counterparts. The nomenclature and description of the variants are tabulated in Table 4.1. For example, W15/F7CdnsΔ refers to a TM OmpA mutant with tryptophan donor at position 15, and Dns acceptor conjugated at a cysteine residue at position 7. The acceptor-only variant contains an acceptor conjugated at a cysteine at position 57, with no tryptophan residues in the protein. This acceptor-only variant is called W0/F57CdnsΔ. The donor-only variant is called W15Δ and the tryptophan-free, acceptor-free variant is called W0Δ.

Labeling yield of the extrinsic dye on OmpA was experimentally determined by UV/VIS absorption spectroscopy; the yield varied from 46 % to 95 % depending on the batch and mutant. The labeling efficiency is taken into account when calculating the overall energy transfer efficiency according to equation 1.3 (chapter 1), repeated as equation 4.2.[25]

Table 4.1 Summary of OmpA mutants. Donor (Trp) and Acceptor (Dns) locations as well as description of each mutant are indicated.

OmpA Mutants	Donor location	Acceptor location	Description
W15/F7CdnsΔ	15	7	D-A on same strand, across bilayer
W57/F7CdnsΔ	57	7	D-A across bilayer
W143/F7CdnsΔ	143	7	D-A across bilayer
W129/F57CdnsΔ	129	57	D-A across bilayer
W129/F7CdnsΔ	129	7	D-A across pore (outside of vesicle)
W143/F57CdnsΔ	143	57	D-A across pore (inside of vesicles)
W0Δ	-	-	Neither Donor nor Acceptor
W15Δ	15	-	Donor-only
W57Δ	57	-	Donor-only
W129Δ	129	-	Donor-only
W143Δ	143	-	Donor-only
W0/F7CdnsΔ	-	7	Acceptor-only
W0/F57CdnsΔ	-	57	Acceptor-only

4.2.2 Refolding, adsorption, and unfolding of OmpA

OmpA was refolded and inserted into liquid-crystalline phase of small unilamellar vesicles (SUVs) or detergent micelles. SUVs were prepared based on an established protocol.[23,24] For reconstitution of OmpA into SUVs, OmpA stock was added to 1 mg/mL of 1,2-dimyristoyl-*sn*-glycero-3-phosphocholine (DMPC, Avanti Polar Lipids) at a temperature above the phase transition temperature for DMPC, which is 24 °C. OmpA was also refolded into detergent micelles by combining protein with 10 mg/mL of the detergent n-octyl-b-D-glucopyranoside (OG) at room temperature. The adsorbed, but not inserted, form of OmpA was generated by adding the protein to a 1 mg/mL solution of 1,2-dipalmitoyl-*sn*-glycero-3-phosphocholine (DPPC, Avanti Polar Lipids) at a temperature below the phase transition temperature of DPPC, which is 41 °C; at the experimental temperature or 33 °C, DPPC is in the gel phase. Unfolded OmpA refers to OmpA that was solubilized in 8 M urea phosphate buffer (pH 7.3). SDS-PAGE and fluorescence spectroscopy were utilized to characterize the conformations of OmpA in a given solution.[13,26]

4.2.3 Steady-state absorption, circular dichroism, and fluorescence spectroscopy

Steady-state absorption spectra were recorded on an Agilent 8453 UV-visible spectrophotometer to determine the protein concentration and labeling efficiency. OmpA stock solutions were diluted immediately prior to collecting absorption spectra to remain in the appropriate range for the spectrometer. The protein concentration and labeling yields were estimated using the following extinction coefficients: ε_{280} = 26,018 $M^{-1}cm^{-1}$ (all donor-only TM OmpA with the exception of W129Δ), 24,441 $M^{-1}cm^{-1}$ (W129Δ

OmpA), and ε_{337} = 5960 $M^{-1}cm^{-1}$ (all acceptor-only OmpA mutants). The acceptor (Dns molecule) has an extinction coefficient at 280 nm of 1192 $M^{-1}cm^{-1}$.

Circular dichroism (CD) measurements were performed on an AVIV CD-215 (Aviv Associates, Lakewood, NJ). CD spectra were acquired from 190 nm to 260 nm at 1 nm interval steps, with an averaging time of 5 seconds per step, and a bandwidth of 1 nm. A ~ 6 μM protein sample was generated by manually mixing the protein in appropriate solution, and then placed in a fused quartz cuvette with a 1 mm pathlength that was quickly placed in a sample chamber purged with nitrogen gas held at 33 °C during the measurements. Corrected CD spectra were obtained by subtracting the corresponding blank spectra (buffer solution without protein).

Steady-state fluorescence spectra were obtained with a Jobin Yvon-SPEX Fluorolog FL3-11 spectrofluorometer. Protein samples of ~ 5 μM were excited at 290 nm (4 nm band-pass), and OmpA emission was recorded from 305 nm to 570 nm (4 nm band-pass) in 2 nm intervals and an integration time of 0.8 seconds. Spectra were collected in a 10 mm x 4 mm fused silica cuvette sealed with a rubber septum and stirred with a micro stir bar at 33 °C. The spectra for the corresponding buffer solutions were also obtained under the same experimental conditions to correct for background signal from lipid scattering and water Raman.

4.2.4 Data analysis for tryptophan fluorescence spectra

The observed OmpA emission contains not only tryptophan fluorescence but also scattering from lipids, water Raman, tyrosine fluorescence, and possibly dye fluorescence. In order to isolate fluorescence signal from tryptophan, contributions from lipids, buffer, tyrosine, and dye must be subtracted from the raw data. The data workup

procedure is as follows: first, the fluorescence signal was normalized by the protein concentration and lamp power. Lamp power was determined by comparing the water Raman signal on a given day with a standard Raman signal. Then, residual background from lipid scattering and tyrosine fluorescence was subtracted from spectra of donor+acceptor OmpA and donor-only OmpA by the following method. Donor+acceptor OmpA fluorescence spectra were corrected by subtracting spectra of the acceptor-only (tryptophan-free OmpA, which is either F7CdnsΔ or F57CdnsΔ). Similarly, the donor-only spectra were corrected by subtracting spectra of the tryptophan-free OmpA mutant (W0Δ). The scalars for these subtractions were systematically varied, and the resulting difference spectrum was compared to the known spectra of fully folded or unfolded OmpA. The scaling factor was optimized by focusing on the slope of the corrected fluorescence spectra in the rising portion of the spectrum (~ 305 nm to 355 nm). The scalar was varied until the slope converged to a value between the known slopes for OmpA of 0.025 (folded) and 0.030 (unfoleded). These slopes were previously determined by analyzing high-concentration OmpA in fully folded or unfolded conformations, and determining the slopes for these basis spectra that were normalized to maximum intensity of 1.0. Results of the workup procedure for W15Δ and W15/F7CdnsΔ are shown in Figure 4.2, and the results of other OmpA variants are shown in Figure 4.3 – Figure 4.5.

In addition to intensity analysis, average wavelengths of emission were determined. The average emission wavelength, $< \lambda >$ is calculated by $< \lambda > = \Sigma(F_i\lambda_i) / \Sigma(F_i)$ where λ_i and F_i are the wavelength and fluorescence intensity between 310 and 370 nm.[27] The average emission wavelength was utilized to probe the change of local environments near

tryptophan from hydrophilic to hydrophobic. All data analysis was performed using Igor Pro 6 (WaveMetrics) software.

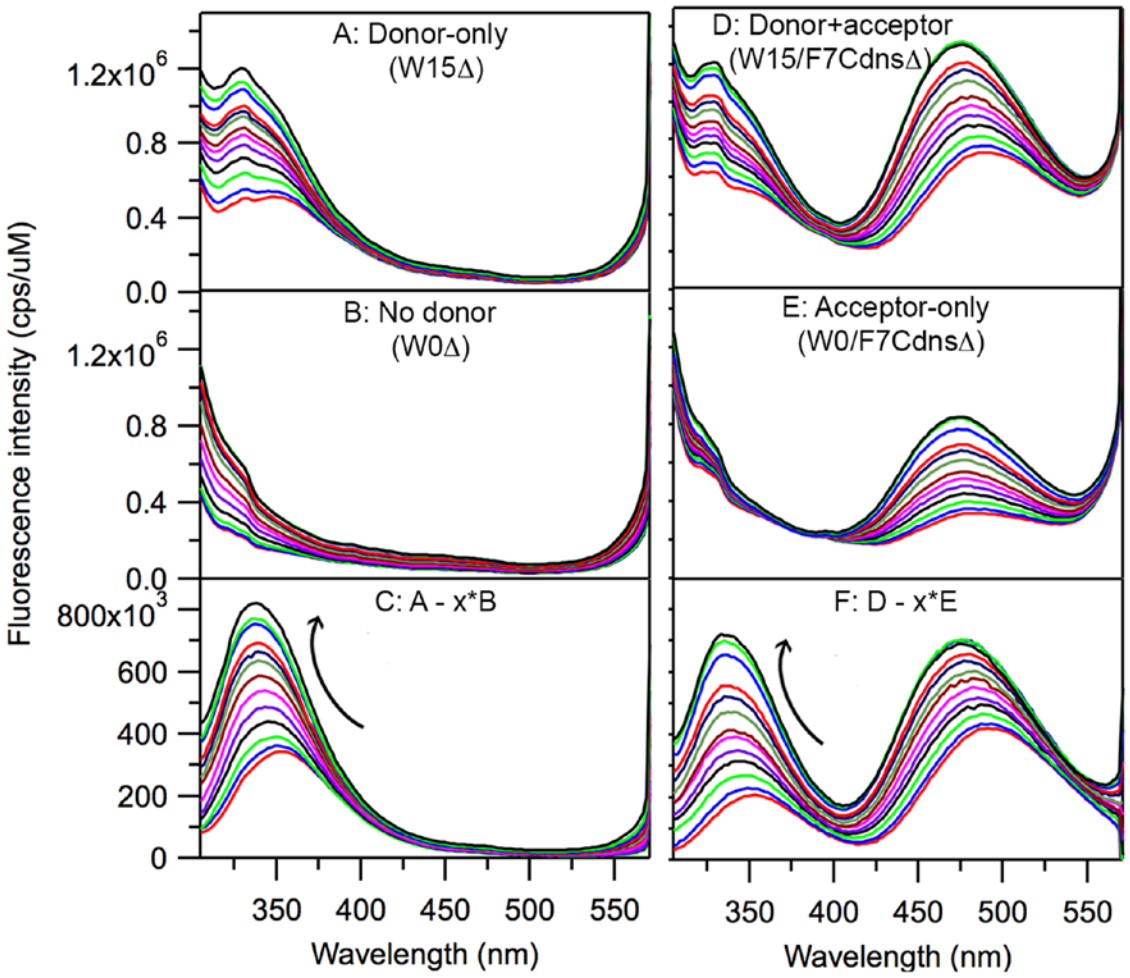

Figure 4.2 Representative workup procedure for FRET data. Fluorescence spectra of OmpA with donor-only at position 15 (W15Δ, panel A), no donor (W0Δ, panel B), and difference (panel C = A – x*B, where x is a scalar). Fluorescence spectra of OmpA with donor and acceptor (W15/F7CdnsΔ, panel D), acceptor-only (W0/F7CdnsΔ, panel E), and difference (panel F = D – x*E). Spectra were collected 2, 5, 10, 15, 20, 25, 30, 40, 50, 60, 120, 180, and 240 minutes after initiation of folding reaction. Difference spectra in panel C show signal from donor after tyrosine and scattering contributions have been subtracted. Difference spectra in panel F show signal from donor and remaining acceptor after tyrosine, acceptor-only, and vesicle scattering contributions have been subtracted.

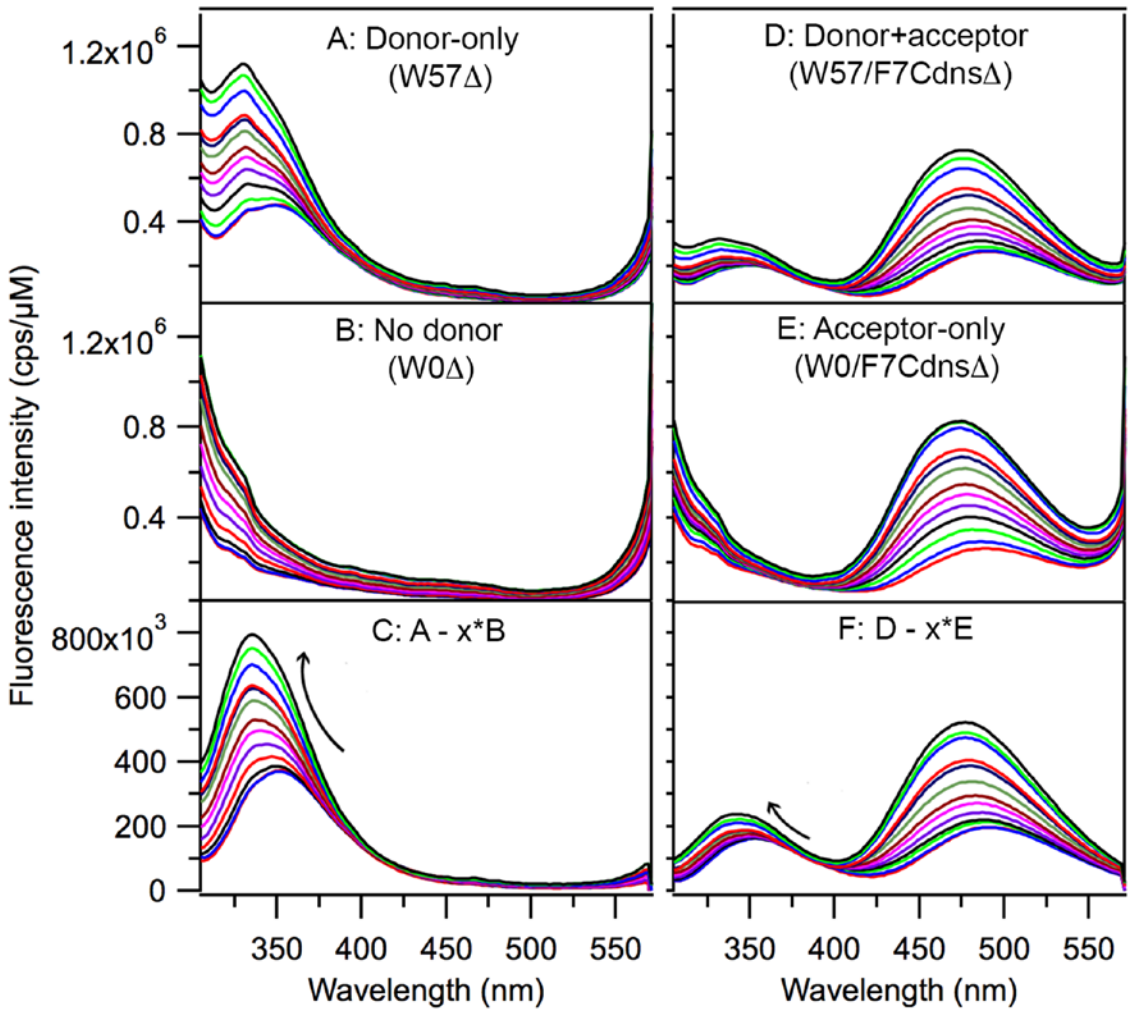

Figure 4.3 Fluorescence spectra of OmpA with donor-only at position 57 (W57Δ, panel A), no donor (W0Δ, panel B), and difference (panel C = A – x*B, where x is a scalar). Fluorescence spectra of OmpA with donor and acceptor (W57/F7CdnsΔ, panel D), acceptor-only (W0/F7CdnsΔ, panel E), and difference (panel F = D – x*E). Spectra were collected 2, 5, 10, 15, 20, 25, 30, 40, 50, 60, 120, 180, and 240 minutes after initiation of folding reaction. Difference spectra in panel C show signal from donor after tyrosine and scattering contributions have been subtracted. Difference spectra in panel F show signal from donor and remaining acceptor after tyrosine, acceptor-only, and vesicle scattering contributions have been subtracted.

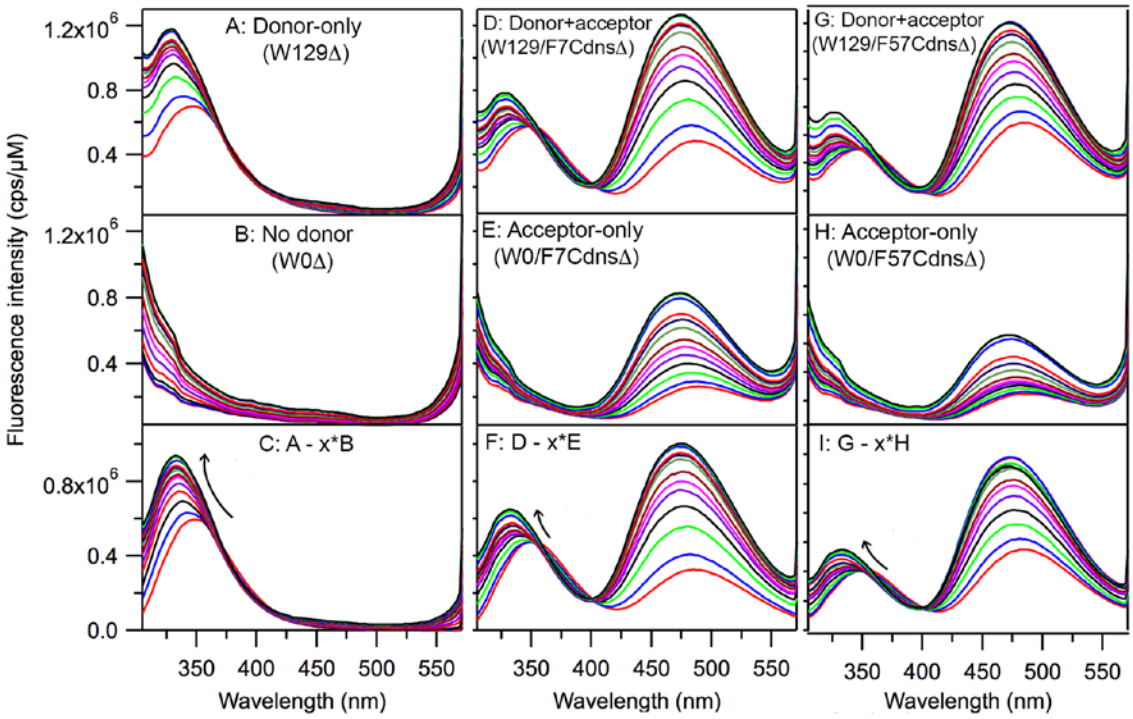

Figure 4.4 Fluorescence spectra of OmpA with donor-only at position 129 (W129Δ, panel A), no donor (W0Δ, panel B), and difference (panel C = A – x*B, where x is a scalar). Fluorescence spectra of OmpA with donor and acceptor (W129/F7CdnsΔ, panel D; W129/F57CdnsΔ, panel G), acceptor-only (W0/F7CdnsΔ, panel E; W0/F57CdnsΔ, panel H), and difference (panel F = D – x*E; panel I = G - x*H). Spectra were collected 2, 5, 10, 15, 20, 25, 30, 40, 50, 60, 120, 180, and 240 minutes after initiation of folding reaction.

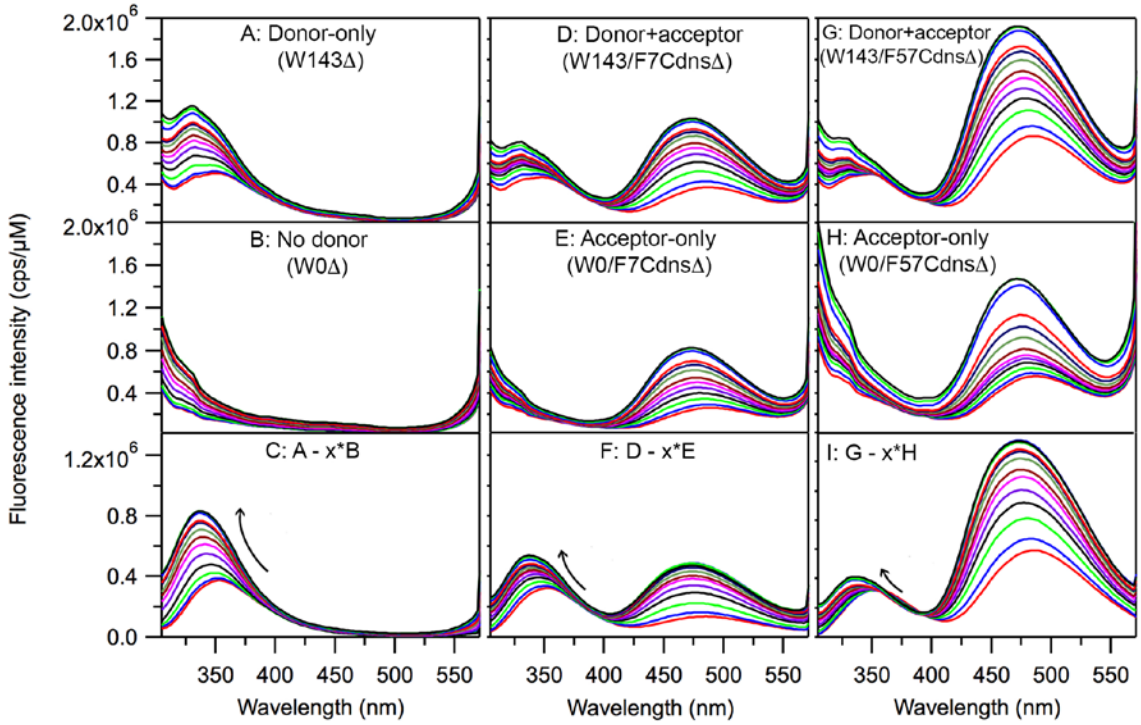

Figure 4.5 Fluorescence spectra of OmpA with donor-only at position 143 (W143Δ, panel A), no donor (W0Δ, panel B), and difference (panel C = A – x*B, where x is a scalar). Fluorescence spectra of OmpA with donor and acceptor (W143/F7CdnsΔ, panel D; W143/F57CdnsΔ, panel G), acceptor-only (W0/F7CdnsΔ, panel E; W0/F57CdnsΔ, panel H), and difference (panel F = D – x*E; panel I = G - x*H). Spectra were collected 2, 5, 10, 15, 20, 25, 30, 40, 50, 60, 120, 180, and 240 minutes after initiation of folding reaction.

4.3 Results

4.3.1 Structures of OmpA in different environments

Representative CD spectra of TM OmpA mutants in different folding/unfolding conditions are shown in Figure 4.6. In 0.5 M urea solution in the absence of SUVs or detergent, CD spectra of OmpA did not show spectral characteristics of β-sheet structure. When OmpA was adsorbed on gel-phase DPPC SUVs, the CD spectra showed a minimum at ~ 212 nm, which is consistent with at least partial β-sheet. The CD spectra of OmpA refolded into liquid-crystalline phase DMPC SUVs and detergent micelle are virtually identical, with a minimum at ~ 216, which indicates formation of significant β-sheet content. CD spectra were also acquired for a set of FRET mutants to ensure that the folding process was not affected by attachment of the extrinsic acceptor label: donor-only (W15Δ, dotted line), acceptor-only (W0/F7CdnsΔ, dashed line), and donor+acceptor (W15/F7CdnsΔ, solid line) OmpA. The results indicate that the secondary structure was preserved upon addition of the label for almost all the donor-acceptor mutants. One donor+acceptor mutant, W57/F7CdnsΔ, failed to form native-like secondary structure; it did not correctly form β-sheet structure like the other mutants. We will further discuss this mutant below. All CD spectra of donor-only mutants were identical to those from a previous study, indicating native-like β-sheet structure regardless of the location of tryptophan residue.[13]

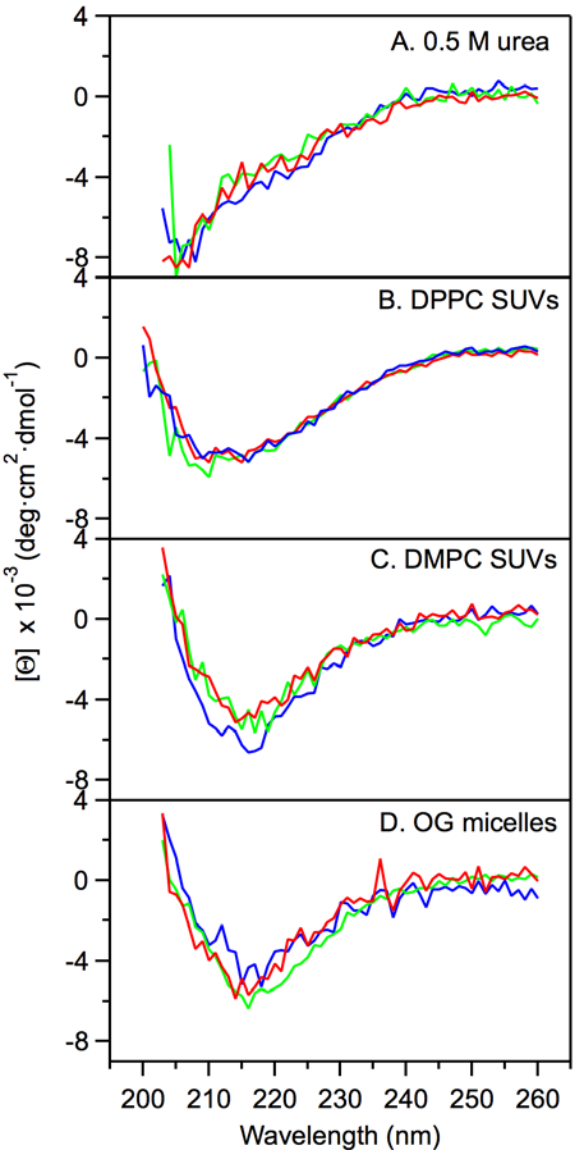

Figure 4.6 CD spectra of donor-only (W15Δ, blue), acceptor-only (W0/F7CdnsΔ, green), donor+acceptor (W15/F7CdnsΔ, red) TM OmpA in various buffer solutions: (A) 0.5 M urea solution, (B) DPPC SUVs, (C) DMPC SUVs, (D) OG detergent micelles.

FRET efficiencies were determined for all mutants. Representative tryptophan fluorescence spectra for W129/F7CdnsΔ (donor+acceptor TM OmpA) and W129Δ (donor-only TM OmpA) are shown in Figure 4.7. The quenching of tryptophan fluorescence in the presence of an acceptor directly reveals change in structure as a result of conformational change. In 8 M urea, OmpA has no secondary and tertiary structure and is considered random coil.[28] The FRET data support that the donor and acceptor are far apart in this random coil; the fluorescence intensity of W129/F7CdnsΔ decreased about 6 % compared to that of W129Δ, indicating negligible energy transfer from donor to acceptor in this unfolded state. As an adsorbed species, the fluorescence intensity of OmpA decreased 12 % in the presence of an energy acceptor because the overall structure of OmpA is more compact relative to the unfolded state. When W129/F7CdnsΔ was completely reconstituted and folded in DMPC SUVs, the fluorescence intensity was quenched 31 % compared to that of donor-only W129Δ. The quenching was similar when the protein was folded in detergent micelles: For refolded W129/F7CdnsΔ in OG, tryptophan fluorescence was attenuated about 28 %. Based on the steady-state measurements, we calculated energy transfer efficiencies for all OmpA mutants in various folding conditions.

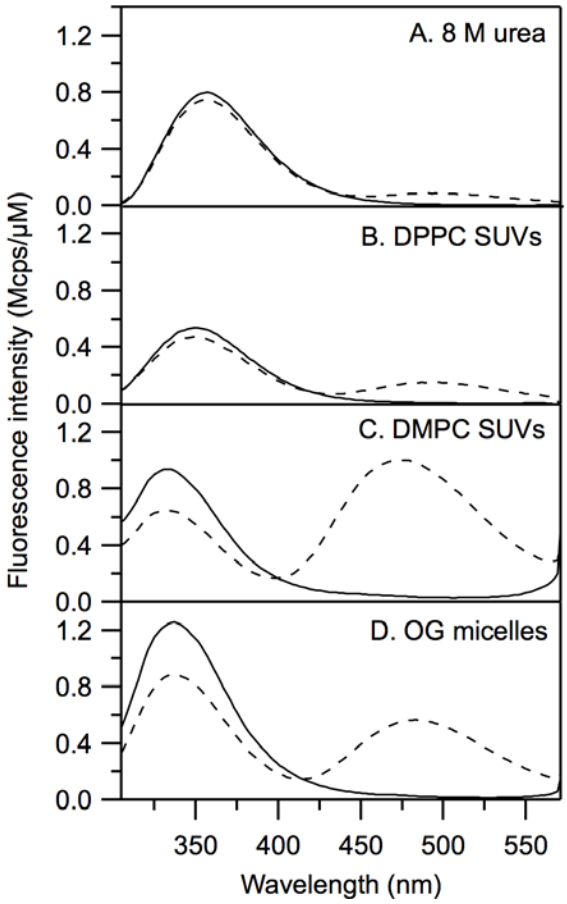

Figure 4.7 Representative fluorescence spectra of donor+acceptor (W129/F7CdnsΔ, dashed) and donor-only (W129Δ, solid) OmpA in various solutions (conformation): (A) 8 M urea (unfolded), (B) DPPC SUVs (adsorbed), (C) DMPC SUVs (folded), and (D) detergent micelle (folded).

4.3.2 Kinetics for formation of secondary and tertiary structures

Figure 4.8 displays steady-state CD spectra for one set of donor-only (W15Δ), acceptor-only (W0/F7CdnsΔ), and donor+acceptor (W15/F7CdnsΔ) OmpA mutants during refolding into DMPC SUVs. CD spectra were acquired at: 0, 10, 20, 30, 40, 50, 60, 80, 100, 120, 150, and 180 minutes (spectra colored from red to purple). CD spectra of OmpA in 0.5 M urea solution without DMPC SUVs are also shown as black solid line, and this spectrum is similar to the early CD spectra during refolding of OmpA in DMPC SUVs. It indicates that the initial state of refolding is close to the denatured state in the absence of DMPC SUVs. Within 10 - 20 minutes (orange spectra), β-sheet featured peak where centered at 216 nm was started to develop for donor+acceptor, donor-only and acceptor-only OmpA spectra, suggesting the early stage of secondary structure formation and the completion of evolution within one hour. As noted in Figure 4.6, the kinetics of formation of secondary structure were also not hindered regardless of the attachment of dye chromophore at position 7 by comparison of donor-only and donor+acceptor OmpA mutants.

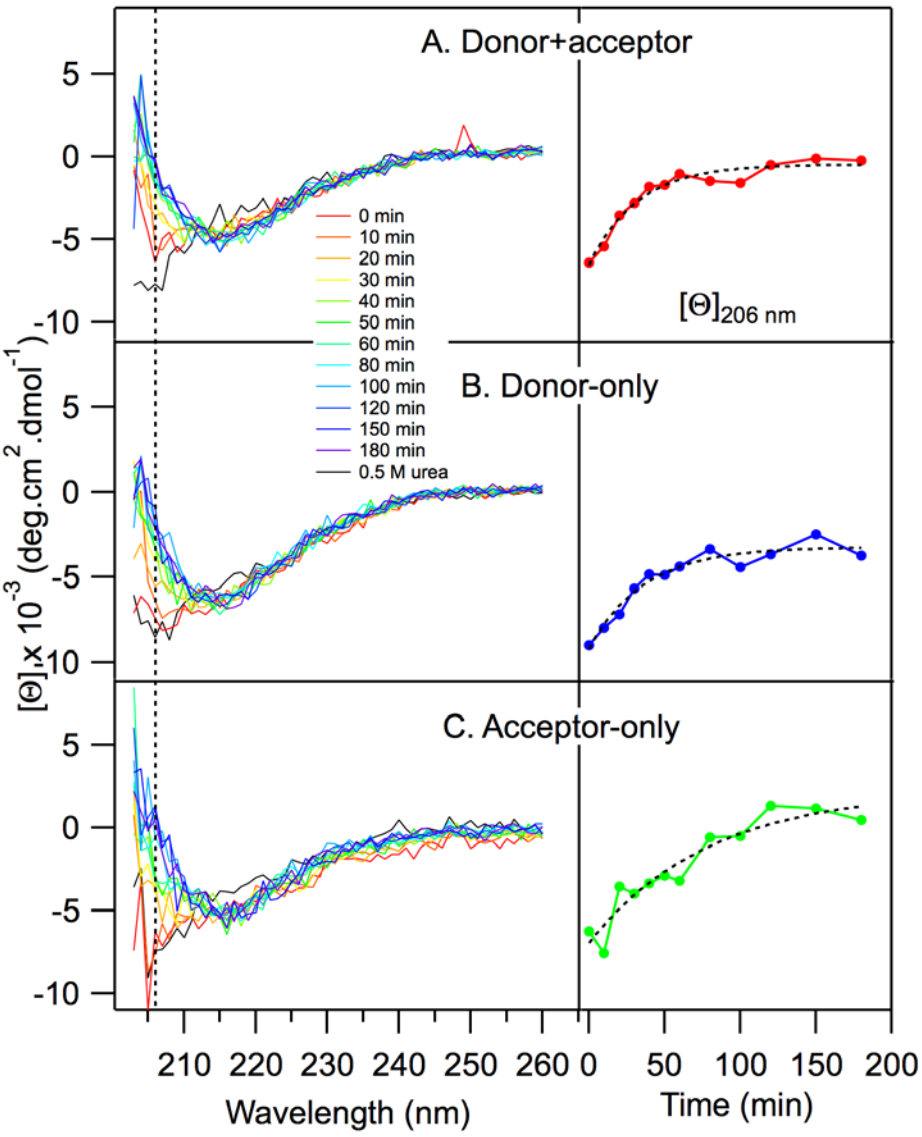

Figure 4.8 CD spectra (left panels) and kinetics of ellipticity at 206 nm (right panels) of OmpA during refolding in DMPC SUVs for 180 minutes after initiation of folding reaction. The black solid curve is the unfolded state in 0.5 M urea solution. (A) donor+acceptor (W15/F7CdnsΔ), (B) donor-only (W15Δ), and (C) acceptor-only (W0/F7CdnsΔ) TM OmpA. The colored curves (from red to purple) are 0, 10, 20, 30, 40, 50, 60, 80, 100, 120, 150, and 180 minutes after initiation the folding event.

Förster distance, R_0, of the donor tryptophan and acceptor Dns was calculated using the following Equation 4.1:

$$R_0^6 = (8.79 \times 10^{23})(\kappa^2 n^{-4} \Phi_D J_{DA}) \quad 4.1$$

in which R_0 is the Förster distance, κ^2 is the orientation factor, n is refractive index, Φ_D is the quantum yield of donor in the absence of acceptor, and J_{DA} is the spectral overlap between the emission spectra of donor-only and the absorption spectra of acceptor-only TM OmpA. We applied the averaging value of 2/3 for κ^2, 1.33 for n, 0.13 – 0.25 for Φ_D, and experimentally determined J_{DA}, obtaining average R_0 of 24.1 Å consistent with the previously reported value for Trp-Dns pair.[25]

Equation 4.2 was used to calculate FRET efficiency to account for incomplete labeling yield

$$E = \left(1 - \frac{F_{DA}}{F_D}\right)\frac{1}{f_A} \quad 4.2$$

where E is the FRET efficiency, F_{DA} and F_D are tryptophan fluorescence intensity at 350 nm in the presence and absence of the acceptor, respectively, and f_A is the experimentally determined labeling yield of the acceptor. To calculate the energy transfer efficiency depending for all FRET pairs, donor-only, donor-acceptor, acceptor-only, and no-tryptophan OmpA mutants were exposed to various aqueous conditions: 8 M urea, 1 mg/mL DPPC SUVs, 1 mg/mL DMPC SUVs, and 10 mg/mL OG micelles. The distances between donor and acceptor were calculated by the following equation: $E = R_0^6/(R_0^6 + r^6)$ from the energy transfer efficiency, which are shown for six TM OmpA variants in Figure 4.6.

During four hours of observation for folding process into DMPC SUVs, significant structural changes were completed within one hour except for two mutants, W15/F7CdnsΔ and W143/F7CdnsΔ. Additionally, the donor and the acceptor moved toward each other during folding for all variants except W15/F7CdnsΔ, which moved apart during folding because they are located on the same strand. For W143/F7CdnsΔ, two out of three experiments displayed the trends that donor and acceptor came close to each other within the first hour, and then they moved apart during the last three hours. This motion may be related to the equilibration of structure after major conformational change was completed within the first hour. For refolded OmpA in detergent micelle, the distances between the donor and the acceptor were larger compared to that in DMPC SUVs, suggesting slight different structures of folded states depending on environment. Two mutants were designed to investigate changes in pore size during folding: W143/F57CdnsΔ places donor and acceptor at the inserting portion of OmpA (interior of vesicle) and W129/F7CdnsΔ places donor-acceptor at the trailing portion of OmpA (exterior of vesicle). Figure 4.9 (b) shows the average distances across the pore. In DMPC SUVs, the diameters for the inserting portion (interior of vesicle, W143/F57CdnsΔ) and trailing portion (W129/F7CdnsΔ) were 21.6 Å and 24.8 Å, respectively. In contrast to the refolded state in DMPC SUVs, refolded state of W143/F57CdnsΔ and W129/F7CdnsΔ in detergent micelles displayed almost identical pore size of 25.8 Å and 26.9 Å, respectively.

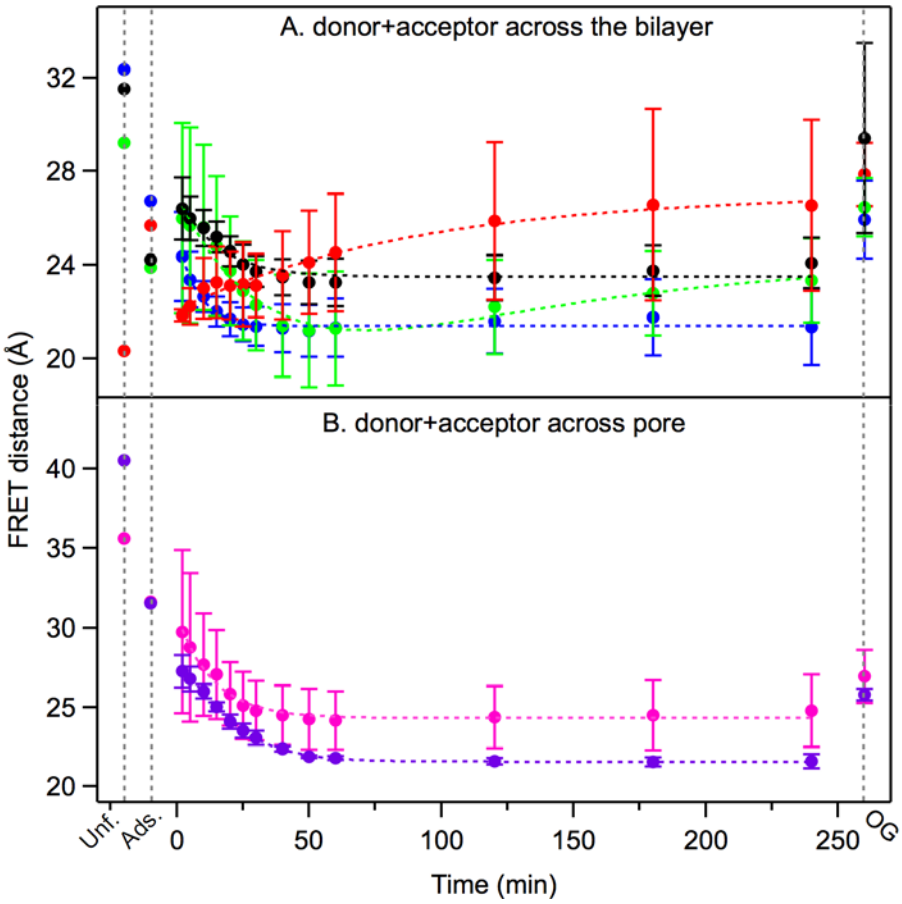

Figure 4.9 FRET distances of OmpA in 8 M urea ('Unf.'), adsorbed on DPPC SUVs ('Ads.'), during folding in DMPC SUVs at 2 to 240 minutes after initiation of the folding reaction, and in detergent micelles ('OG'). Data are for OmpA mutants with (A) donor + acceptor across the bilayer: W15/F7CdnsΔ (red), W129/F57CdnsΔ (black), W143/F7CdnsΔ (green), and W57/F7CdnsΔ (blue); (B) donor + acceptor OmpA across pore: W129/F7CdnsΔ (pink), W143/F57CdnsΔ (purple). All data were fit to single exponential functions with the exception of W143/F7CdnsΔ (green), which was fit to a double exponential function. Fits are shown as dashed curves, and parameters are in Table 4.2.

Figure 4.10 displays the average emission wavelength of tryptophan fluorescence for donor-only OmpA. The average tryptophan emission wavelength of unfolded OmpA in 8 M urea was ~ 347 nm regardless of the mutant. In gel phase DPPC SUVs, the tryptophan residue was partially buried with average emission wavelengths of 341, 344, and 345 nm. During folding and insertion into DMPC SUVs, the emission peaks blue-shifted to ~ 340 nm. The W129Δ mutant had the most blue-shifted emission maximum. We also measured the thermodynamics of W129 and W129Δ mutants to augment previous reports.[23,29] Free energies of unfolding were determined by plotting the fraction unfolded as a function of urea concentration and fitting with two-state model.[30] As shown in Figure 4.11, the calculation gave rise to free energies of 7.0 kcal/mol and 5.9 kcal/mol, respectively.

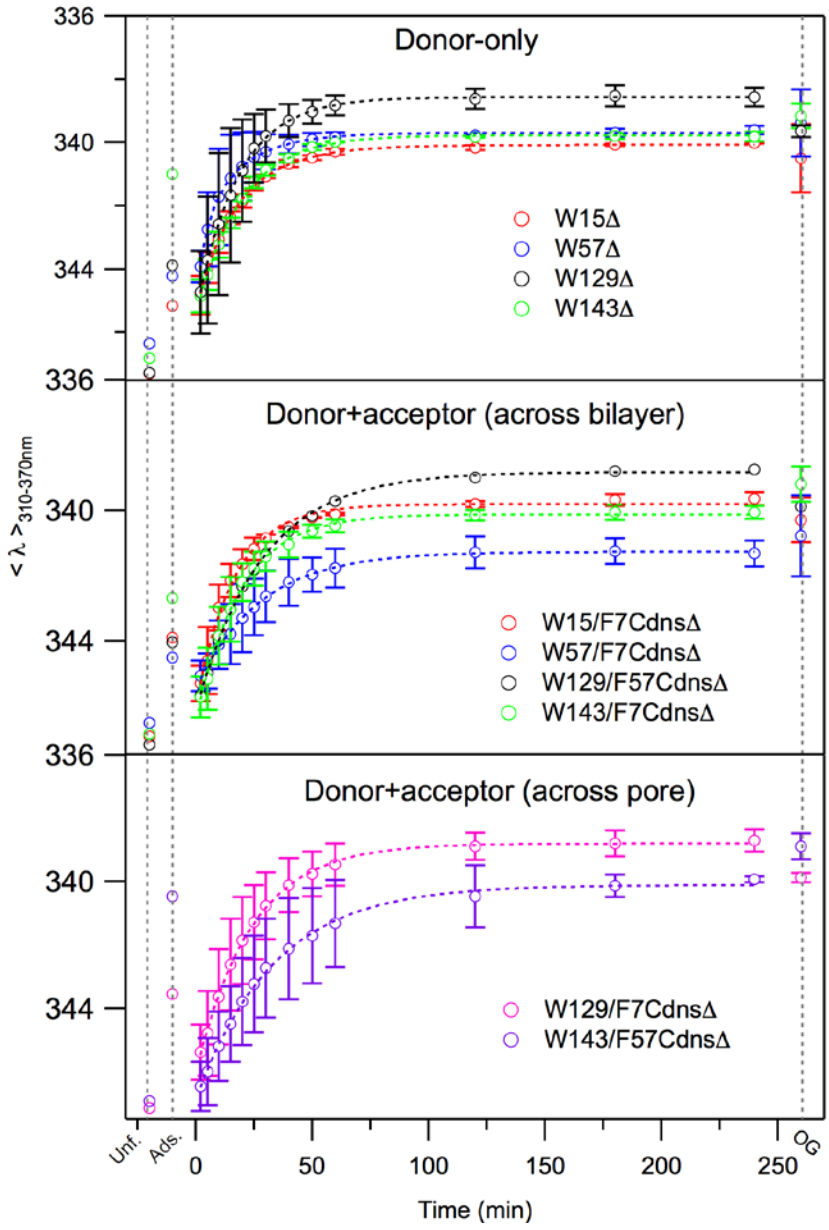

Figure 4.10 Average tryptophan emission for unfolded OmpA in 8 M urea (Unf.), adsorbed OmpA in DPPC SUVs, during folding in DMPC SUVs, and folded in detergent micelles (OG). (Top) Four donor-only OmpA mutants: W15Δ (red), W57Δ (blue), W129Δ (black), and W143Δ (green). (Middle) Four donor+acceptor OmpA mutants where donor and acceptor are positioned across the bilayer: W15/F7CdnsΔ (red), W57/F7CdnsΔ (blue), W129/F57CdnsΔ (black), and W143/F7CdnsΔ (green). (Bottom) two donor+acceptor OmpA mutants where donor and acceptor are positions across the pore: W129/F7CdnsΔ (pink), and W143/F57CdnsΔ (purple). Dashed curves are fits to the data using a single exponential function. Fit parameters are listed in Table 4.2.

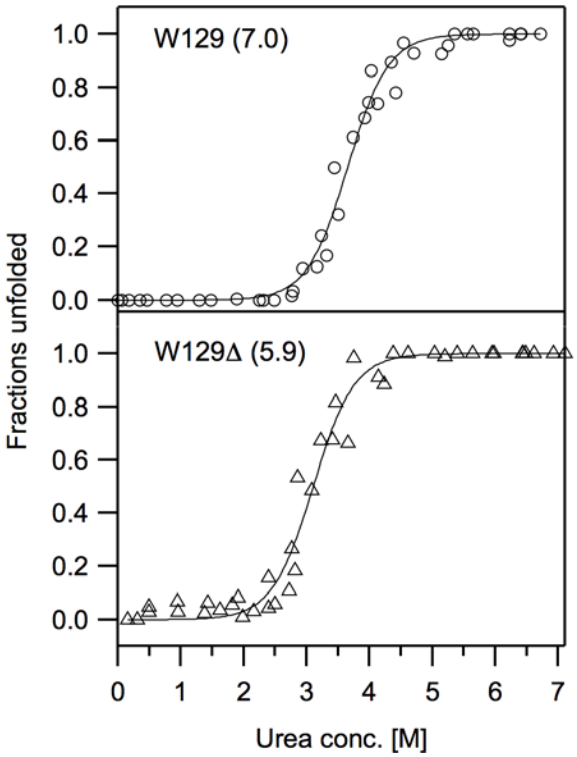

Figure 4.11 Unfolding curves and Gibbs free energies of unfolding (kcal/mol) of W129 and W129Δ OmpA based on tryptophan fluorescence decomposition method. See text for details.

4.4 Discussion

4.4.1 Formation of secondary and tertiary structure during folding

We have probed the evolution of the distance between donor and acceptor during folding of OmpA into lipid bilayer. Based on the FRET results, major conformational change is completed within the first hour, followed by minor structural changes attributed to strand extension and equilibration. Previous experiments with brominated lipids determined that each tryptophan residue moves across the membrane at similar rates.[10] The current CD data and FRET results suggest that the evolution of secondary and tertiary structures occur in similar time scales. As shown in Figure 4.8, the β-sheet structure appears within 20 minutes, yet the CD spectra continue to evolve for 50 minutes. Therefore, both CD and FRET data show changes that continue for 50-60 minutes. A summary of the kinetics associated with CD and fluorescence spectra are shown in Table 4.2.

Table 4.2 Summary of kinetics for average tryptophan emission (from Figure 4.10), FRET distance (from Figure 4.9), and ellipticity at 206 nm (from Figure 4.8). The curves that describe the average tryptophan emission (three trials), FRET distance (three trials), and ellipticity (one trial) were fitted to single exponential functions. Protein:lipids = 1:250-300. *FRET data for W143/F7CdnsΔ were fit to double exponential function.

	Trp emission shift	FRET distance	$[\theta]_{206nm}$ of CD spectra	description
mutants	tau (min) ± stdv (min)	tau (min) ± stdv (min)	tau (min) ± stdv (min)	
W15Δ	17.9 ± 0.4	NA	37 ± 7	Donor-only
W15/F7CdnsΔ	16.4 ± 0.9	90 ± 20	32 ± 5	Across pore, Same strand D and A
W0/F7CdnsΔ			80 ± 30	Acceptor-only
W57Δ	12.3 ± 0.7	NA		Donor-only
W57/F7CdnsΔ	27 ± 1	8 ± 1		Incomplete folding
W143Δ	19.2 ± 0.6	NA		Donor-only
W143/F7CdnsΔ*	19.2 ± 0.7	46 ± 150 and 67 ± 300		Across bilayer
W143/F57CdnsΔ	33 ± 1	21.6 ± 1.4		Across pore
W129Δ	18.0 ± 0.4	NA		Donor-only
W129/F7CdnsΔ	23.6 ± 0.6	14.0 ± 1.5		Across bilayer
W129/F57CdnsΔ	28.1 ± 0.5	15 ± 3		Across pore

Our FRET data show differences in structure of OmpA in lipid bilayer and in OG micelles. The distances between donor and acceptor were overall larger for OmpA in micelles than in SUVs. This observation suggests that the refolded conformation in SUVs is more compact than in micelles. Furthermore, while the distance across the pore was nearly identical in both sides of the pore, the distances were not symmetric for OmpA in SUVs, with one end of the pore larger than the other end. Specifically, the inserting end of the pore in SUVs is more compact than the trailing end, which might reflect differences in pressure between the inner and external portions of the vesicle. In contrast, detergent micelles may apply equal pressure on the entire β-barrel. The compactness of the barrel may affect the penetration of water and overall flexibility of the structure.[12] The structural variation in DMPC SUVs vs. in OG detergent micelles was also reported from previous experimental and theoretical studies.[12,13]

4.4.2 Limitation and possible error in FRET calculation

Depending on the distance of interest, a specific donor and an acceptor are chosen to measure the energy transfer efficiency. As discussed earlier, we utilized an intrinsic fluorophore, tryptophan residue, as an energy donor and an extrinsic fluorophore, 1,5-IAEDANS, as an energy acceptor. This FRET-pair is a commonly used donor-acceptor pair and reveals relevant distances of ~$0.5R_0$ (12 Å) to ~$1.5R_0$ (36 Å). The FRET technique is also suited for monitoring relative conformational changes (e.g. folding process) as opposed to absolute distances in case some properties of the dyes are not known, or if the size of the dye chromphore artificially gives rise to larger absolute distance.[31] Generally, the introduction of dye molecule does not impede the development of structure in biomolecular systems.[31] Yet, we observed that one of the labeled mutants

did not form secondary structure properly; W57/F7CdnsΔ did not show the spectral feature of β-sheet. Figure. 4.12 compares CD spectra of donor+acceptor, donor-only, and acceptor-only OmpA variants, and shows that W57/F7CdnsΔ did not fold properly. In addition to improper folding, incomplete labeling of an extrinsic dye is another potential complication that results in misinterpretation of FRET efficiency. Thus, the calculation of the energy transfer has to be carefully done by considering the labeling efficiency of protein.

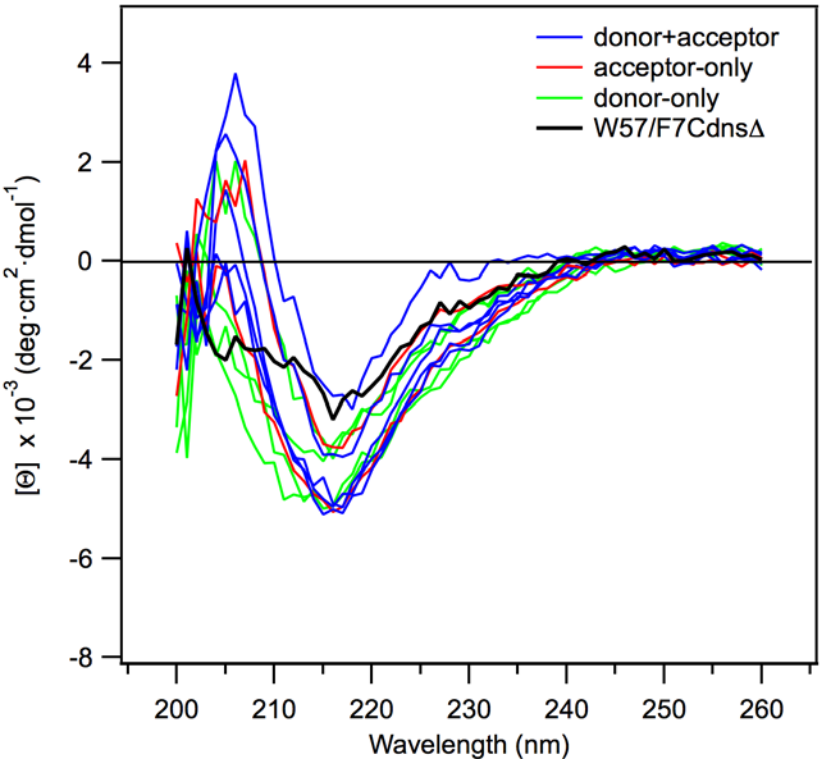

Figure 4.12 CD spectra for refolded states of donor+acceptor mutants (blue), acceptor-only mutants (red), and donor-only mutants (green) in DMPC SUVs. The single, improperly folded mutant W57/F7CdnsΔ is shown as a solid black curve.

4.5 Summary

FRET is useful to monitor the relative conformational change of membrane protein during folding process. Incomplete labeling yield and effect of label on structure should be considered before calculating FRET efficiencies. Our fluorescence data illustrate the kinetics of formation of structure, and show that the tertiary structure is formed within the first hour. CD and FRET data suggest that the formation of secondary and tertiary structure occur on similar timescales. Furthermore, the folded structure of OmpA in lipid bilayer may be different from that in detergent micelles. The compactness of the barrel and asymmetric pore size affect the overall structure on OmpA and water permeability of OmpA. As an ongoing project, FRET can be carried out to explore the effects of Skp, one of the native perisplasmic chaperones of OmpA, on the folding kinetics and structural modifications of OmpA during folding,[32] and this project is being pursued in our group.

4.6 Acknowledgements

Chapter 4, in part, is currently being prepared for submission for publication of the material. Kang, Guipeun; Asamoto, Deeann; and Kim, Judy E. The dissertation author was the primary investigator and author of this material.

4.7 References

(1) Fagerberg, L.; Jonasson, K.; von Heijne, G.; Uhlen, M.; Berglund, L. *Proteomics* **2010**, *10*, 1141.

(2) Wallin, E.; Heijne, G. V. *Protein Sci.* **1998**, *7*, 1029.

(3) von Heijne, G. *Annu Rev Bioph Biom* **1994**, *23*, 167.

(4) Kleinschmidt, J. *Cell. Mol. Life Sci.* **2003**, *60*, 1547.

(5) Chen, G. Q.; Gouaux, E. *Biochemistry-Us* **1999**, *38*, 15380.

(6) Surrey, T.; Jahnig, F. *P Natl Acad Sci USA* **1992**, *89*, 7457.

(7) Kleinschmidt, J. H.; Tamm, L. K. *Biochemistry-Us* **1996**, *35*, 12993.

(8) Surrey, T.; Jahnig, F. *J Biol Chem* **1995**, *270*, 28199.

(9) Kleinschmidt, J. H.; Tamm, L. K. *J Mol Biol* **2002**, *324*, 319.

(10) Kleinschmidt, J. H.; den Blaauwen, T.; Driessen, A. J. M.; Tamm, L. K. *Biochemistry-Us* **1999**, *38*, 5006.

(11) Kleinschmidt, J. H.; Wiener, M. C.; Tamm, L. K. *Protein science : a publication of the Protein Society* **1999**, *8*, 2065.

(12) Bond, P. J.; Sansom, M. S. P. *Journal of Molecular Biology* **2003**, *329*, 1035.

(13) Kim, J. E.; Arjara, G.; Richards, J. H.; Gray, H. B.; Winkler, J. R. *J Phys Chem B* **2006**, *110*, 17656.

(14) Arora, A.; Abildgaard, F.; Bushweller, J. H.; Tamm, L. K. *Nat. Struct. Biol.* **2001**, *8*, 334.

(15) Pautsch, A.; Schulz, G. E. *Nat Struct Biol* **1998**, *5*, 1013.

(16) Pautsch, A.; Schulz, G. E. *J Mol Biol* **2000**, *298*, 273.

(17) Forster, T. *Discuss Faraday Soc* **1959**, 7.

(18) Förster, T. *Ann Phys-Berlin* **1948**, *2*, 55.

(19) Corradi, G. R.; Adamo, H. P. *Journal of Biological Chemistry* **2007**, *282*, 35440.

(20) Sanchez, K. M.; Schlamadinger, D. E.; Gable, J. E.; Kim, J. E. *J. Chem. Educ.* **2008**, *85*, 1253.

(21) dosRemedios, C. G.; Moens, P. D. J. *J Struct Biol* **1995**, *115*, 175.

(22) dos Remedios, C. G.; Miki, M.; Barden, J. A. *J Muscle Res Cell Motil* **1987**, *8*, 97.

(23) Sanchez, K. M.; Gable, J. E.; Schlamadinger, D. E.; Kim, J. E. *Biochemistry-Us* **2008**, *47*, 12844.

(24) Kang, G. P.; Lopez-Pena, I.; Oklejas, V.; Gary, C. S.; Cao, W. H.; Kim, J. E. *Biochimica Et Biophysica Acta-Biomembranes* **2012**, *1818*, 154.

(25) Lakowicz, J. R. *Springer: New York* **2006**.

(26) Arora, A.; Rinehart, D.; Szabo, G.; Tamm, L. K. *J Biol Chem* **2000**, *275*, 1594.

(27) Huysmans, G. H. M.; Baldwin, S. A.; Brockwell, D. J.; Radford, S. E. *Proceedings of the National Academy of Sciences of the United States of America* **2010**, *107*, 4099.

(28) Schweizer, M.; Hindennach, I.; Garten, W.; Henning, U. *European journal of biochemistry / FEBS* **1978**, *82*, 211.

(29) Kang, G. L.-P., Ignacio;Bhakta, Saajan; Kim, Judy E. *Encyclopedia of Analytical Chemistry* **2013**, 1.

(30) Pace, C. *Methods Enzymol.* **1986**, *131*, 266.

(31) Lakey, J. H.; Baty, D.; Pattus, F. *J Mol Biol* **1991**, *218*, 639.

(32) Bulieris, P. V.; Behrens, S.; Holst, O.; Kleinschmidt, J. H. *Journal of Biological Chemistry* **2003**, *278*, 9092.

Chapter 5. Probing membrane protein structure and dynamics by fluorescence

Chapter 5, in part, is a reprint of the material as it appears

in *Encyclopedia of Analytical Chemistry*, 1-21, 2013.

5.1 Introduction

Fluorescence spectroscopy is a primary research tool for the study of biomolecules. The inherent sensitivity of the fluorescence process to chromophore structure and dynamics allows for the investigation of a wide range of microscopic properties, such as local hydrophobicity and viscosity, excited-state proton and electron transfer rates, conformational changes, as well as rotational flexibility of the chromophore.[1-7] Other properties can also be easily interrogated by utilizing a variety of biologically-compatible fluorescent molecules; for example, macromolecular images of complex systems as well as measurements of nanometer-scale distances on the single-molecule level can be achieved.[8,9] This breadth of information may be obtained for a diverse set of biomolecules, including nucleic acids, peptides, ligands, proteins, and complex higher-ordered systems. The fact that fluorescence spectroscopy is capable of providing insights on families of proteins that are both very easy and extremely challenging to handle makes this tool a significant one in the general study of protein structure and dynamics.

Membrane proteins constitute a large family of biomolecules that continue to challenge experimentalists and theorists. They comprise a significant fraction of proteins in the genome and constitute the majority of drug targets.[10] Additionally, membrane-

bound proteins and peptides are associated with a broad range of diseases, such as type 2 diabetes and cystic fibrosis.[11,12] Despite their prevalent roles in biology as gates, pumps, and receptors, there is a lack of knowledge on the structure and dynamics of membrane proteins, especially in comparison to soluble proteins. This limitation is a direct consequence of the inherent difficulties associated with handling these hydrophobic biomolecules. Therefore, techniques that exhibit high sensitivity on low concentrations of protein are preferred and ideal for the study of membrane proteins. In particular, fluorescence spectroscopy is one of the most widely-utilized and successful tools for the study of membrane-associated proteins. The goal of this review is to provide a brief overview of fluorescence spectroscopy, and illustrate the insights that can be gained on membrane proteins with this straightforward technique. Special focus will be placed on the most widely-utilized native fluorophore, tryptophan, but some examples of extrinsic fluorescence quenchers and dyes will be described.

5.2 Background

5.2.1 Molecular processes in excited states

Several events may occur immediately following photoexcitation of a chromophore. Excess energy that has been absorbed by a non-reactive molecule is released in the form of thermal and photon energy. (Here, we limit our discussion to photophysical, not photochemical, processes associated with chromophores.) Thermal relaxation occurs for all excited molecules, and may proceed with conservation of spin angular momentum in a process termed internal conversion (e.g. singlet-to-singlet, $S_1 \rightarrow S_0$), or with change in angular momentum during intersystem crossing (e.g. triplet-to-singlet, $T_1 \rightarrow S_0$).[13] The emission of a photon as a means to dissipate energy during

relaxation from an excited to ground state is defined as luminescence. When photon emission occurs during internal conversion, the process is called fluorescence. Because internal conversion is an allowed transition, fluorescence emission occurs rapidly; for tryptophan in proteins, the fluorescence lifetime is typically less than 10 ns.[4] On the other hand, phosphorescence refers to photon emission that accompanies intersystem crossing. Because intersystem crossing is a formally forbidden process, the timescales for phosphorescence are much longer than those of fluorescence; the phosphorescence lifetime for tryptophan in proteins is on the order of milliseconds and even up to seconds.[14]

Fluorescence competes with other processes, including intersystem crossing and non-radiative decay (e.g. thermal relaxation). The probability for fluorescence emission for a photoexcited molecule is described quantitatively by the fluorescence quantum yield. Alternatively, one may think of fluorescence quantum yield as the number of photons emitted via fluorescence per photon absorbed; this number ranges from 0 to 1. The fluorescence quantum yield (Φ_{fluo}) compares the rate of radiative decay (k_{rad}) to the total rate of decay due to both radiative and non-radiative (k_{nonrad}) mechanisms, including thermal deactivation via internal conversion, and intersystem crossing, shown in equation 5.1:

$$\Phi_{fluo} = \frac{Number\ of\ fluorescence\ photons}{Number\ of\ absorbed\ photons} = \frac{k_{rad}}{k_{rad}+k_{nonrad}} \qquad 5.1$$

The fluorescence lifetime is defined as $\tau_{fluo} = (k_{rad} + k_{nonrad})^{-1}$. The absolute and relative values of τ_{fluo} and Φ_{fluo} can be measured in a laboratory relatively easily, and provide a wealth of information about the chromophore.[15] For example, collision

between a solvent-exposed chromophore (e.g. indole) and freely-diffusing fluorescence quencher (e.g. acrylamide) may result in an electron transfer reaction that quickly depopulates the indole excited state and thereby causes a reduction in Φ_{fluo}, also known as quenching of fluorescence. Alternatively, collisions between indole and heavy atoms, such as bromine, enhance intersystem crossing rates and subsequently also results in quenched fluorescence. Another common mechanism for reduction of quantum yield is dipole-dipole energy transfer, known as Förster resonance energy transfer (FRET). These processes are discussed in greater detail in subsequent sections of this review.

The most fluorescent natural amino acid is tryptophan, and here we provide brief background on the photophysical properties of this residue (Figure 5.1). The fluorescent portion of tryptophan is the aromatic moiety indole. Indole possesses two nearly-degenerate excited singlet states referred to as ^1L_a and ^1L_b whose transition dipole moments are perpendicular to one another.[16] The ^1L_a state is typically the fluorescent state for indole in aqueous solution, with a fluorescence lifetime of 4.8 ns that becomes multiexponential in tryptophan (0.5 and 3.1 ns lifetimes).[17] This excited state exhibits a large permanent dipole moment which gives rise to the high sensitivity of tryptophan fluorescence to local environment and large Stokes shift. In contrast, emission from the ^1L_b state in proteins is rare, and has only been associated with a tryptophan residue in a highly hydrophobic protein pocket.[18] The emission properties of the ^1L_a and ^1L_b states are different; for example, emission from the ^1L_b state is blue-shifted, or higher energy, than emission from the ^1L_a state. Other excited states may also be populated. Intersystem crossing results in population of the triplet ^3L_a state;[16] in contrast to the ^1L_a state, the triplet state exhibits a small excited-state dipole moment, but displays a large

range of decay kinetics, on the order of microseconds to seconds depending on local environment and temperature. Additionally, unlike the broad fluorescence spectrum, the phosphorescence spectrum exhibits vibronic features. In this review, we primarily focus on the steady-state fluorescence, not phosphorescence, properties of tryptophan.

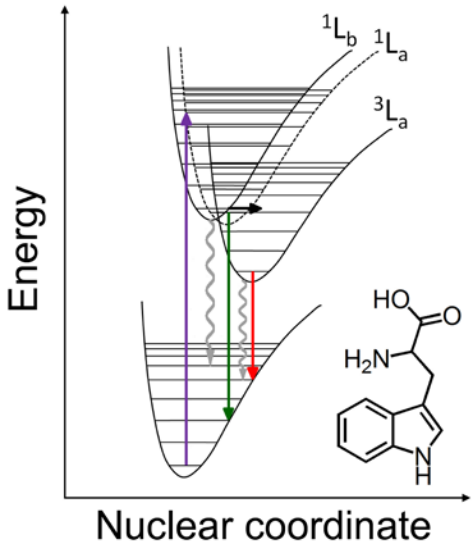

Figure 5.1 Photophysics of tryptophan. The indole moiety is the fluorescent component of the amino acid tryptophan, which is shown as the inset. Energy from photon absorption (purple arrow) is released as thermal energy (wavy arrows) or in the form of fluorescence (green arrow) or phosphorescence (red arrow). Intersystem crossing is denoted by the solid horizontal arrow.

5.2.2 Steady-state fluorescence measurements

A spectrofluorometer is used to record steady-state fluorescence spectra. The components, as shown in Figure 5.2, include a white light source, such as a high-pressure xenon arc lamp (250-750 nm), scanning excitation and emission monochromators to select excitation and emission wavelengths, respectively, sample holder, detector, and optional polarizers. The most common geometry is one in which the fluorescence signal is detected perpendicular to the excitation source; this geometry, in combination with appropriate polarizers, minimizes interference from stray light, in particular elastically-scattered light from the sample.[19] A photomultiplier tube (PMT) is the most common single-channel detector for fluorescence experiments; these are sensitive devices capable of counting single photons. For imaging experiments, multichannel detectors, such as a charge-coupled device (CCD) may be utilized.

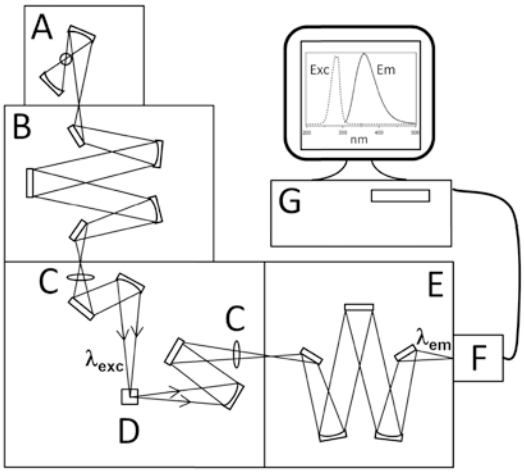

Figure 5.2 Schematic of steady-state spectrofluorometer. Key components are shown. A, lamp; B, excitation monochromator; C, polarizers; D, sample holder; E, emission monochromator; F, detector: G, computer. The excitation wavelength, λ_{exc}, is determined by the excitation monochromator, and the emission wavelength, λ^{em}, is selected by the emission monochromator. The incident and emitted photons are collected in a right angle geometry. Representative excitation ('Exc') and emission ('Em') spectra are shown.

Two types of fluorescence spectra may be acquired. In a standard fluorescence spectrum, the excitation wavelength is held constant and the emission monochromator is scanned to reveal the intensity of fluorescence at different emission wavelengths. An excitation spectrum complements a fluorescence spectrum and is obtained by scanning the excitation monochromator throughout the absorption band of the chromophore while keeping the emission monochromator fixed at an optimal fluorescence wavelength; the selected fluorescence wavelength is typically in an intense region of the fluorescence spectrum. As expected, an excitation spectrum often resembles an absorption spectrum. An excitation spectrum is especially useful when impurities are suspected of affecting the fluorescence spectrum because it allows for identification of the absorption transition that gives rise to the observed emission peak.

Optical polarizers may be placed before and after the sample to determine the rotational flexibility of the chromophore in anisotropy measurements. If the initially populated excited state and fluorescent state of a static, non-rotating chromophore are identical, the polarization of the emitted radiation is unchanged from that of the excitation radiation, and is governed by the direction of the intrinsic transition dipole moment. If the chromophore is allowed to rotate freely, the emitted polarization will no longer be parallel to the excitation polarization; in other words, it will become depolarized or isotropic. The extent of fluorescence anisotropy, or degree of rotational hindrance, is determined by measuring the intensity of light that is emitted parallel (polarized) or perpendicular (depolarized) to the excitation; this measurement reveals the extent of rotational flexibility of the chromophore within the timescale of the fluorescence lifetime. Anisotropy provides insight about the rigidity of the local environment; for example, a

solvent-exposed tryptophan residue in an unfolded membrane protein exhibits low anisotropy because it is able to tumble randomly during the window of fluorescence whereas a residue in a buried region of a membrane-inserted, folded membrane protein exhibits high anisotropy, shown below.

5.2.3 Selection of fluorophores

The spectral properties of fluorescent molecules, such as excitation and emission maxima as well as quantum yields, are sensitive to environmental factors, including pH, temperature, and hydrophobicity. As a result of this sensitivity, control experiments must be carefully planned and executed. The particular chromophore that is selected for any given fluorescence experiment depends strongly on the type of experiment. In the case of proteins, tryptophan is the primary intrinsic chromophore whose fluorescence is utilized to reveal insights into the structures and dynamics of the protein. As discussed above, tryptophan has a large excited-state dipole moment that makes it a sensitive and straightforward reporter of local environment; emission maxima for tryptophan in proteins have been reported in the range 308-352 nm.[2] Tryptophan also exhibits a reasonable oscillator strength (extinction coefficient of 5517 $M^{-1}cm^{-1}$) and a decent quantum yield of 0.14.[20,21] While tryptophan offers the advantage that the protein does not require modification, there are some limitations associated with it. Tryptophan requires UV-excitation and detection, has a low fluorescence quantum yield compared to other dyes, and is susceptible to photodamage. Extrinsic dyes, discussed further below, are generally more robust and fluorescent than tryptophan, but require labeling reactions that are not easily achievable for systems such as membrane proteins. Nonetheless, a

great deal of molecular insight has been gained with the use of both intrinsic and extrinsic dyes.

Tryptophan is not a prevalent amino acid in soluble proteins,[22] but becomes more abundant in membrane proteins because this aromatic amino acid plays a key role in the anchoring and positioning of membrane proteins. Tryptophan exhibits the greatest driving force of all the amino acids for the interfacial region between the lipid bilayer and bulk water and therefore, provides significant stability to the overall structure.[23-26] There are several reasons why tryptophan is believed to play such a critical role in membrane protein stability, such as the fact that it is an amphiphilic molecule that can act as a hydrogen-bond donor in a hydrophobic region. Insertion of tryptophan from bulk water into a lipid bilayer results in a characteristic blue-shift of the emission maximum from ~350 nm (solvent-exposed) to ~330 nm (in bilayer) as well as ~1.5-fold increase in fluorescence quantum yield. These and other dynamic properties make tryptophan emission a good reporter of the structure and dynamics of membrane proteins.

Given the prevalent use of extrinsic fluorophores, we make some brief comments on common dyes that are used with membrane proteins. Fluorescent probes can be introduced into the protein, as is commonly achieved for soluble proteins (e.g. thiol-reactive iodoacetamide and maleimide dyes linked to cysteine residues). One of the challenges with extrinsic labels is that these typically hydrophobic and aromatic molecules may affect the inherent structure and dynamics of a membrane protein. This challenge has limited the number of types of extrinsic labels that can be successfully incorporated into membrane proteins, and has also prohibited analogous extrinsic fluorescence-based studies reported for soluble proteins. Despite these challenges,

several membrane proteins have been successfully labeled for analysis.[27-30] One useful label is the naphthalene derivative, IAEDANS, whose absorption spectrum overlaps with the emission of tryptophan such that tryptophan and IAEDANS comprise a suitable FRET pair.[1,9]

Extrinsic labels in different regions of the lipid bilayer also provide valuable insight.[31] A fluorescent label on the phospholipid head group may provide information on the dynamics of a fluid bilayer in the presence of a membrane protein, or whether a membrane protein is bound to the bilayer via FRET. The phospholipid acyl chains can also be modified to monitor the conformational changes of membrane proteins in the lipid bilayer by embedding a heavy atom quencher such as bromine at different acyl positions.[32] These and other modifications can reveal the depth of insertion of a protein in the lipid bilayer.[33] The variety of intrinsic and extrinsic fluorescent probes is a valuable aid to the challenging spectroscopic experiments that investigate the dynamics of membrane proteins in lipid bilayer.

5.3 Membrane proteins and bilayers

5.3.1 Properties of lipid bilayers

It is beneficial to understand some of the general properties of natural and synthetic bilayers prior to planning fluorescence experiments on membrane proteins. Natural cellular membranes exist in a fluid (liquid-crystalline, L_α) phase, containing a complex and diverse milleu of lipids, fatty acids, peripheral and integral proteins, and sugars. Studies of membrane protein structure and function are simplified by using synthetic bilayers with well-defined lipid compositions. Model bilayers include planar bilayers or closed bilayers, such as small or large unilamellar lipid vesicles (SUVs and

LUVs, respectively). Because membrane proteins exist in equilibrium with the bilayer, the structural and physical properties of the lipid bilayer, including the lipid chain phase (gel versus fluid), curvature stress, and bilayer thickness are important to membrane protein function.[34] The energetics of aggregation of the pore-forming oligomer alamethicin, for example, is sensitive to the curvature of the bilayer,[35] and the thermodynamic stability of the outer membrane protein A favors a bilayer thickness that reduces hydrophobic mismatch with the lipid acyl chains.[36]

A molecular dynamics (MD) simulation of a POPC (1-palmitoyl-2-oleoylphosphatidylcholine,16:0/18:1-PC) bilayer (Figure 5.3) shows a synthetic bilayer in the fluid phase.[37] The electron density profile of the MD simulation depicts the equilibrium distribution of water molecules and lipid components, e.g. phosphate, choline, carbonyl, and methylene, in the bilayer. There are two distinct regions that arise from this chemical heterogeneity, the interfacial region and the hydrophobic core. A well-defined boundary between these regions does not exist, and a folding protein experiences a steep dielectric gradient when partitioning from bulk water to the hydrophobic core. Therefore, the amino acid composition and structure of membrane proteins must be well suited for stability and function in the heterogeneous environment of the lipid bilayer.

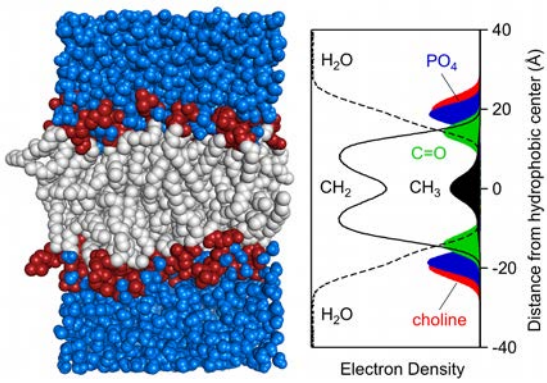

Figure 5.3 Molecular dynamics simulation of a POPC bilayer. Left: A cut-away view of an equilibrated bilayer with three regions indicated: blue, water molecules; red, head group components choline, phosphate, and carbonyl; grey, acyl chains. Right: Thermal distribution of electron density in the bilayer.

The macroscopic properties of a bilayer are influenced by the properties of the phospholipid molecules themselves, such as hydrocarbon chain length, head group charge and size, and degree of chain unsaturation. An important consideration is the gel-to-fluid phase transition temperature. Some membrane proteins, such as the one that is the focus of this review, only insert into fluid phases of bilayers and remain adsorbed onto bilayers in the gel phase.[38] DMPC (1,2-dimyristoyl-sn-glycero-3-phosphocholine, 14:0-PC) is a convenient lipid for studies of membrane protein folding because the phase transition temperature of DMPC bilayers is 23 °C. Therefore, it is relatively straightforward to initiate folding reactions via temperature jumps. Vesicles of different sizes can be generated in the lab using standard techniques, such as probe sonication or extrusion.[39] It should be noted that the stability and size distribution of SUVs and LUVs depend on the bilayer phase and aqueous properties (pH, temperature, ionic strength, etc), so for experiments that utilize varying conditions, such as different concentrations of denaturant, control studies of the properties of vesicles should be performed.

5.3.2 Membrane protein structures

As further background, we briefly discuss membrane protein structures. The two known structural motifs of integral membrane proteins are the α-helical bundle and the β-barrel pore. The first atomic resolution structure of an integral membrane protein, the α-helical model photosynthetic reaction center, was elucidated in 1985.[40] Since this initial report, approximately 400 unique proteins have been resolved to relatively high resolution.[41] Although membrane proteins comprise about one-third of the human genome, only a few integral membrane proteins have been solved by X-ray crystallography because of the technical challenges of obtaining high-purity samples

combined with the inherent thermal disorder of lipid bilayers. Nonetheless, X-ray and NMR structures on the limited number of membrane proteins have provided detailed information on the membrane protein scaffold. We touch on the important elements of structure, such as amino acid composition, and discuss a model scaffold. We refer readers to comprehensive reviews for extended discussions of the composition and structure of α-helical and β-barrel proteins.[25,42-44]

The pseudo-2D geometry of the bilayer reduces the conformational space available to a membrane protein. Nonetheless, the structures of membrane proteins are well adapted for stability and function in the bilayer. For example, transmembrane (TM) α-helices are longer than those found in globular proteins, requiring about 20 residues, in addition to long stretches of aliphatic amino acids, to span the vertical depth (~30 Å) of a bilayer.[25] Moreover, about 60% of TM helices contain kinks and distortions introduced by proline residues that act as hinges in TM channels and introduce diversity to TM protein function.[45,46] The hydrophobic nature of the bilayer also places constraints on the hydrogen-bonding environment of membrane proteins. Because there is an energetic cost of introducing an amide backbone into the low dielectric of the bilayer, the backbone must participate in an extensive hydrogen-bonding network in the bilayer.[47] This thermodynamic consideration is consistent with the finding that TM protein segments retain secondary structure in a membrane.

The prevalence of certain residues is influenced by the properties of the bilayer. The interface region between bulk water and hydrocarbon core of the membrane is a chemically diverse environment, and is typically enriched with polar-aromatic or charged residues, such as tryptophan and lysine, that provide stabilization for TM protein

segments.[48-50] The side chains of these residues interact with lipid head groups through non-covalent intermolecular interactions, such as dipole-dipole or hydrogen-bonding interactions with head group carbonyls, phosphate, or water molecules.[26,51,52] The distribution of amino acids within the bilayer also follows some general trends. The lipid-exposed residues of membrane proteins are more hydrophobic than those buried in the protein interior; a sequence analysis of X-ray structures reveals that the average hydrophobicity of buried residues in a α-helical bundle is comparable to that of globular proteins.[53] Integral proteins that exhibit the β-barrel fold as porins are not unlike reverse-micelles in which the interior of the pore through which solvents pass is more polar than the protein surface that interacts with lipids.[54]

In the present discussion of fluorescence, we focus on a model membrane protein, outer membrane protein A (OmpA) of *Escherichia coli.* This is an abundant integral membrane protein that is believed to serve primarily as an anchor between the outer membrane and the cell wall peptidoglycan; other possible functions are as a phage receptor, channel, and transporter.[55,56] OmpA contains 325 residues and two distinct domains: an N-terminal domain (1-171), which embeds into the membrane, and a globular C-terminal domain (172-325), which binds to peptidoglycan. The transmembrane domain forms a β-barrel containing eight antiparallel β-strands. In planar bilayers, OmpA has been observed to form two types of channels: one channel is essentially impermeable to solutes, and the other is about 1nm in diameter.[55,57]

OmpA serves as a model membrane protein for optical spectroscopy because it is naturally abundant in the bacterial outer membrane, can be purified to high purity, and folds reversibly from a starting unfolded state in 8 M urea by rapid dilution of the

denaturant in the presence of detergents or lipid bilayers. Additionally, there are five native tryptophan residues at positions 7, 15, 57, 102, and 143, as shown in Figure 5.4. We have added additional tryptophan positions at positions 129 and 170. The native and non-native tryptophan residues serve as spectroscopic probes for the protein. For example, the fluorescence spectrum of folded protein is blue-shifted relative to unfolded protein (Figure 5.4). Wild-type and single tryptophan mutants exhibit reasonable thermodynamic stabilities. This protein can also be labeled with extrinsic dyes that only mildly perturb the stability. Finally, OmpA in which the periplasmic domain has been deleted can be expressed relatively easily; this truncated mutant that contains only the transmembrane portion (residues 1-171) serves as an ideal platform for focused studies of β-barrel protein folding, and the significance of the physics of the lipid bilayer to transmembrane stability.

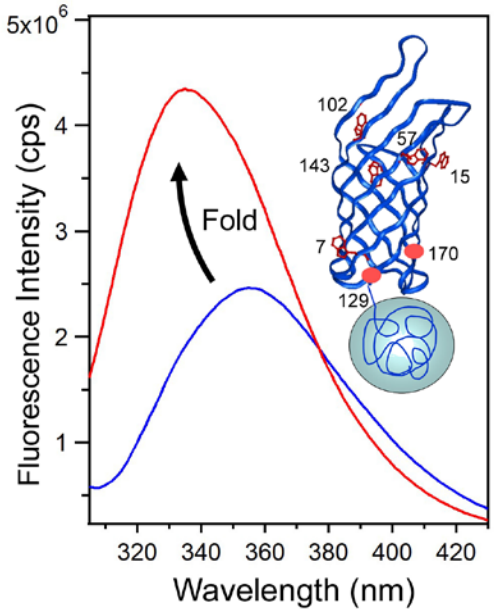

Figure 5.4 Inset: X-ray structure of transmembrane domain of OmpA (PDB: 1QJP); periplasmic domain is shown as a cartoon. Native tryptophan residues are shown, and non-native tryptophan residues that have been probed are indicated as red filled ovals. The fluorescence spectra of the tryptophan residues are sensitive to environment; the emission maximum is 355 nm when OmpA is unfolded in 8.0 M urea, shown in blue, and shifts to 335 nm when folded in a lipid bilayer, indicated in red.

5.4 Characterization of membrane protein stability

Membrane protein folding is an expanding area of research that is relevant for diverse scientific disciplines, including biology, chemistry, health, disease, and pathogenesis. A simple, yet experimentally challenging, goal in this field is to characterize the thermodynamics associated with a natively folded protein in a bilayer. The stability of a membrane protein is quantified by measurements of changes in Gibbs free energy, ΔG°, where the reaction may be from folded to unfolded, or unfolded to folded, conformations. Non-covalent interactions that contribute to the change in Gibbs free energy include hydrogen-bond networks, hydrophobic contacts, and electrostatic interactions. Hydrogen bonding along the peptide backbone is especially important because these intramolecular interactions become significant as the protein is dehydrated, and hence drive the formation of secondary structure in a bilayer.[47] Hydrophobic contacts and specific amino acids also stabilize membrane proteins in the hydrophobic bilayer.[48,58] For example, aromatic amino acids typically reside in the water-lipid interface to help anchor the protein within the lipid bilayer,[26,52] and charged amino acids can form stabilizing through-space electrostatic interactions, such as those between negative lysine and positive arginine residues.[25,26,50] Quantitative determination of ΔG° is the first step towards discerning the relative contributions of these and other non-covalent interactions to the overall stability of a membrane protein.

As expected, laboratory-based measurements of ΔG° are sensitive to experimental conditions, such as type of model membrane (e.g. micelle or vesicle, charged or neutral lipid head group, acyl chain length), surface curvature of vesicle, and pH.[36,39,59] Therefore, careful systematic experiments must be performed. Denaturation, or

unfolding, curves are one of the most straightforward and reliable methods to determine ΔG° for folding and unfolding reactions. Common denaturants include chemical agents, temperature, and pH. A typical experiment involves measuring the shift in relative populations of folded and unfolded states upon exposing folded protein to varying amounts of denaturant (e.g. different denaturant concentrations, temperatures, or pH); results from this titration can be fit to models, the simplest being a two-state model in which folded protein cooperatively converts to unfolded conformation.[60] Analysis of additional protein mutants or different lipid bilayers could yield insight into intra- and intermolecular interactions that impact values of ΔG° associated with unfolding reactions.[36,39]

The most widely used chemical denaturants are urea and guanidinium. The mechanisms by which denaturants unfold proteins are complex, and involve direct solvation of hydrophobic regions as well as breaking of hydrogen-bond networks.[61,62] Analysis of a chemical unfolding curve involves determination of ΔG° at each denaturant concentration via experimental determination of populations of folded and unfolded conformations. Extrapolation to zero denaturant concentration reveals ΔG°_{H2O} which is the desired change in Gibbs free energy in the absence of denaturant. The simplest model for determining ΔG°_{H2O} assumes a linear dependence of change in Gibbs free energy with denaturant concentration.[63]

$$\Delta G^{\circ} = \Delta G^{\circ}_{H2O} - mC \qquad 5.2$$

In equation 5.2, C is the independent variable (i.e. concentration of urea), and ΔG° is the dependent variable (i.e. change in Gibbs free energy at specific C). A linear fit to

this curve yields a slope, m, and intercept, ΔG°_{H2O}. Under equilibrium conditions, there is a denaturant concentration, $C_{1/2}$, at which the population of folded and unfolded conformations is equivalent and therefore, $\Delta G^{\circ} = 0$. At this point in the denaturation curve, ΔG°_{H2O} can be obtained because $\Delta G^{\circ}_{H2O} = mC_{1/2}$, and the parameters m and $C_{1/2}$ are relatively easy to measure in a lab (discussed below). It should be pointed out that unfolding curves are measured under equilibrium conditions such that ΔG°_{H2O} values are independent of whether the reaction proceeds in the direction of folded → unfolded, or unfolded → folded. In other words, the folding reaction should be fully reversible. However, given the high propensity for membrane proteins to aggregate, it is challenging to find suitable conditions where the reaction is 100% reversible. We have found that it is optimal to confirm the reversibility of the folding reaction as well as measure the change in Gibbs free energy using complementary methods as opposed to relying on a single technique.

The reversibility of OmpA unfolding in the presence of urea has been illustrated using SDS-PAGE measurements.[36,39,64] The gels indicate that the urea concentration that results in equal population of folded and unfolded protein is independent of whether the reaction proceeds as a folding or unfolding reaction. This observation supports a primarily reversible reaction for OmpA in this particular chemical denaturant.

The relative populations of equilibrium folded and unfolded conformations, and hence Gibbs free energy for folding or for unfolding, can be directly measured using a variety of tools, such as circular dichroism, gel electrophoresis, or fluorescence spectroscopy, that provide clear markers for folded and unfolded states. Among these techniques, fluorescence is the most sensitive method, and typically requires significantly

less protein that the other methods. The drawback to fluorescence spectroscopy is that this technique requires presence of a fluorescence chromophore whose emission maximum and/or emission intensity differ for the folded and unfolded states.

Tryptophan residues in membrane proteins easily satisfy this requirement because the emission maximum and quantum yield are highly sensitive to the polarity of the local solvent. Specifically, tryptophan residues buried in a bilayer exhibits an emission maximum of ~330 nm whereas a solvent-exposed indole emits at ~350 nm (see Figure 5.4). This 20-nm blue shift is also typically accompanied by a change in fluorescence quantum yield. These shifts in emission maximum and intensity may be utilized to determine the population of folded and unfolded protein. An important experimental consideration is that the urea concentration should be determined by index of refraction measurements because it is hygroscopic.[65]

It has been shown that the corrected fluorescence intensity at a given wavelength shows a linear dependence on the faction of folded (or unfolded) conformations.[19] This is the most straightforward method to analyze the fraction of folded protein, but can be experimentally challenging because of the need to know absolute protein concentrations. Given the highly scattering nature of membrane proteins, techniques that do not require knowledge of protein concentrations for all samples are preferred.

Intensity-weighted emission maxima have also been utilized to determine fraction of folded protein.[36,66] The intensity-weighted emission maximum, $< \lambda >$, over the wavelength range 305-450 nm is defined as $< \lambda >= \frac{\sum_i I_i \lambda_i}{\sum_i I_i}$ where i is the index for wavelength (e.g. i would range from 1 to 146 if data were available from 305 to 450 nm

in increment of 1 nm), I_i is the intensity at a given wavelength of index i, and λ_i is the wavelength at index i. It is important to note that the intensity-weighted emission maximum, not simply the emission maximum, must be utilized for proper analysis because of possible differences in the shapes, including intensities, of the spectra for folded and unfolded conformations.[66]

A final technique that is preferred in our lab is the intensity-corrected decomposition method in which an observed fluorescence spectrum is decomposed into basis spectra corresponding to folded and unfolded populations. Our preference for this method is based on a few considerations. Unlike the method that relies on absolute intensities, protein concentrations at each denaturant concentration are not needed for decompositions. Instead, only two absolute fluorescence spectra of the fully folded and unfolded samples are essential. Additionally, the decomposition method is insensitive to the selected range of wavelengths or shapes of the spectra for analysis since full Gaussian curves over the entire window are generated.

The decomposition method proceeds as follows. Tryptophan fluorescence spectra of fully folded (~0 M urea) and unfolded (~8 M urea) OmpA are measured, and the spectra are corrected for background scattering as well as normalized for concentration. These two corrected spectra are then fit to individual Gaussian curves, G_{fold}^{corr} and G_{unf}^{corr}, that provide the essential Gaussian parameters of peak wavelength (λ_{fold}^{max} and λ_{unf}^{max}) and width (σ_{fold} and σ_{unf}) for the basis spectra. The ratio of the areas of G_{fold}^{corr} to G_{unf}^{corr} provides a quantum yield correction term, $C_{QY} = \frac{Area\ of\ G_{fold}^{corr}}{Area\ of\ G_{unf}^{corr}}$. For

OmpA mutants that contain single tryptophan residues, the average C_{QY} across all mutants is 1.8.

With knowledge of the Gaussian parameters for folded and unfolded conformations, an experimental fluorescence spectrum that contains a mixture of folded and unfolded conformations is decomposed into two Gaussian basis spectra, G_{fold} and G_{unf}, that have peak wavelengths and widths that correspond to those of folded (λ_{fold}^{max} and σ_{fold}) and unfolded (λ_{unf}^{max} and σ_{unf}) populations. The best fit is obtained by holding the Gaussian wavelengths and widths constant, and allowing the amplitudes of the Gaussian basis spectra to vary. The sum of the two decomposed basis spectra forms a model spectrum which should closely reproduce the experimental result. This process is repeated for each experimental fluorescence spectrum that is obtained with different urea concentration. We utilize multipeak fitting packages in Igor Pro Software 6.22A, though any fitting program will suffice.

Representative data for a truncated OmpA mutant with a single tryptophan residue at position 143 are illustrated in Figure 5.5. These data show fluorescence spectra of the protein in the presence of DMPC SUVs and five urea concentrations of 8,4 M (fully unfolded), 3.3 M, 2.9 M (midpoint), 2.8 M, and 0.1 M (fully folded). Peak wavelength and width parameters based on Gaussian functions that correspond to fully folded, G_{fold}^{corr}, and fully unfolded, G_{unf}^{corr}, protein are obtained from the 0.1 M and 8.4 M urea spectra, and are utilized to decompose spectra at urea concentrations where a mixture of folded and unfolded populations are expected.

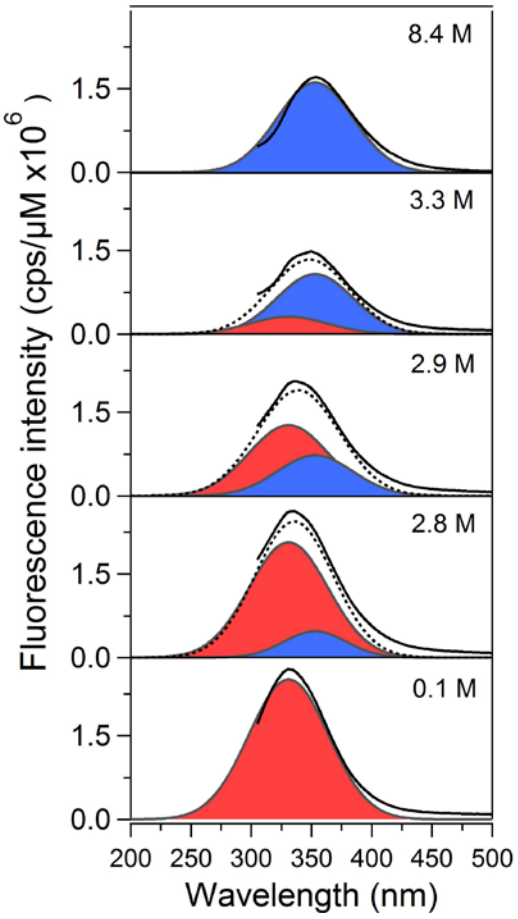

Figure 5.5 Representative fluorescence spectra of truncated OmpA mutant with single tryptophan residue at position 143. Spectra were acquired from 305-500 nm at different urea concentrations, as indicated. The experimental spectra were decomposed into Gaussian basis spectra that represent folded and unfolded populations shown as red solid band and blue solid bands, respectively. The sum of the two Gaussian curves is shown as dashed curves. See main text for details.

The area of the Gaussian basis spectrum that corresponds to folded protein is normalized by C_{QY} to finally reveal the fraction of unfolded OmpA, f_{unf}, as determined by this decomposition technique.

$$f_{unf} = \frac{Area\ of\ G_{unf}}{Area\ of\ G_{unf} + \frac{1}{C_{QY}}(Area\ of\ G_{fold})} \quad 5.3$$

The fraction unfolded is plotted as a function of urea concentration to generate an unfolding curve. Finally, the free energy of folding is obtained by fitting the data in the unfolding curve to a two-state model to reveal m and $C_{1/2}$ and therefore ultimately, ΔG°_{H2O}.[60]

$$f_{unf} = \frac{\exp\left[-m\left(\frac{C_{1/2}-C}{RT}\right)\right]}{1+\exp\left[-m\left(\frac{C_{1/2}-C}{RT}\right)\right]} \quad 5.4$$

$$\Delta G^{\circ}_{H2O} = mC_m \quad 5.5$$

Unfolding curves for full-length and truncated OmpA in which the periplasmic domain is cleaved are shown in Figure 5.6. Full-length mutants with single tryptophan residues at positions 7, 15, 57, 102, 143, or 170 are indicated W7, W15, W57, W102, W143, or W170, respectively. These single-tryptophan mutants contain phenylalanine in the remaining four or five native tryptophan positions. Wild-type OmpA is indicated as WT, and a tryptophan-free mutant in which all native tryptophan residues have been replaced with phenylalanine is called W0. Truncated OmpA in which the periplasmic domain has been deleted starting at residue 177 is indicated with the symbol Δ following the nomenclature for full-length OmpA.

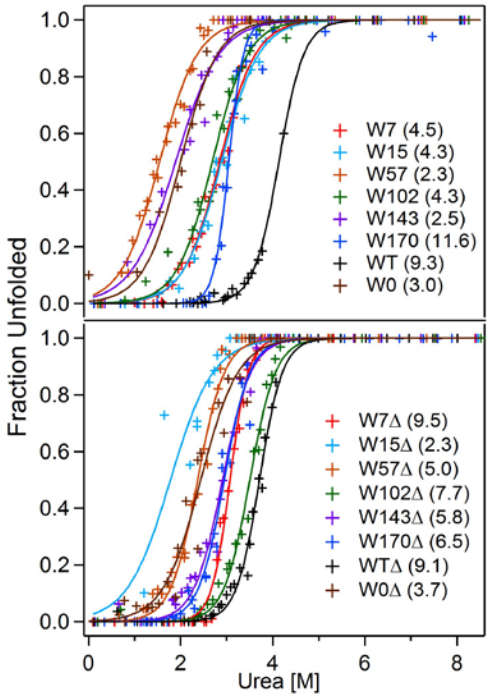

Figure 5.6 Unfolding curves and Gibbs free energies of unfolding (kcal/mol) of full-length (top) and truncated (bottom) OmpA based on tryptophan fluorescence decomposition method, or SDS-PAGE data for a mutant that lacks tryptophan. See text for details.

These data illustrate the range of Gibbs free energies for the various OmpA mutants. In a prior report,[39] we analyzed unfolding curves by plotting emission maxima (λ_{max}) as a function of denaturant concentration and reported Gibbs free energies with estimated errors of 15%. This method is appropriate if there is no difference in shapes and integrated areas of the fully folded and fully unfolded spectra. However, given the variations in spectral width and fluorescence quantum yield between folded and unfolded states, the λ_{max} method does not provide accurate results for OmpA. Here, we re-analyze the data after improving our technique to obtain more precise and accurate protein concentrations of fully folded and unfolded states, and utilize the decomposition method to generate unfolding curves. The specific values for Gibbs free energies are systematically decreased by an average of 16% using the decomposition method relative to using λ_{max}. However, the trends reported previously are reproduced with the decomposition method. As expected, native OmpA with five tryptophan residues is most stable (ΔG°_{H2O} of 9.3 kcal/mol), and mutants that contain single tryptophan residues in native locations are destabilized relative to native OmpA, but by varying degrees. For example, OmpA with a single tryptophan residue at position 7 is relatively stable, whereas a mutant with a single tryptophan at position 143 exhibits a similar Gibbs free energy as a tryptophan-free mutant. It is interesting to note that a tryptophan residue in the non-native position of 170 is a particularly stable mutant, and that deletion of the soluble periplasmic domain generally stabilizes the protein; this latter observation was discussed in our previous report.[39] These thermodynamic insights can be coupled to structural studies to illustrate the relative contributions of intermolecular interactions to the overall stability of a membrane protein.

5.5 Rotational freedom and anisotropy

Anisotropy experiments elucidate changes in rotational flexibility associated with structural changes, such as binding of proteins to membranes. The anisotropy value, *r,* reflects the rotational diffusion of a fluorophore during the lifetime of the excited state. Anisotropy (equation 5.6) is determined by collecting the polarized vertical (I_{VV}) and horizontal emission (I_{VH}) following vertical excitation, where the first and second subscripts represent incident and emitted polarizations, respectively.[78,79] The G factor is a corrective term that characterizes differential instrument sensitivity to vertically (S_V) and horizontally (S_H) polarized light as a function of wavelength, and is determined by collecting the vertically (I_{HV}) and horizontally polarized (I_{HH}) emission following horizontal excitation (equation 5.7). Anisotropy of a membrane protein is sensitive to changes in rotational diffusion, and thus can be used to report changes in molecular size, viscosity, and binding events.

$$r = \frac{I_{VV} - G\, I_{VH}}{I_{VV} + 2G\, I_{VH}} \qquad 5.6$$

$$\mathrm{G} = \frac{S_V}{S_H} = \frac{I_{HV}}{I_{HH}} \qquad 5.7$$

The measured anisotropy value depends on the viscosity of solvent and the mobility of the fluorophore of interest. Thus, anisotropy provides valuable information about structural motion of membrane proteins affected by a viscous membrane as well as inherent rigidity of native structures. As shown in the Perrin equation (equation 5-6), anisotropy (r) is comprised of the fundamental anisotropy (r_o) in the absence of any depolarization process, fluorescence lifetime (τ) of the fluorophore, and rotational correlation time (θ). The latter term depends on viscosity (η), volume of rotating protein

(V), and temperature (T); R is the gas constant.[1] A plot of (1/r) as a function of (T/η) for a given protein at different temperatures and viscosities reveals the apparent volume of a protein, V.

$$\frac{1}{r} = \frac{1}{r_0} + \frac{\tau}{r_0 \theta} = \frac{1}{r_0} + \frac{\tau RT}{r_0 \eta V} \qquad 5.8$$

For membrane proteins, the insertion and folding events can be monitored by anisotropy measurements. Figure 5.7 shows the change in anisotropy of OmpA as it inserts and folds into a lipid bilayer (DMPC). As expected, the extent of depolarization is greater for the solvent-exposed tryptophan in unfolded protein (r=0.03) relative to the folded state (r=0.1). The enhanced anisotropy of the folded state is consistent with the fact that tryptophan is in a more viscous environment of the membrane and may also be localized to a rigid pocket of the protein. As discussed here, anisotropy can be utilized to obtain overall structural information during folding and to help to understand lipid-protein interactions in viscous membrane.

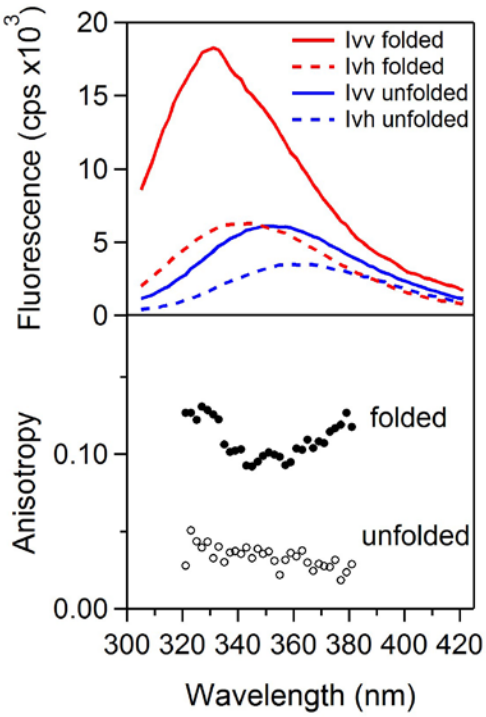

Figure 5.7 Polarized tryptophan fluorescence and anisotropy of folded and unfolded truncated OmpA that contains a single tryptophan residue at position 143. The periplasmic domain has been cleaved at position 177. Top: Polarized tryptophan fluorescence spectra indicating I_{VV} (red solid) and I_{VH} (red dashed) of folded protein, as well as I_{VV} (blue solid) and I_{VH} of unfolded (blue dashed) OmpA. The first and second subscripts refer to the polarization of the incident and emitted radiation, respectively. Bottom: Resulting anisotropy of folded (filled circles) and unfolded (open circles) OmpA.

5.6 Tertiary structure: distance measurement via FRET

Förster resonance energy transfer (FRET) is a mechanism by which electronic energy is transferred from an excited donor (D) molecule to a nearby acceptor (A) molecule without the emission or reabsorption of light.[80-82] The FRET process occurs because of through-space dipole-dipole coupling between the electronic states of D and A. The rate of energy transfer depends on several factors: (1) relative orientation of the transition dipole moments between the D and A pair; (2) fluorescence quantum yield of the donor; (3) index of refraction of the medium; (4) the extent of spectral overlap between the donor emission and acceptor absorption; and (5) distance between D and A. Of these variables, distance is the most critical parameter; the FRET efficiency scales as $\frac{1}{r^6}$, where r is the D-A distance. This strong distance dependence enables FRET to be used as a spectroscopic ruler to measure molecular separations in the range 10-100 Å.[82] For example, FRET has been used to map the distance between the subunits of cytochrome *c* oxidase,[2] the effect of the retinal cofactor on the thermodynamic stability of bacteriorhodopsin (bR),[3] and the conformational distribution of prion protein (PrP) repeating peptides.[4]

5.6.1 Practical aspects of FRET

There are several practical considerations that must be addressed prior to performing FRET measurements. The first questions that one must answer are, what D and A pairs will be used, and where will they be located on the protein? These questions are related in that the D-A pair that is selected depends on the distance that one seeks to access. A given D-A pair exhibits a characteristic Förster radius, $R_{o,}$ at which the efficiency (E) for FRET is 50%:

$$R_0{}^6 = \left(8.79 \times 10^{23} \frac{\text{Å}^6\text{M}}{\text{cm}^3}\right) (\kappa^2 n^{-4} \Phi_\text{D} J_\text{DA}) \quad 5.9$$

$$E = \frac{R_0{}^6}{R_0{}^6 + r^6} = 1 - \frac{F_{DA}}{F_D} = 1 - \frac{\tau_{DA}}{\tau_D} \quad 5.10$$

The variables are defined: κ^2 is the orientation factor, n is the index of refraction of the medium, Φ_D is the fluorescence quantum yield of the donor, J_DA is the overlap integral, F_DA is the fluorescence intensity of the donor in the presence of acceptor, F_D is the fluorescence intensity of the donor in the absence of acceptor, τ_{DA} is the lifetime of the donor in the presence of acceptor, and τ_D is the lifetime of the donor in the absence of acceptor. The overlap integral is given in equation 6.3, and shown graphically in 5.11 for a D-A pair.

$$J_{DA} = \frac{\int F_D(\lambda)\, \varepsilon_A(\lambda)\, \lambda^4\, d\lambda}{\int F_D(\lambda)\, d\lambda} \quad 5.11$$

$F_\text{D}(\lambda)$ is the fluorescence intensity at wavelength λ, and $\varepsilon_\text{A}(\lambda)$ is the extinction coefficient at λ. The denominator serves to normalize the value of J_DA to the integrated fluorescence intensity, which simplifies the calculation by eliminating the need to know absolute fluorescence intensities. As can be seen in equation 5.10, FRET efficiencies can be measured in the form of steady-state emission intensities or fluorescence lifetimes. Experiments with fluorescence intensities are straightforward. Fluorescence lifetime measurements can be more complex in implementation and analysis, because decay kinetics are fast (nanoseconds) and rarely mono-exponential, especially in biological samples; however, lifetime measurements have the advantage that they are insensitive to differences in sample concentrations and are more likely to reveal heterogeneous

populations. In the case of multi-exponential kinetics, the average lifetime, which is proportional to the steady-state integrated intensity, is typically utilized.

The range of distances that can be accessed depends on R_o; a general rule of thumb is that values within a factor of two of R_o may be measured,[1] though in practice it can be challenging to achieve this level of dynamic range. If emission intensities or lifetimes can be accurately measured for 5% – 95% FRET efficiency, which is a conservative range for most instruments, distances between $0.6R_o$ and $1.6R_o$ can be determined fairly easily. For example, a FRET pair comprised of tryptophan as the donor and a naphthalene-based dye as the acceptor exhibits a R_o of 21 Å, which allows distances between ~13 to 34 Å to be readily measured. Other FRET pairs have greater R_o values, such as pyrene (D) and coumarin (A) with R_o of 39 Å.[83]

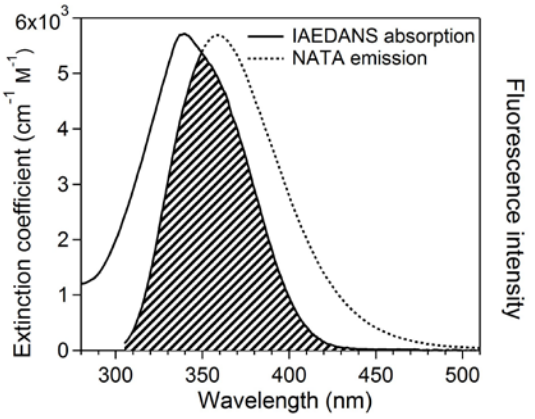

Figure 5.8 Absorption spectrum of IAEDANS acceptor (left axis), and fluorescence spectrum of NATA donor (right axis). The overlap region is shown by the hashed region.

5.6.2 Challenges associated with FRET and membrane proteins

In the case of membrane proteins, the natural abundance of aromatic amino acids, in particular tryptophan makes them excellent intrinsic donors. Nonetheless, there are several challenges that must be overcome in order to perform successful FRET measurements. One problem associated with biological FRET measurements is that the D-A distance is typically not fixed and instead, varies because of the inherent fluctuations of the protein and/or labels. Additionally, the finite volumes of the labels themselves are not considered. Therefore it is sometimes preferred to utilize FRET measurements to reveal relative structural changes rather than absolute distances between two atoms. This inherent source of error that originates from the averaging of D-A positions and assumption of point dipoles places limitations on the accuracy of the distances, but this error is not as significant as others associated with the experiments themselves.[84,85] An ongoing challenge is low labeling yields of extrinsic donors. Not only is it a difficult task to label membrane proteins, but it is a challenge to quantitatively determine the labeling yield itself because it requires successful separation and analytical measurements. Once the labeling efficiency is known, the method suggested by Lakowicz *et. al.* can be utilized to take into consideration the emission intensity and lifetime that reflects incompletely labeled protein.[1,86]

Another challenge associated with FRET experiments for membrane proteins (as well as soluble proteins) is determining the correct value for R_o, including characterizing the evolution of R_o during a folding reaction. The Förster radius depends on orientation factor, κ^2, as noted earlier. The value of κ^2 is 2/3 when the D and A dipoles sample all orientations within the timescale of the FRET process; in other words, the D-A dipoles

are effectively oriented randomly relative to one another. However, the range of κ^2 is quite large, between 0-4, where 0 indicates the dipoles are perpendicular, 1 represents parallel dipoles, and 4 results from collinear, parallel orientations. Additionally, this value is likely to evolve when a protein inserts into the membrane because of the loss of rotational flexibility.

Fluorescence polarized emission measurements, i.e. anisotropy experiments, can be used to establish the upper and lower limits of the orientation factor.[87,88] However, these experiments and analyses are not trivial, so a great deal of effort has been placed to determine appropriate approximations. In practice, many FRET researchers simply utilize $\kappa^2 = 2/3$; some authors publish reports with little or no acknowledgement of this assumption, while others devote large studies to this topic. Fortunately, the assumption of orientational averaging implicit in $\kappa^2 = 2/3$ is not always incorrect. When all angles are considered, the uncertainty in distance is relatively small, on the order of 20 %.[9,89] One of the reasons why $\kappa^2 = 2/3$ is not so erroneous is because in the case where there is structural heterogeneity, such as for proteins, a distribution of static structures is effectively equivalent to orientational averaging. Additionally, certain chromophores, including tryptophan, possess multiple, nearly degenerate excited states. The presence of these multiple levels means that there is more than one transition dipole moment for absorption and therefore, supports some degree of orientational averaging. Despite the fact that some systems are more prone to the difficulties associated with κ^2, many systems have been studied successfully, and FRET results have been shown to compare well with X-ray diffraction data, as reviewed in Dos Remedios *et al*.[90]

In addition to determining the value of R_o, the change in R_o must be investigated during a folding process. This analysis is essential because the photophysical properties of the donor and acceptor are likely to evolve as the protein transfers from aqueous to membrane environments. In the case of tryptophan as a donor, the emission spectrum blue-shifts and the quantum yield increases. Fortunately, these spectral shifts associated with tryptophan do not significantly impact the overlap integral, as discussed below for folded and unfolded states of labeled OmpA.

5.6.3 Application of FRET in OmpA

The dynamics of a handful of membrane-associated systems have been monitored with FRET.[91-93] Currently, our group is investigating tertiary structure changes associated with the folding reaction of OmpA. An intrinsic donor, tryptophan, and an extrinsic acceptor from IAEDANS (abbreviated dns), were introduced using a combination of mutagenesis (to generate single tryptophan and cysteine residues) and labeling reaction.[93] Figure 5.9 shows representative data for a mutant that is designed to elucidate evolution of the pore structure during insertion and folding into DMPC bilayers (up to four hours). In this mutant, the donor at position 129 and acceptor at position 7 are on opposite sides of the pore, and located on the periplasmic side of the protein. OmpA has the advantage that it exhibits directional folding in which the periplasmic end inserts last, even when the periplasmic portion is removed.[38] For simplicity, we refer to the leading portion of the protein which contains large loops and positions 102, 57, 15, etc. as the 'front' during the folding reaction, and the opposite, periplasmic portion with residues 7, 170, etc. as the 'tail' (see Figure 5.4 for clarification). In our FRET studies, the

periplasmic domain has been removed and our FRET experiments have been performed on truncated OmpA mutants.

Fluorescence spectra of donor-only, donor+acceptor, acceptor-only, and tryptophan-free truncated OmpA are analyzed to reveal changes in distance during the folding reaction. The tryptophan-free mutant provides isolated signal from the thirteen tryrosine residues in the transmembrane portion of the protein. Fluorescence spectra of these four OmpA mutants in which scattering from vesicle has been removed are shown in the left panel of Figure 5.9. The spectral region of interest is ~305-400 nm, which is the range of tryptophan fluorescence. Contributions from tyrosines and the acceptor are subtracted from the spectra, and these corrected spectra are shown in the middle panel. These corrected spectra are further analyzed to reveal the FRET efficiency (E) using equation 5.10, which describes the extent of tryptophan fluorescence quenching in the presence of acceptor. Finally, we utilize the experimentally determined R_0 value of 21 Å, assuming constant orientation factor of $\kappa^2=2/3$, to construct the structural evolution of the pore during the folding reaction (right panel in Figure 5.9). The FRET efficiency and distance are shown for unfolded OmpA in 8 M urea for comparison.

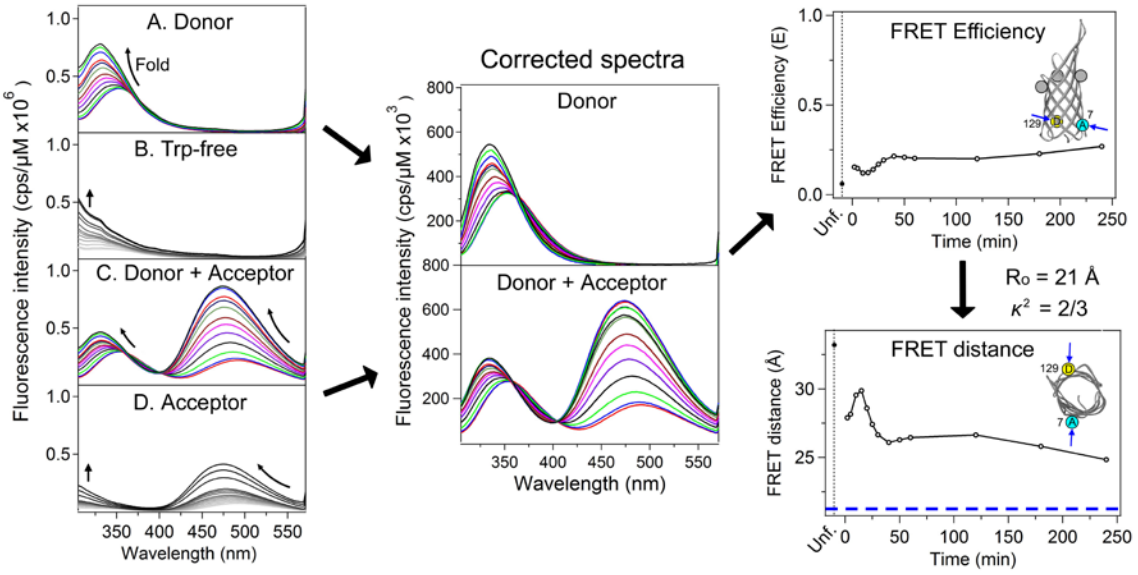

Figure 5.9 FRET data for truncated OmpA mutant with tryptophan donor at position 129, and extrinsic acceptor at position 7. Left panel: Spectra for (A) donor, (B) tryptophan-free mutant, (C) donor+acceptor, and (D) acceptor. Middle panel: Contribution from tyrosine has been subtracted to reveal corrected spectra for donor (panel A minus panel B) and corrected spectra for donor+acceptor (panel C minus panel D). Right panel: Efficiencies are calculated from the data in the middle panel, and converted to distances using the experimentally determined value for R_0, which assumes a constant κ^2 value. The crystal structure distance between donor and acceptor γ-carbons of the native residues is shown as the blue dashed line. Results for unfolded OmpA in 8 M urea are indicated as "Unf." See main text for additional details.

Our FRET data indicate the relative timescale for pore formation of the tail end of OmpA. Initially, upon dilution of urea in the presence of SUVs, there is a rapid collapse of the protein, supported by the decrease in donor-acceptor distance immediately following the mixing reaction (t=2 minutes). This collapse may indicate adsorption of the protein onto the bilayer. As the protein begins to insert and fold, the distance between donor and acceptor first increases, and after approximately 15 minutes, the distance decreases and begins to stabilize at the 50-minute mark. These data support a picture in which the collapsed, adsorbed structure undergoes structural changes as the front of the protein inserts (first 15 minutes), followed by complete insertion and pore formation of the tail retion. This pore continues to compress until a relatively stable structure with pore size of ~26 Å is reached within an hour, after which continued equilibration persists for the duration of the interrogation time. The FRET-based pore distance of 26 Å can be compared to the static structural data from X-ray diffraction, which indicates a distance of 21.3 Å between the donor (position of native Y129 C_γ) and acceptor (position of native W7 C_γ).

Additional mutants provide other insights. For example, we are also investigating a mutant that probes the evolution of the pore on the front, leading portion of OmpA (donor+acceptor at positions 143+57). We have also generated several mutants that interrogate distances across the bilayer, such as donor+acceptor at positions 57+7. Thus far, our FRET data support a concerted folding mechanism in which pore formation and bilayer transversal occur on similar timescales. These results, especially when coupled to other tools such as circular dichroism, help reveal the *in vitro* folding behavior of transmembrane proteins.[74,94]

5.7 Summary

In this review, we summarize the applications of steady-state fluorescence measurements as valuable aids for the study of membrane-associated biomolecules. The excited states of molecules provide powerful insights into their local microenvironments. Consequently, the simple technique of fluorescence reports on the structures and dynamics of membrane proteins. Fluorescence quenching measurements can be used to estimate the depth of insertion of a fluorophore into a bilayer, the hydration level of a membrane protein, and evolution of tertiary structure. Anisotropy measurements can be used to monitor the rotational freedom of fluorophores and indicate the binding of a protein to a membrane. The Gibbs free energies of unfolding can also be determined by titration of the folded state of a membrane protein with denaturants. Many challenges persist in these experiments, such as correcting for light scattering from vesicles, membrane protein aggregation, and in examples of FRET measurements, consideration of the error in the orientation factor, κ^2. Despite these obstacles, fluorescence spectroscopy is a simple and valuable tool to reveal fundamental properties of a large class of experimentally challenging biomolecules, membrane proteins.

5.8 Acknowledgments

We thank Dr. Katheryn M. Sanchez for leading the efforts on the initial studies of OmpA folding, Dr. Diana E. Schlamadinger and Ms. Dina I. Kats for quenching experiments on Cyt c, and Dr. Yi Wang for providing MD results on POPC. G.K is supported by the Heme and Blood Proteins Training Grant (T32DK007233), and I.L.P. is supported by the San Diego Fellowship program as well as the Molecular Biophysics

Training Program (GM008326) at UCSD. We gratefully acknowledge funding from the National Science Foundation to J.E.K. (CHE-0645720).

Chapter 5, in part, is a reprint of the material as it appears in Encyclopedia of Analytical Chemistry, 2013, Kang, Guipeun; López-Peña, Ignacio; Bhakta, Saajan; Kim, Judy E. Wiley. The dissertation author was primary investigator and author of this paper. Sections 5.5.1 and 5.5.2 from the original publication focused on hydration, and these sections have been removed from Chapter 5 of this dissertation because previous group members were the lead researchers for hydration studies.

5.9 References

(1) Lakowicz, J. R. *Principles of fluorescence spectroscopy*; Springer: New York, 2006.

(2) Vivian, J. T.; Callis, P. R. *Biophysical Journal* **2001**, *80*, 2093.

(3) Reshetnyak, Y. K.; Koshevnik, Y.; Burstein, E. A. *Biophysical Journal* **2001**, *81*, 1735.

(4) Beechem, J. M.; Brand, L. *Annual Review of Biochemistry* **1985**, *54*, 43.

(5) Ladokhin, A. S. *Analytical Biochemistry* **1999**, *276*, 65.

(6) Chen, Y.; Barkley, M. D. *Biochemistry* **1998**, *37*, 9976.

(7) Toptygin, D.; Savtchenko, R. S.; Meadow, N. D.; Roseman, S.; Brand, L. *Journal of Physical Chemistry B* **2002**, *106*, 3724.

(8) Schuler, B.; Eaton, W. A. *Curr. Op. Struct. Biol.* **2008**, *18*, 16.

(9) Stryer, L. *Ann. Rev. Biochem.* **1978**, *47*, 819.

(10) Arinaminpathy, Y.; Khurana, E.; Engelman, D. M.; Gerstein, M. B. *Drug Discov Today* **2009**, *14*, 1130.

(11) Sanders, C. R.; Myers, J. K. *Annu. Rev. Biophys. Biomol. Struct.* **2004**, *33*, 25.

(12) Khemtemourian, L.; Killian, J. A.; Hoppener, J. W. M.; Engel, M. F. M. *Experimental Diabetes Research* **2008**, *2008*, 1.

(13) Lower, S. K.; El-Sayed, M. A. *Chemical Reviews* **1966**, *66*, 199.

(14) Vanderkooi, J. M.; Calhoun, D. B.; Englander, S. W. *Science* **1987**, *236*, 568.

(15) Callis, P. R.; Liu, T. Q. *Journal of Physical Chemistry B* **2004**, *108*, 4248.

(16) Callis, P. R. *Fluorescence Spectroscopy* **1997**, *278*, 113.

(17) Szabo, A. G.; Rayner, D. M. *Journal of the American Chemical Society* **1980**, *102*, 554.

(18) Broos, J.; Tveen-Jensen, K.; de Waal, E.; Hesp, B. H.; Jackson, J. B.; Canters, G. W.; Callis, P. R. *Angewandte Chemie-International Edition* **2007**, *46*, 5137.

(19) Ladokhin, A. S.; Jayasinghe, S.; White, S. H. *Analytical Biochemistry* **2000**, *285*, 235.

(20) Pace, C. N.; Vajdos, F.; Fee, L.; Grimsley, G.; Gray, T. *Protein Science* **1995**, *4*, 2411.

(21) Eftink, M. R.; Jia, Y. W.; Hu, D.; Ghiron, C. A. *Journal of Physical Chemistry* **1995**, *99*, 5713.

(22) Overton, I. M.; van Niekerk, C. A. J.; Carter, L. G.; Dawson, A.; Martin, D. M. A.; Cameron, S.; McMahon, S. A.; White, M. F.; Hunter, W. N.; Naismith, J. H.; Barton, G. J. *Nucleic Acids Research* **2008**, *36*, W190.

(23) Hong, H.; Park, S.; Jiménez, R. H. F.; Rinehart, D.; Tamm, L. K. *J. Am. Chem. Soc.* **2007**, *129*, 8320.

(24) White, S. H.; Wimley, W. C. *Annu. Rev. Biophys. Biomol. Struct.* **1999**, *28*, 319.

(25) MacKenzie, K. R. *Chemical Reviews* **2006**, *106*, 1931.

(26) Killian, J. A.; von Heijne, G. *Trends Biochem. Sci.* **2000**, *25*, 429.

(27) Veatch, W.; Stryer, L. *Journal of Molecular Biology* **1977**, *113*, 89.

(28) Lakowicz, J. R.; Gryczynski, I.; Laczko, G.; Wiczk, W.; Johnson, M. L. *Protein Sci.* **1994**, *3*, 628.

(29) Cha, A.; Snyder, G. E.; Selvin, P. R.; Bezanilla, F. *Nature* **1999**, *402*, 809.

(30) Nannepaga, S. J.; Gawalapu, R.; Velaszuez, D.; Renthal, R. *Biochemistry* **2004**, *43*, 550.

(31) Maier, O.; Oberle, V.; Hoekstra, D. *Chemistry and Physics of Lipids* **2002**, *116*, 3.

(32) Bolen, E. J.; Holloway, P. W. *Biochemistry* **1990**, *29*, 9638.

(33) Keller, R. C. A.; ten Berge, D.; Nouwen, N.; Snel, M. M. E.; Tommassen, J.; Marsh, D.; deKruijff, B. *Biochemistry* **1996**, *35*, 3063.

(34) Andersen, O. S.; Koeppe, R. E. *Annual Review of Biophysics and Biomolecular Structure* **2007**, *36*, 107.
(35) Keller, S. L.; Bezrukov, S. M.; Gruner, S. M.; Tate, M. W.; Vodyanoy, I.; Parsegian, V. A. *Biophysical Journal* **1993**, *65*, 23.

(36) Hong, H.; Tamm, L. K. *Proc. Natl. Acad. Sci. USA* **2004**, *101*, 4065.

(37) Schlamadinger, D. E.; Wang, Y.; McCammon, J. A.; Kim, J. E. *J Phys Chem B* **2012**, *116*, 10600.

(38) Surrey, T.; Jahnig, F. *Proc. Natl. Acad. Sci. USA* **1992**, *89*, 7457.

(39) Sanchez, K. M.; Gable, J. E.; Schlamadinger, D. E.; Kim, J. E. *Biochemistry* **2008**, *47*, 12844.

(40) Deisenhofer, J.; Epp, O.; Miki, K.; Huber, R.; Michel, H. *Nature* **1985**, *318*, 618.

(41) Raman, P.; Cherezov, V.; Caffrey, M. *Cell Mol Life Sci* **2006**, *63*, 36.

(42) Bowie, J. U. *Nature* **2005**, *438*, 581.

(43) Tamm, L. K.; Hong, H.; Liang, B. *Biochim. Biophys. Acta, Rev. Biomembr.* **2004**, *1666*, 250.

(44) Schulz, G. E. *Current Opinion in Structural Biology* **2000**, *10*, 443.

(45) Yohannan, S.; Faham, S.; Yang, D.; Whitelegge, J. P.; Bowie, J. U. *Proc Natl Acad Sci U S A* **2004**, *101*, 959.

(46) Cordes, F. S.; Bright, J. N.; Sansom, M. S. *J Mol. Biol.* **2002**, *323*, 951.

(47) White, S. H. *Peptide Solvation and H-Bonds* **2006**, *72*, 157.

(48) Wimley, W. C.; White, S. H. *Nat. Struct. Biol.* **1996**, *3*, 842.

(49) de Planque, M. R. R.; Kruijtzer, J. A. W.; Liskamp, R. M. J.; Marsh, D.; Greathouse, D. V.; Koeppe, R. E.; de Kruijff, B.; Killian, J. A. *Journal of Biological Chemistry* **1999**, *274*, 20839.

(50) Chamberlain, A. K.; Lee, Y.; Kim, S.; Bowie, J. U. *Journal of molecular biology* **2004**, *339*, 471.

(51) Reithmeier, R. A. *Curr Opin Struct Biol* **1995**, *5*, 491.

(52) Yau, W. M.; Wimley, W. C.; Gawrisch, K.; White, S. H. *Biochemistry* **1998**, *37*, 14713.

(53) Rees, D.; DeAntonio, L.; Eisenberg, D. *Science* **1989**, *245*, 510.

(54) Pautsch, A.; Schulz, G. E. *Nature Structural Biology* **1998**, *5*, 1013.

(55) Sugawara, E.; Nikaido, H. *Journal of Biological Chemistry* **1992**, *267*, 2507.

(56) Wang, Y. *Biochem. Biophys. Res. Commun.* **2002**, *292*, 396.

(57) Arora, A.; Rinehart, D.; Szabo, G.; Tamm, L. K. *J Biol. Chem.* **2000**, *275*, 1594.

(58) White, S. H.; Wimley, W. C. *Biochim. Biophys. Acta, Rev. Biomembr.* **1998**, *1376*, 339.

(59) Ladokhin, A. S. *Methods in Enzymology: Biothermodynamics, Vol 466, Pt B* **2009**, *466*, 19.

(60) Pace, C. *Methods Enzymol.* **1986**, *131*, 266.

(61) O'Brien, E. P.; Dima, R. I.; Brooks, B.; Thirumalai, D. *Journal of the American Chemical Society* **2007**, *129*, 7346.

(62) Monera, O. D.; Kay, C. M.; Hodges, R. S. *Protein Science* **1994**, *3*, 1984.

(63) Pace, C. N. *CRC Crit Rev Biochem* **1975**, *3*, 1.

(64) Sanchez, K. M.; Kang, G. P.; Wu, B. J.; Kim, J. E. *Biophysical Journal* **2011**, *100*, 2121.

(65) Shirley, B. A. *Methods in molecular biology*; Humana Press Inc.: Totowa, 1995; Vol. 40.

(66) Moon, C. P.; Fleming, K. G. *Methods in Enzymology: Biothermodynamics, Vol 492, Pt D* **2011**, *492*, 189.

(67) Bright, F. V.; Pandey, S.; Baker, G. A. In *Encyclopedia of Anal. Chem.*; John Wiley & Sons, Ltd: 2006.

(68) Rodionova, N. A.; Tatulian, S. A.; Surrey, T.; Jahnig, F.; Tamm, L. K. *Biochemistry* **1995**, *34*, 1921.

(69) Eftink, M. R.; Ghiron, C. A. *Analytical Biochemistry* **1981**, *114*, 199.

(70) Mcintosh, T. J.; Holloway, P. W. *Biochemistry* **1987**, *26*, 1783.

(71) Chattopadhyay, A.; London, E. *Biochemistry* **1987**, *26*, 39.
(72) Abrams, F. S.; London, E. *Biochemistry* **1992**, *31*, 5312.

(73) Gable, J. E.; Schlamadinger, D. E.; Cogen, A. L.; Gallo, R. L.; Kim, J. E. *Biochemistry* **2009**, *48*, 11264.

(74) Kleinschmidt, J. H.; Tamm, L. K. *Biochemistry* **1999**, *38*, 4996.

(75) Ladokhin, A. S. *Fluorescence Spectroscopy* **1997**, *278*, 462.

(76) Ladokhin, A. S.; Holloway, P. W.; Kostrzhevska, E. G. *Journal of Fluorescence* **1993**, *3*, 195.

(77) Ladokhin, A. S. *Biophysical Journal* **1999**, *76*, 946.

(78) Weber, G. *Biochem J* **1952**, *51*, 145.

(79) Weber, G. *Biochem J* **1952**, *51*, 155.

(80) Förster, T. *Annalen Der Physik* **1948**, *437*, 55.

(81) Förster, T. *Delocalized excitation and excitation transfer*; Academic Press: New York, 1965.

(82) Stryer, L.; Haugland, R. P. *Proc Natl Acad Sci U S A* **1967**, *58*, 719.

(83) Wu, P. G.; Brand, L. *Analytical Biochemistry* **1994**, *218*, 1.

(84) dos Remedios, C. G.; Miki, M.; Barden, J. A. *J Muscle Res Cell Motil* **1987**, *8*, 97.

(85) Moens, P. D. J.; Yee, D. J.; Dosremedios, C. G. *Biochemistry* **1994**, *33*, 13102.

(86) Lakowicz, J. R.; Gryczynski, I.; Wiczk, W.; Kusba, J.; Johnson, M. L. *Analytical Biochemistry* **1991**, *195*, 243.

(87) Dale, R. E.; Eisinger, J.; Blumberg, W. E. *Biophys J* **1979**, *26*, 161.

(88) Dale, R. E.; Eisinger, J. *Biopolymers* **1974**, *13*, 1573.

(89) Cerione, R. A.; Hammes, G. G. *Biochemistry* **1982**, *21*, 745.

(90) dosRemedios, C. G.; Moens, P. D. J. *Journal of Structural Biology* **1995**, *115*, 175.

(91) Curnow, P.; Booth, P. J. *Journal of Molecular Biology* **2010**, *403*, 630.

(92) Haldar, S.; Raghuraman, K.; Chattopadhyay, A. *Journal of Physical Chemistry B* **2008**, *112*, 14075.

(93) Kang, G. P.; Lopez-Pena, I.; Oklejas, V.; Gary, C. S.; Cao, W. H.; Kim, J. E. *Biochimica Et Biophysica Acta-Biomembr.* **2012**, *1818*, 154.

(94) Kleinschmidt, J. H.; den Blaauwen, T.; Driessen, A. J. M.; Tamm, L. K. *Biochemistry* **1999**, *38*, 5006.

Chapter 6. Future experiments: FRET studies for refolding OmpA in a new membrane mimic, nanodiscs

6.1 Introduction

In 2002, nanodiscs were first synthesized in the Sligar lab; these nanodiscs have the shape of a discoidal phospholipid bilayer surrounded by membrane scaffold proteins (MSPs) or belt peptides, with an overall diameter of ~ 10 nm.[1] Figure 6.1 provides a surface image showing the constant size of nanodiscs composed of DPPC lipids and one type of MSP, MSP1. To achieve a homogeneous distribution of nanodiscs, it is important to use the correct stoichiometry of lipids to MSP/belt peptide; this stoichiometry was established in previous work.[2,3] Compared to liposomes or micelles, nanodiscs provide more controllable environments and greater solubility than vesicles or micelles, which opens up new doors for studying membrane proteins.[4]

Nanodiscs facilitate examinations of the relationship between membrane protein activity and structure by supplying native-like environments for membrane proteins. For example, the kinase activation of the receptor TAR embedded in nanodiscs was successfully investigated and showed the effects on the order of dimerization when the number of dimers per nanodisc was varied.[5] Furthermore, nanodiscs make the reconstituted membrane proteins soluble, thus overcoming experimental problems such as the aggregation of detergents and vesicles.[6] In some early experiments, OmpA was reconstituted into preformed DMPC nanodiscs without the aid of a detergent. To our knowledge, there are no studies of membrane protein folding in nanodiscs. Our goal is to

probe the folding dynamics of membrane proteins and the driving forces of the folding process using a combination of FRET and UVRR spectroscopy in nanodiscs.

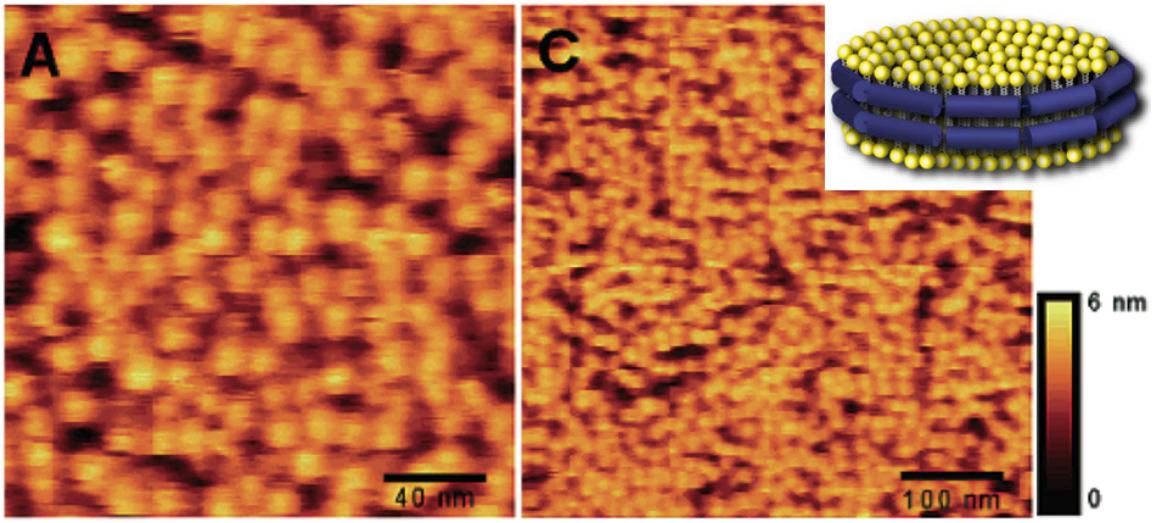

Figure 6.1 Surface images of nanodiscs obtained using scanning probe microscopy from reference.[1] Nanodiscs of ~ 10 nm diameter were composed of DPPC and MSP1. The cartoon of a single nanodisc on the top right corner was adapted from the website of Heinrich-Heine-Universität.
(https://www.uni-duesseldorf.de/MathNat/ipb/index.php?index=1501)

6.2 Preparation of preformed nanodiscs

Nanodiscs of ~ 10 nm diameter were generated from DMPC phospholipids and a belt peptide (Ac-DYLKAFYDKLKEAF-NH_2). The belt peptide was kindly gifted by the Opella group. The final concentrations of DMPC and the peptide solution were 1.475 mM and 0.875 mM, respectively, giving rise to a DMPC to belt peptide molar ratio of 1.67 for the formation of nanodiscs of ~ 10 nm diameter.[2] The procedure for producing nanodiscs is as follows. 25 mg of DMPC dissolved in chloroform was dried under nitrogen gas for several hours, and then dried DMPC powder was resuspended in 5 mL of phosphate buffer (20 mM KPi, pH 7.3). Subsequently, an aliquot of belt peptide from a stock solution (10 mg/mL = 5.58 mM peptide) was added to the hydrated DMPC solution to achieve a molar ratio of 1.67 to produce 10 nm diameter nanodiscs (final concentration of 0.875 mM in 20 mM KPi, pH 7.3). When the belt peptide solution was added to the DMPC solution, the cloudy DMPC solution became clear within 1 minute. The preformed DMPC nanodisc solution was freshly prepared for fluorescence, gel-electrophoresis, and UVRR experiments.

6.3 Preliminary data: SDS-polyacrylamide gel electrophoresis

SDS-polyacrylamide gel electrophoresis (PAGE) was carried out at constant voltage of 200 V for one of the single tryptophan TM OmpA mutants (W15Δ) and one of the dye-conjugated TM OmpA mutants (W15/F7CdnsΔ) to test the folding of OmpA in the presence of preformed DMPC nanodiscs. OmpA stock in 8 M urea solution was injected into preformed DMPC nanodiscs, and the dilution factor was such that the residual urea concentration was ~ 0.4 M in the solution. The targeted ratio was 1:1 for OmpA to nanodiscs, but the actual ratio values were 0.7 to 1.5, as indicated by the

absorption spectra of W15Δ OmpA and W15/F7CdnsΔ, respectively. Samples of reconstituted OmpA in nanodiscs were incubated at 37 °C overnight. The next morning, the samples were divided into two Eppendorf tubes; the solution in one tube was boiled, and the other remained refolded. These OmpA samples and protein marker were loaded into each well of a 12.5 % polyacrylamide gel; the resulting data are shown in Figure 6.2. The apparent molecular weight for unfolded and refolded TM OmpA is 19 kDa and 21 kDa, respectively.[7] W15/F7CdnsΔ was completely denatured by boiling, appearing as one band at 19 kDa (lane 1). For reconstituted W15/F7CdnsΔ, a folded band of 21 kDa appeared, but another band coexisted at 19 kDa due to a residual unfolded or aggregated population (lane 2). The folding yield of W15/F7CdnsΔ in nanodiscs was approximately 50 % or slightly higher. W15Δ was mostly denatured by heat, but a faint band at 21 kDa appeared, in contrast to the boiled W15/F7CdnsΔ (lane 3). Without heat treatment to keep OmpA refolded, nearly two equivalent populations were observed for the W15Δ in nanodiscs, indicating a folding yield of approximately 50 %, similar to that of W15/F7CdnsΔ in nanodiscs. Despite the failure of some population to integrate into nanodiscs, the preliminary data are promising, showing that OmpA can successfully refold into preformed nanodiscs directly. Nevertheless, it is necessary to find an optimal folding condition for refolding in preformed nanodiscs to increase the folding yields.

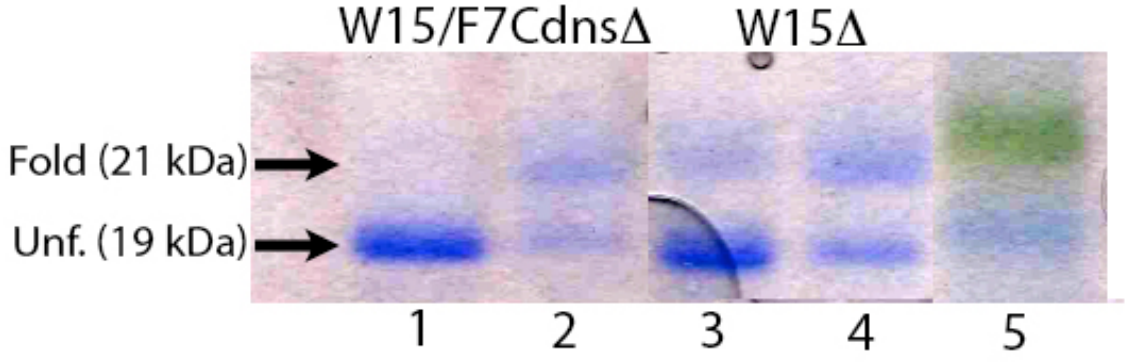

Figure 6.2 SDS-PAGE gel showing the refolded TM OmpA in preformed nanodiscs of ~ 10 nm diameter and heat-denatured TM OmpA. Lane 1, boiling-denatured W15/F7CdnsΔ in the presence of nanodiscs; lane 2, refolded W15/F7CdnsΔ in nanodiscs; lane 3, boiling-denatured W15Δ in the presence of nanodiscs; lane 4, refolded W15Δ in nanodiscs; lane 5, protein marker (green band: 23 kDa and blue band: 17 kDa)

Digestion experiments were designed to confirm that OmpA is correctly reconstituted in nanodiscs. Arg-C endoproteinase was selected over trypsin protease for digestion experiments because Arg-C is predicted to cleave full-length OmpA without affecting the belt peptide. The cleavage sites for Arg-C and trypsin are shown in Figure 6.3. The protease experiments were performed by adding Arg-C to the OmpA sample to achieve a final Arg-C:OmpA ratio of 20:1. This sample was incubated at 37 °C for 3 hours, and then analyzed by SDS-PAGE. None of the samples were boiled.

Prior to the digestion experiments of OmpA in nanodiscs, Arg-C was tested with refolded OmpA in DMPC SUVs. This digestion experiment is valuable because OmpA spontaneously inserts in a directional manner, with the peripheral domain on the outside of vesicles.[8] Therefore, the transmembrane domain of OmpA remains protected by the lipid bilayer, and the soluble peripheral domain can be cleaved by Arg-C or trypsin protease. As shown in Figure 6.4, the refolded and the unfolded bands of the full-length OmpA appear at 30 kDa and 35 kDa, respectively. In the presence of Arg-C, refolded and unfolded OmpA was cleaved into several fragments of lower apparent molecular weight. A fragment of ~ 25 kDa in lane 2 (folded OmpA in SUV) is expected to be the transmembrane domain protected by the lipid bilayer, but some residual undigested population of folded OmpA still remains. The incomplete digestion reaction could be resolved by a higher concentration of enzyme or longer incubation time. Compared to lane 2, where refolded OmpA was digested with Arg-C, the mixture of unfolded OmpA and Arg-C resulted in approximately twice the number of fragments, reflecting cleavage of the transmembrane domain. This test shows that Arg-C is suitable for cleaving the soluble domain, and will help determine whether OmpA folds into nanodiscs.

A P K_3 D N T W_7 Y T G A K_{12} L G W_{15} S Q Y H D T G F I N N N G P T H E N

Q L G A G A F G G Y Q V N P Y V G F E Met G Y D W_{57} L G R_{60} Met P Y K_{64}

G S V E N G A Y K_{73} A Q G V Q L T A K_{82} L G Y P I T D D L D I Y T R_{96} L G

G Met V W_{102} R_{103} A D T K_{107} S N V Y G K_{113} N H D T G V S P V F A G G V E

Y A I T P E I A T R_{138} L E Y Q W_{143} T N N I G D A H T I G T R P D N G Met L S L

G V S Y R_{169} F G Q G E A A P_{177} V V A P A P A P A P E V Q T K_{192} H F T L

K_{197} S D V L F N F N K_{206} A T L K_{210} P E G Q A A L D Q L Y S Q L S N L D P

K_{230} D G S V V V L G Y T D R_{242} I G S D A Y N Q G L S E R_{255} R_{256} A Q S V V

D Y L I S K_{267} G I P A D K_{273} I S A R_{277} G Met G E S N P V T G N T C D N V

K_{294} Q R_{296} A A L I D C L A P D R_{307} R_{308} V E I E V K_{314} G I K_{317} D V V T Q P

Q A

Figure 6.3 Comparison of the cleavage sites for wild-type OmpA in the presence of Arg-C or trypsin protease. The cleavage sites for the activity of both enzymes are shown in red color. Trypsin protease cleaves at the lysine residue (blue) as well.

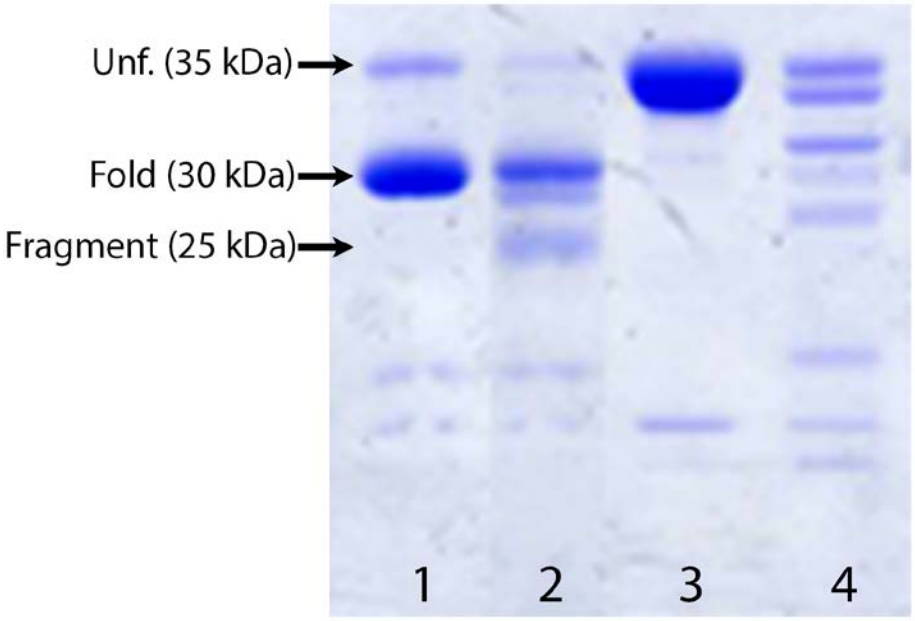

Figure 6.4 SDS-PAGE showing that Arg-C digested the reconstituted OmpA in DMPC SUVs and the unfolded OmpA. Lane 1, refolded wild-type (WT) OmpA in DMPC SUVs; lane 2, refolded WT OmpA in DMPC SUVs with Arg-C endoproteinase; lane 3, unfolded WT OmpA in 0.5 M urea solution; lane 4, unfolded WT OmpA in 0.5 M urea solution with Arg-C endoproteinase. The experiment was performed by Ivan Kozachenco.

6.4 Preliminary data: UV resonance Raman spectroscopy

We further investigated whether OmpA folds into nanodiscs using vibrational spectroscopy. UV resonance Raman spectra were obtained using the Ti:sapphire laser setup described elsewhere.[9,10] An excitation beam of 228 nm was used to irradiate the OmpA samples in various aqueous solutions to probe the vibrational modes of the tryptophan residue. OmpA samples at a protein concentration of ~ 20 μM were prepared for three aqueous solutions: 0.8 M urea solution, 1 mg/mL DMPC SUVs with 0.8 M urea, and 1 mg/mL DPPC SUVs with 0.8 M urea. For the nanodisc studies, the concentration of OmpA was about half that in SUV solutions, with 0.8 M urea in the solution. A sample of ~ 10 μM OmpA in the nanodisc solution provided a 1:1 ratio of OmpA to nanodisc. We focused on W129 OmpA and W129Δ OmpA for the nanodiscs experiments because these mutants exhibit a unique vibrational mode at ~ 785 cm^{-1} near the W18 mode that we interpret as an enhanced hydrogen-out-of-plane (HOOP) mode. This HOOP mode is only present for tryptophan residue at position 129, and only when the protein is folded in preformed DMPC SUVs and OG detergent micelles. Thus, this new vibrational mode can be utilized as a marker to detect whether OmpA folds properly in preformed nanodiscs.

Figure 6.5 shows normalized and corrected UVRR spectra of W129 and W129Δ in various solutions: 10 mg/mL OG detergent micelles, 1 mg/mL DMPC SUVs, 1 mg/mL DPPC SUVs, 0.8 M urea, and 10 μM nanodiscs (only for Y129WΔ)). The proposed HOOP mode at the shoulder of the W18 peak is evident only under refolding conditions in the presence of detergent micelles, DMPC SUVs, and the DMPC nanodisc solution, indicating that OmpA was successfully reconstituted into DMPC nanodiscs. Evolution of

the HOOP intensity is evident in the UVRR spectra collected during a folding reaction of W129Δ in DMPC SUVs (Figure 6.6). We hypothesize that the HOOP mode gains intensity because of perturbation of the indole π electrons because of interaction with a nearby charge.[10,11] The perturbation is apparently induced by intramolecular interactions rather than intermolecular interactions, such as protein-lipid interactions, because the mode is intense when OmpA is folded in OG micelles, which have no charged groups, and in DMPC bilayers, which have zwitterionic head groups. Possibly, a charged residue of the protein interacts with the indole side chain and perturbs the π electrons to break the symmetry. In further investigations, molecular interactions that drive the folding process can be probed by UVRR spectroscopic studies due to the sensitivity of vibrational modes to environmental changes, such as the formation of hydrogen bonds and hydrophobic interactions.

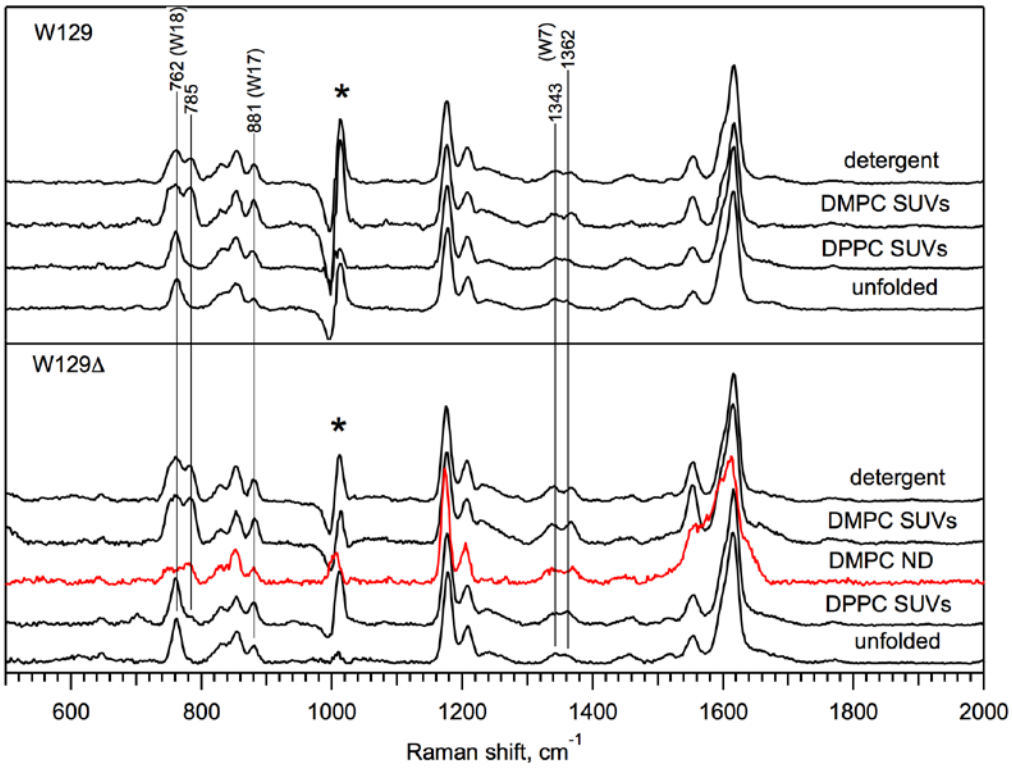

Figure 6.5 UVRR spectra for W129 and W129Δ OmpA in various aqueous conditions: 10 mg/mL OG detergent micelles, 1 mg/mL DMPC SUVs, 1 mg/mL DPPC SUVs, 0.8 M urea solution (unfolded), and DMPC nanodisc (ND) solution (indicated by red solid line). All spectra were collected for 10 minutes, but the acquisition time of the spectra for OmpA in nanodiscs was 5 minutes. The region near 1000 cm^{-1} (indicated with *) has strong urea signal, resulting in a subtraction artifact.

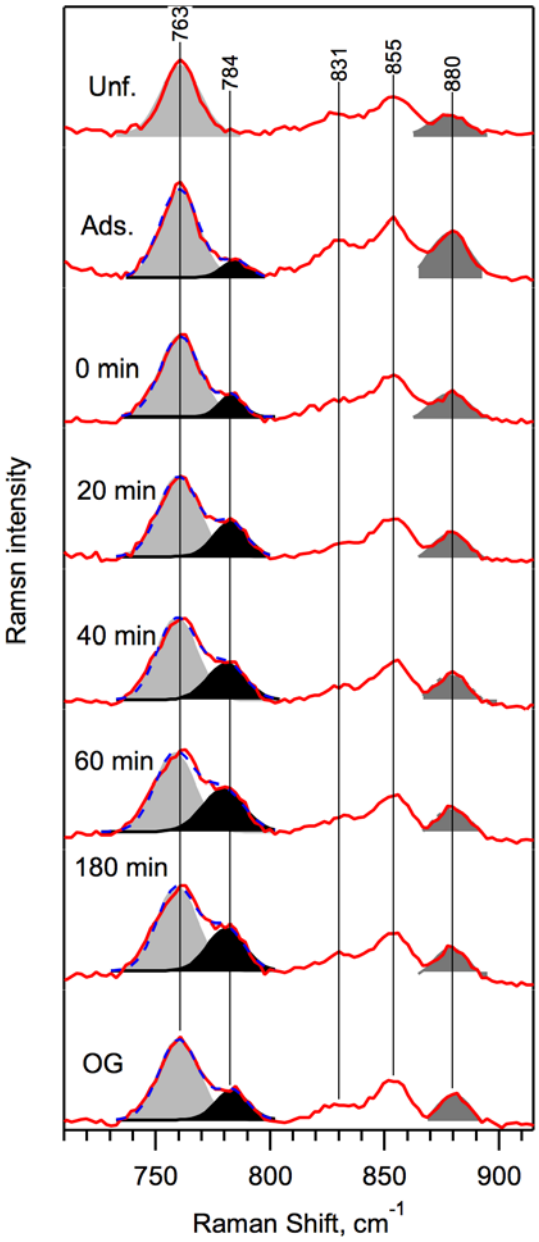

Figure 6.6 UVRR spectra of W129Δ OmpA under various conditions: Unfolded in 0.8 M urea ("Unf."); adsorbed in 1 mg/mL DPPC SUVs ("Ads"); during folding at the indicated time points of 0, 20, 40, 60, and 180 min following addition of OmpA to DMPC SUVs; and folded in 10 mg/mL OG detergent micelles ("OG."). All spectra were collected for 5 minutes. Red curves are experimental data. The bands at 763 (W18) and 784 (HOOP) cm^{-1} were decomposed to two Gaussian bands (solid gray and black bands), and the sum of the bands is indicated as the blue dashed curves. The W17 mode at 880 cm^{-1} was fit to a single Gaussian, shown as the solid gray band.

6.5 Preliminary data: Förster resonance energy transfer

Steady-state fluorescence spectroscopy was performed for W15/F7CdnsΔ and W15Δ to measure the energy transfer efficiency in the refolded state in DMPC nanodiscs. Figure 6.7 shows fluorescence spectra ~ 2 minutes after injection of the protein sample into the preformed DMPC nanodisc solutions, as well as after 12 hours of incubation at 37 °C. For W15Δ in DMPC nanodiscs, the emission maximum shifted from 355 to 343 nm during folding, indicating that the environment of the indole side chain became more hydrophobic. As comparison, the emission max of W15Δ in DMPC SUVs shifted from 353 to 337 nm. These spectra are shown in Figure 6.7. The blue-shift for folding in nanodiscs and in SUVs are qualitatively similar, but the magnitudes differ. This difference in magnitude can be attributed to variation in folding yields for OmpA in nanodisc vs SUV. A more appropriate comparison is intensity-weighted emission maximum, which, as described in Chapter 5, properly takes into account differences in shape of the spectra for folded and unfolded states. The intensity-weighted (from 310-370 nm) emission wavelength for OmpA in nanodiscs blue-shifted from 345.1 nm (at 2 min) to 341.7 nm (at 12 hours). For reference, the analogous intensity-weighted blue-shift of W15Δ in DMPC SUVs was from 344.8 nm (average of three trials at 2 minutes after the initiation of folding) to 340.0 nm (average of three trials at 4 hours).

We performed a preliminary FRET analysis of OmpA in nanodiscs, and compared the result to OmpA in SUVs. The distance between the donor and acceptor for W15/F7CdnsΔ increased from 23.9 Å to 26.0 Å during folding into DMPC nanodiscs. This evolution can be compared to the folding reaction in DMPC SUVs, where a shift in

distance from 21.8 Å to 26.5 Å occurred within 4 hours. The increased distance for W15/F7CdnsΔ originates from the fact that the donor and acceptor are placed on the same strand that spans the bilayer, so it is expected that the donor and acceptor move apart as the folded structure evolves in the bilayer. These preliminary data show that FRET can used to monitor the structural evolution of OmpA as it folds in preformed nanodiscs.

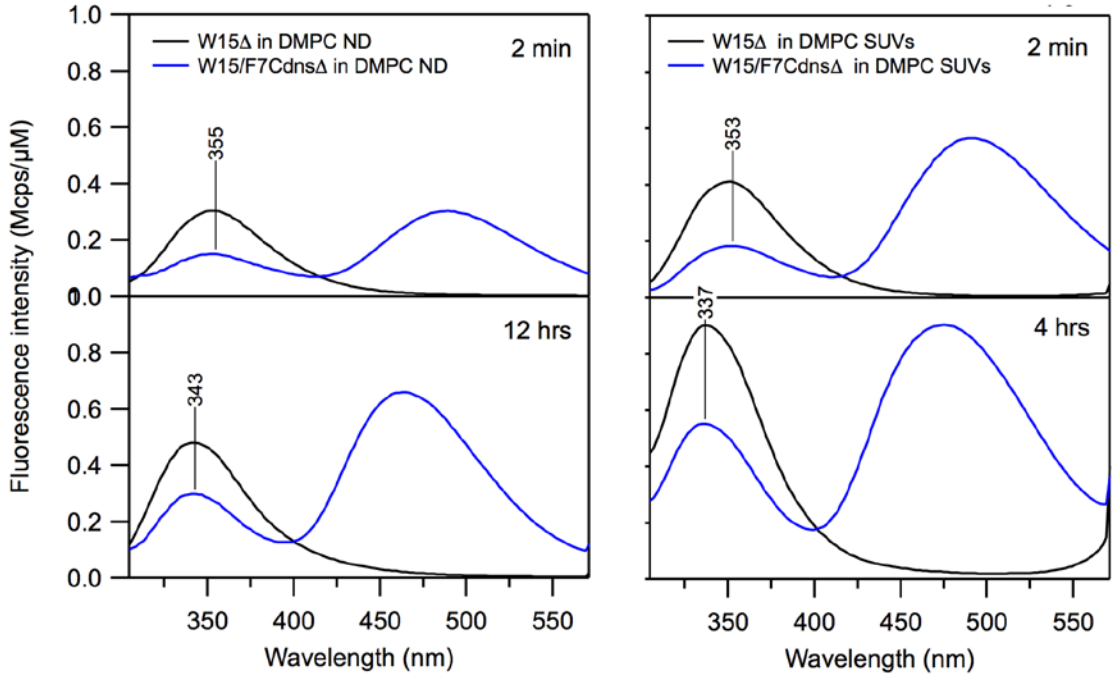

Figure 6.7 Steady-state fluorescence spectra of donor+acceptor OmpA (W15/F7CdnsΔ, blue solid line) and donor-only OmpA (W15Δ, black solid line) during folding reaction into DMPC nanodiscs (left) or into DMPC vesicles (right). Top: Fluorescence spectra of OmpA approximately 2 min after initiation of folding reaction. Bottom: Fluorescence spectra of OmpA after 12 and 4 hours incubation at 37 °C.

6.6 Summary and outlook

These initial efforts to integrate OmpA into preformed nanodiscs without the aid of detergent, and to analyze the folding process by FRET, UVRR and SDS-PAGE have yielded promising results. Based on the preliminary results, OmpA successfully refolds into preformed nanodiscs from the denatured state. These results suggest that the nanodiscs can be used to investigate the folding dynamics and molecular interactions of membrane proteins while refolding into preforemed nanodiscs. There are several advantages for using nanodiscs in membrane protein studies. They are homogeneous and their sizes are controllable. Also, nanodiscs are membrane templates that stabilize membrane proteins while providing better solubility than liposomes. Our long-terms goals are to probe folding mechanisms and inter/intra molecular interactions associated with membrane protein folding, and nanodiscs provide a valuable opportunity to investigate membrane proteins in more controlled and homogeneous environments. This new platform combined with spectroscopic tools, such as FRET and UVRR, may reveal new insights into this complex biological problem.

6.7 References

(1) Bayburt, T. H.; Grinkova, Y. V.; Sligar, S. G. *Nano Lett* **2002**, *2*, 853.

(2) Park, S. H.; Berkamp, S.; Cook, G. A.; Chan, M. K.; Viadiu, H.; Opella, S. J. *Biochemistry* **2011**, *50*, 8983.

(3) Denisov, I. G.; Grinkova, Y. V.; Lazarides, A. A.; Sligar, S. G. *J Am Chem Soc* **2004**, *126*, 3477.

(4) Hebling, C. M.; Morgan, C. R.; Stafford, D. W.; Jorgenson, J. W.; Rand, K. D.; Engen, J. R. *Anal Chem* **2010**, *82*, 5415.

(5) Boldog, T.; Grimme, S.; Li, M. S.; Sligar, S. G.; Hazelbauer, G. L. *P Natl Acad Sci USA* **2006**, *103*, 11509.

(6) Borch, J.; Hamann, T. *Biol Chem* **2009**, *390*, 805.

(7) Arora, A.; Rinehart, D.; Szabo, G.; Tamm, L. K. *J Biol Chem* **2000**, *275*, 1594.

(8) Surrey, T.; Jahnig, F. *Proc. Natl. Acad. Sci. USA* **1992**, *89*, 7457.

(9) Sanchez, K. M.; Neary, T. J.; Kim, J. E. *J. Phys. Chem. B* **2008**, *112*, 9507.

(10) Schlamadinger, D. E.; Gable, J. E.; Kim, J. E. *J. Phys. Chem. B* **2009**, *113*, 14769.

(11) Sanchez, K. M.; Kang, G. P.; Wu, B. J.; Kim, J. E. *Biophys. J.* **2011**, *100*, 2121.